U.S. DEPARTMENT OF THE INTERIOR
U.S. GEOLOGICAL SURVEY

PETROGENESIS OF LATE-STAGE GRANITES AND Y-REE-ZR-NB-ENRICHED VEIN DIKES OF THE BOKAN MOUNTAIN STOCK, PRINCE OF WALES ISLAND, SOUTHEASTERN ALASKA

by

John A. Philpotts[1], Cliff D. Taylor[2], Mitsunobu Tatsumoto[2], and Harvey E. Belkin[1]

[1] U.S. Geological Survey, Reston, VA 20192 U.S.A.
[2] U.S. Geological Survey, Denver, CO 80225 U.S.A.

Open-File Report 98-459

PETROGENESIS OF LATE-STAGE GRANITES AND Y-REE-ZR-NB-ENRICHED VEIN DIKES OF THE BOKAN MOUNTAIN STOCK, PRINCE OF WALES ISLAND, SOUTHEASTERN ALASKA

by

John A. Philpotts, Cliff D. Taylor, Mitsunobu Tatsumoto, and Harvey E. Belkin

ABSTRACT

A suite of samples, constituting a 3-km transect southeast from the margin of the Bokan Mountain peralkaline granite stock along a Y-REE-Zr-Nb-enriched micro-pegmatite and aplite vein-dike system, have been studied geochemically and petrographically in order to assess the nature and origin of the enrichment. Noteworthy minerals include arfvedsonite, taeniolite, gittinsite, and a host of rare-earth-, zirconium-, and niobium-bearing phases. Textures range from primary igneous assemblages, through autometasomatic replacements, to late-stage fracture fillings of hydrothermal aegirine, zircon, iron oxide, iron hydroxide, and clay minerals. Fluid inclusions are abundant. Mineral rare-earth abundance patterns show diversity that contrasts with the limited range of whole-rock patterns. Yttrium and heavy rare earths are unusually enriched in these samples. The rocks display a pronounced negative europium anomaly ($Eu/Eu^{*} = 0.27 \pm 0.03$) that is consistent with their sampling the same evolutionary stage of an igneous system that has undergone extensive feldspathic fractionation. The enrichment of trace elements in the vein dikes likely resulted from separation of solid, fluid, and vapor phases. Evidence for immiscible fluid separation include silicate-, fluoride-, and sulfate-phases. Neodymium isotope measurements indicate depleted source rocks for the magma and subsequent open geochemical systems.

INTRODUCTION

Bokan Mountain (lat 54°55′N., long 132°9′W.) is located between the South Arm of Moira Sound and the West Arm of Kendrick Bay on southern Prince of Wales Island in the Dixon Entrance D1 quadrangle, 60 km southwest of the town of Ketchikan (Figs. 1,2). In 1955, airborne and subsequent ground surveys identified areas of high radioactivity due to concentrations of uranium and thorium minerals. Follow-up work led to the development of the Ross Adams mine which produced 94,000 short tons of high-grade uranium ore, averaging one percent U_3O_8, between 1957 and 1971. Subsequently, significant resources of rare earth elements (REE), yttrium, zirconium, and niobium were discovered at Bokan Mountain. Details of the local geology and of the thorium- and uranium-rich mineral occurrences have been reported by MacKevett (1963), Staatz (1978), Thompson and others (1982), De Saint-Andre and others (1983), Warner & Mardock (1987), Thompson (1988), Barker & Mardock (1988), and Warner & Barker (1989).

Prince of Wales Island is in the Craig subterrane of the allochthonous Alexander terrane (Berg and others, 1972; 1978; Churkin & Eberlein, 1977), which consists of up to 35,000 feet of predominantly marine sedimentary and volcanic strata, and plutonic rocks, of latest Precambrian(?) to Middle(?) Jurassic age (Gehrels & Saleeby, 1987; Gehrels & Berg, 1994). Samson and others (1989) suggest that the terrane has the characteristics of an oceanic island arc. Paleomagnetic, paleontologic, and detrital zircon studies (Hillhouse, 1977; Hillhouse & Gromme, 1984; Haeussler and others, 1992; Bazard and others, 1994; Gehrels and others, 1994; Savage, 1994; Gehrels & Berg, 1994) place the terrane within 10 to 20 degrees of the equator and apparently in close proximity to a continent prior to the Late Jurassic, followed by rifting and transport northwards to its present location. Continental docking of the Alexander terrane (and the adjoining Wrangellia terrane) began in the Jurassic (McClelland & Gehrels, 1990; Saleeby, 1994) and was complete by about Middle Cretaceous as indicated by the intrusion of subduction-related magmatic-epidote-bearing plutons and the development of the Jurassic-Cretaceous Chugach accretionary prism outboard of the superterrane. In the southernmost portion of the Craig subterrane, the oldest rocks recognized are arc-type sediments and volcanics of the Wales Group that were metamorphosed and deformed during the Middle Cambrian to Early Ordovician Wales orogeny. These rocks form the basement for an arc-type volcano-plutonic-sedimentary complex of Early Ordovician to Early Silurian age which underlies most of the southern portion of the terrane and comprises the host rocks for the Bokan Mountain stock. The subsequent (Middle Silurian to earliest Devonian) Klakas orogeny resulted in metamorphism, intrusion, uplift, and erosion of the arc edifice (Gehrels & Berg, 1994). Upper Paleozoic shallow marine carbonates, clastic sediments, and lesser volcanic rocks, indicative of a tectonically stable environment, occur as erosional remnants in the Craig subterrane; they are largely absent in the Bokan Mountain area.

Bokan Mountain is a circular stock, about 10 km^2 in area, composed of peralkaline granite of Jurassic age (Armstrong, 1985). The geologic map of Gehrels (1992) divides the Bokan Mountain stock into a core of riebeckite granite porphyry (with subordinate aplitic felty-aegirine granite) surrounded by an outer annulus that is predominantly aegirine granite porphyry (Fig. 2). The Bokan Mountain stock intrudes country rock that consists predominantly of Late Ordovician and (or) Early Silurian quartz monzonite and

granite and Late Ordovician quartz diorite and diorite (Fig. 2). The stock is surrounded by a 3 km-wide albitized contact-metamorphic aureole. Collot (in De Saint-Andre and others, 1983) interpreted the stock as the apex of a large composite intrusion made up largely of outer aegirine granite around a core of amphibole granite. Collot identified the amphibole in the granite as arfvedsonite. Collot distinguished three main facies from border to center: (1) albitic aegirine granite, (2) albitic arfvedsonite granite, and (3) fine-grained albitic arfvedsonite-aegirine granite. Collot considered the Bokan Mountain granite to be hypoaluminous, an extreme example of peralkalinity, and highly differentiated. Thompson and others (1982) and Thompson (1988) mapped 12 intrusive phases in the complex; in their interpretation, a key feature is the subsidence or collapse of the central part of the complex that led to the emplacement of ring dikes, devolatilization of the magma, and a change from aegirine granite to riebeckite granite crystallization.

The thorium-uranium deposits occur as pegmatites, vein dikes, and pipe-like bodies that are spatially and genetically associated with the stock, and are believed to have formed during devolatilization of the magma; the mineralization is thought to be of magmato-hydrothermal origin (Thompson and others, 1982; Thompson, 1988). Alteration is characterized by albitization and silicification of the igneous host rock and destruction of potassium feldspars. Iron and manganese oxides locally mark the position of shear zones and faults along which the fluids travelled. Later movement on these faults has offset some of the mineralization (MacKevett, 1963). Temperature estimates obtained from water-rich and carbon dioxide-rich fluid inclusions in late-stage quartz, and independently from sulfur isotopes in coexisting sulfide phases, range from 150 to 450°C; $\delta^{18}O$ of calcite indicates magmatic rather than meteoric water (Thompson, 1988). Although most of the early work focused on the uranium occurrences, MacKevett (1963) recognized abnormal REE-enrichments in some rocks at Bokan Mountain. The resources of REE, yttrium, zirconium, and niobium in Bokan Mountain granites and vein dikes have been emphasized in recent reports from the U.S. Bureau of Mines (Warner & Mardock, 1987; Warner & Barker, 1989).

Bokan Mountain is of interest for a number of reasons: (1) Unusually high abundances of yttrium, zirconium, hafnium, and REE indicate an unusually high degree of fractionation; (2) Ratios of HREE (heavy REE, gadolinium to lutetium) to LREE (light REE, lanthanum to samarium) are much higher than HREE/LREE ratios of typical REE ore deposits and this could have economic significance should demand rise for one or more of the HREE; (3) the Bokan Mountain stock magma likely formed from relatively simple source material, either in the mantle or in juvenile rocks of the Alexander terrane (Samson and others, 1989); and (4) a possible petrologic scenario for the genesis of the Bokan Mountain stock has been outlined by Thompson (1988).

The purpose of the present paper is to develop a detailed petrogenetic model for the origin of the late-stage granites and vein dikes at Bokan Mountain based on a comprehensive geochemical and petrographic study giving particular emphasis to the REE. Much of the earlier geochemical data were determined by semiquantitative emission spectroscopy. The more accurate analytical data we report here are particularly necessary for the petrogenetic interpretation of the REE data. We also obtained samarium-neodymium isotopic systematics in the hope of reconciling discrepancies in previously reported ages. Sampling by Staatz (1978), Warner & Mardock (1987), Barker & Mardock

(1988), and Warner & Barker (1989) included many composite and channel samples that are well suited for estimating potential grades and tonnages but not suited for paragenetic studies or for petrogenetic interpretation. The petrography of the late-stage granites and the REE-bearing minerals are here examined in detail. A comprehensive model for the evolution of Bokan Mountain is expected to be useful for elucidating the petrogenesis of other similar but less well studied alkalic igneous bodies in southeastern Alaska.

PREVIOUS STUDIES OF THE BOKAN MOUNTAIN VEIN DIKES

The term "vein dike" is used here for dikes and veins at Bokan Mountain that include pegmatitic, aplitic, and quartz-cored varieties. The vein dikes show bifurcating and anastomosing tendencies, particularly away from the stock, and they are, perhaps, more precisely thought of as systems rather than as individual bodies. The Dotson vein dike is a major mineralized (U, Th, REE, etc.) feature at Bokan Mountain. The northwestern terminus appears to be at a right-lateral offset of the "I & L" vein-dike system (Staatz, 1978), which continues to the periphery of the stock (Fig. 2). The Dotson vein dike extends for about 2 km to the southeast with width usually $\geq$1 m and reasonably good exposure on the flanks of the mountain (Warner & Barker, 1989). The Geoduck vein dike crops out south of the Dotson vein dike and continues to the southeast for another 2 km. The Dotson and Geoduck vein dikes are therefore well suited for studying relationships between the vein dikes and the stock, as well as any changes in composition along the lengths of the vein dikes.

Staatz (1978) studied the mineralogy and composition specifically of the I & L vein-dike system, which in his usage included the Dotson vein dike. The I & L vein-dike system is a fracture-bound set that dips steeply northeast. Staatz (1978) considered that uranium, thorium, and REE typically occur together in the same fine-grained minerals. He reported bastnaesite as the most common REE-bearing phase, with monazite being exceedingly rare; REE and yttrium were also reported in xenotime, Fe-Mn carbonate, and other unidentified minerals. According to Staatz (1978), bastnaesite is the only REE mineral in the central and southeast portions of the vein dike, which also contains the only occurrence of calcite and epidote; allanite occurs in the southeast portion; uraninite, and zinc- and niobium-bearing phases occur principally in the northwest portion; pyrite, galena, sphalerite, zircon, fluorite, and phenacite were also reported. Staatz (1978) considered the vein dikes to be atypical of igneous thorium-rich deposits in that they are high in uranium and zirconium and also have abundant albite instead of microcline. He considered the vein dikes in some respects to resemble the deposit at Mountain Pass, California. Maxima in REE abundances at neodymium were interpreted as being due to loss of tetravalent cerium. Distributions of REE were noted as being generally consistent within a particular vein dike.

Warner & Mardock (1987) investigated newly discovered quartz-albite dikes containing enrichments of zirconium, yttrium, REE, niobium, thorium, and uranium, which extend more than 6 km from the Bokan Mountain stock. They reported REE in thalenite and its alteration product tengerite as well as in bastnaesite, parisite, synchysite, xenotime, and monazite. Niobium was found to occur in minerals of the euxenite-polycrase series and in columbite. Thorium and uranium were contained in thorite, uranothorite, and allanite. Other minerals present include zircon, barite, pyrite, and native silver. Warner

& Barker (1989) identified significant niobium, yttrium, REE, and zirconium resources but considered data to be insufficient for description of reserves. They concluded that: the aegirine and riebeckite granites at Bokan Mountain were not economic although they might form placer deposits; uranium- and thorium-rich minerals were concentrated along shear-zones near to the border of the granite; pegmatitic vein dikes host the highest zirconium abundances; and that yttrium and REE abundances increase away from the stock as the dikes bifurcate and become aplitic. Warner & Barker (1989) were unable to link deposit types to any specific granite. Their qualitative, energy-dispersive analyses by scanning electron microscope (SEM) indicated that niobium was contained largely in euxenite-polycrase; yttrium in thalenite, tengerite, and xenotime; and REE in fluorocarbonates, xenotime, monazite, and allanite.

SAMPLE LOCATIONS

Locations of samples are shown in Fig. 2. Granite samples 11 (that is, APP-91-11) and 13 were collected from the periphery of the stock, about 100 m south of the Ross Adams open pit. Granite samples 15A and 15C were selected from talus immediately southwest (Fig. 2) of the I & L vein-dike system (Staatz, 1978) because they have more distinctly porphyritic textures than those of granite samples 11 and 13. The in situ locations of granites 15A and 15C are unknown, but their geochemistry clearly links them to the stock, and sample 15A, which contains relics of large mafic phenocrysts, closely fits the description given by Warner & Barker (1989) for border-zone pegmatite. Samples 17, 19-5, and 19-6 (all porphyritic quartz-albite-potassic feldspar pegmatites) and samples 21A and 21B are from locations on the Dotson vein dike that are increasingly distal from the stock. Sample 21A is a medium-grained granite whereas sample 21B is a mixed rock consisting additionally of fine-grained speckled granite. Sample 21B was interpreted in the field to be from a vein dike interfingering with host sample 21A, although the exact relationship was obscure. The trace element signature, however, indicates that 21A also represents a vein dike or rock contaminated with vein-dike components. Sample 23, is a fine-grained brownish aplite that was collected about 1 km southeast of sample 21. The bifurcating nature of the vein dike and the heavy undergrowth make it uncertain whether the sample is from the extension of the Dotson vein dike or from a nearby parallel vein dike. Sample 6, a tan-colored felsic aplite collected 1.2 km southeast of sample 23, is from another extensive vein dike, the Geoduck system (Warner & Barker, 1989). The Geoduck trends southeast along the southern edge of the West Arm of Kendrick Bay (Fig. 2). Sample 5 was taken from the metabasalt country rock that hosts the Geoduck vein dike in this vicinity. Sample 7 was collected from a metabasalt dike and sample 8 from the local Ordovician and (or) Silurian granodiorite country rock. Samples 7 and 8 were collected about 4 km southeast of the outer-annulus granite of Bokan Mountain and are likely free from albitization or any other metasomatic effects associated with the stock.

WHOLE-ROCK CHEMICAL COMPOSITIONS

Chemical analyses are reported in Table 1. Major and minor elements are reported as weight percent of the oxide except for fluorine, chlorine, and sulfur, which are reported as weight percent of the element. Trace elements are reported as parts per million by

weight. A variety of analytical techniques were used. Major elements (Si, Ti, Al, Fe, Mg, Ca, Na, K, Mn) were determined by wavelength dispersive X-ray fluorescence spectrometric (WDXRF) analysis of glass discs prepared by fusing 800 mg samples with lithium tetraborate. Abundances of the trace elements As, Au, Co, Cr, Cs, Hf, Rb, Sb, Sc, Se, Ta, Th, U, Zn, Zr, La, Ce, Nd, Sm, Eu, Tb, Ho, Yb, and Lu were determined by instrumental neutron activation analysis (INAA) using 6.5 hour irradiations of 0.5 g samples in a TRIGA reactor (U.S. Geological Survey, Denver) and four counts over an 8 week period. Other trace elements (Ba, Be, Cd, Cu, Ga, Li, Ni, P, Pb, Sn, Sr, V, Y) were determined by inductively coupled plasma-atomic emission spectrometry (ICP-AES) using acid dissolution and lutetium as an internal standard. Molybdenum, niobium, and tungsten were determined by ICP-AES following an ion exchange separation. Ferrous iron was determined on 0.5 g samples by colorimetric titration with potassium dichromate. Loss on ignition (LOI 925C) was determined on 800 mg samples ignited in platinum-gold crucibles at 925 °C for 45 minutes. H_2O+ was calculated by subtracting H_2O- from total H_2O determined by coulometric Karl-Fischer titration of water released from a fluxed sample heated to 950 °C. H_2O- was determined gravimetrically after heating a 1 g sample to 110 °C. The abundance of CO_2 was determined on 0.5 g samples by coulometric titration following perchloric acid digestion. Fluorine was determined by selective ion electrode (SIE) analysis on 100 mg samples. Chlorine was determined by SIE analysis of 200 mg samples. Total sulfur was determined by combustion infrared spectroscopy of 200 mg samples. Details of all procedures and of the estimated analytical quality are given by Baedecker (1987). Probable magnitudes of systematic analytical errors are less than ten percent of the reported values in all cases. Table 2 gives CIPW weight percent normative mineralogy for the samples.

The peripheral granite samples 11, 13, and 15C are quite similar to each other in composition, and in the present discussion they will be taken as representing primary magmatic granites. For the major elements, the largest relative difference is in potassium which decreases from sample 11 to 13 to 15C. Porphyritic granite sample 15A and upper Dotson vein-dike sample 17 are not very different from samples 11, 13, and 15C in terms of major element composition except for higher iron (15A being lower in potassium and 17 lower in sodium). Interestingly, the normative mineralogy differs in that samples 11, 13, and 15C have significant acmite abundance and no appreciable magnetite whereas samples 15A and 17 have significant normative magnetite and no appreciable acmite. Upper Dotson vein-dike sample 17 also has appreciable normative zircon as do middle Dotson samples 19-5 and 19-6, (which, however, have abundant normative acmite instead of magnetite). Lower Dotson sample 21B also has high normative zircon. The lower Dotson samples 21A and 21B, and particularly the east Dotson sample 23 have appreciable carbonate. The more distal samples appear to have atypical alkali contents. Lower Dotson vein-dike sample 21B has less sodic normative feldspar than is typical. Sample 21A, east Dotson sample 23, and Geoduck vein-dike sample 6 have more than 90 percent pure albite in their norms and this is more sodic than is typical. This disproportionation of alkalies in distal samples may be another manifestation of the metasomatism that produced the albitic halo around Bokan Mountain and that is shown on a microscopic scale in thin section by the ubiquitous replacement of potassium feldspar by albite. Lithium appears

depleted in most of the vein dikes relative to the granites and was perhaps lost in a hydrothermal fluid or vapor phase. Vein-dike samples 21A and 23 are exceptions with 23 having the highest measured lithium content (510 ppm); these samples both have highly albitic normative feldspar and the high sodium and lithium contents may reflect a metasomatic component.

The vein dikes present a complex picture in terms of trace element enrichments. Yttrium (1.8%), REE (e.g. Ce 0.6%), and rubidium (740 ppm) are highest in lower Dotson sample 21B. Zirconium (2.4%), hafnium (537 ppm), and tin (120 ppm) are highest in middle Dotson sample 19-5. Niobium (2100 ppm) and beryllium (130 ppm) are highest in Geoduck sample 6. Lead (2300 ppm) and zinc (1600 ppm) are highest in east Dotson sample 23. Clearly there are a number of factors involved in the enrichment of these elements at Bokan Mountain. The vein dikes generally differ from the presumed primary granite in terms of considerably higher calcium, zirconium, hafnium, yttrium, HREE, and carbonate abundances. These relationships are brought out in Fig. 3 for the middle Dotson vein-dike sample 19-5 and Bokan Mountain stock granite sample 11 in terms of an element-by-element abundance comparison. Zinc also appears to be enriched in some of the vein dikes relative to the granites, and lead is even more enriched. Correlations discussed next suggest that zinc may have been transported as chloride complexes and lead with carbonate. The zinc/lead ratio ranges from 9 to 16 in granite samples 11, 13, and 15, whereas it is less than unity in some vein-dike samples (19-6 and 23).

In searching for possibly significant geochemical coherence or antipathy of elements we have determined linear (Pearson) inter-element correlation coefficients for the granite and vein-dike data. Correlation coefficients with a significance exceeding 99% are given in Table 3. Paired elements might be expected to show good correlation with each other if they are geochemically similar (i.e. substitute for each other) or if they occur together in an aqueous complex or an abundant mineral. Because only a limited number of samples are involved, any given correlation might be heavily influenced by a single sample. Some of the correlations are as expected: sodium with lithium, and potassium with cesium and rubidium, for example. Zirconium is correlated with hafnium, as expected, but also with tin. Carbon dioxide is best correlated with magnesium, then strontium, cobalt, lead, scandium, zinc and manganese; perhaps some of these elements have a significant abundance in carbonate. Fluorine is well correlated only with barium. Chlorine is correlated with manganese, zinc, and calcium; perhaps these elements were in chlorides. Niobium correlates with tantalum, beryllium, molybdenum, copper, and strontium. Some of the more interesting correlations are with the REE. Yttrium, as expected, shows a correlation with all of the REE, reaching a maximum at about terbium. Thorium shows very similar affinities. Uranium correlates with cerium and europium (but even more so with copper). Copper and barium correlate better with lanthanum and cerium than do ytterbium and lutetium. Chromium and cesium correlate with the HREE. Rubidium and tin correlate best with ytterbium and lutetium.

Chondrite-normalized REE abundance patterns are given in Figs. 4a, b, and c. For each sample the pattern was interpolated through the measured data points (symbols) based on the known regular behavior of the trivalent REE. Each of the three country rock samples has its own unique pattern (Fig. 4c). Sample 7, which is from a metabasalt dike,

has low lanthanum and cerium abundances indicative of a depleted source, and the pattern resembles that of MORB (mid-ocean-ridge basalt; e.g., Philpotts and others, 1969). The lack of any significant europium anomaly indicates that it represents primitive melt that has undergone little (low-pressure) feldspar fractionation since leaving the mantle. The europium anomaly is defined in terms of the ratio of measured europium abundance to a hypothetical trivalent europium abundance (Eu*) which, in the present paper, is based upon interpolation of normalized abundances of the trivalent REE samarium and terbium. Sample 5, another metabasalt, also lacks a europium anomaly. The enriched lanthanum and cerium abundances in sample 5 suggest either a much lower degree of partial melting than for sample 7 or a source that was not as depleted by prior melting events. The REE pattern of sample 5 is similar to that of many diabases and continental flood basalts (Philpotts & Schnetzler, 1968). The lack of a europium anomaly in sample 8 (granodiorite) again suggests little differentiation involving feldspar and hence mantle rather than crustal derivation. The slope of the REE pattern, particularly for the HREE, resembles that of the tonalite-trondhjemite suite.

The degree of HREE enrichment apparent in the vein-dike samples shown in Figs. 4a and 4b is unusual for rocks with such high total REE abundances. Most REE ores, such as those at Mountain Pass, California (Olson and others, 1954) and the world's largest REE deposit at Bayan Obo, China (Philpotts and others, 1991) are highly enriched in LREE. The east Dotson vein-dike sample 23 is the only Bokan Mountain rock showing this tendency (Fig. 4c). The LREE-enriched pattern of sample 23 may reflect its position as the most distal of our Dotson vein-dike samples. The REE data of Staatz (1978), when plotted as chondrite-normalized patterns, show HREE-enriched or bowl-shaped patterns for samples from the I & L vein dikes (which are proximal to the stock) but show LREE enrichment, like that in sample 23, in three samples from the (distal) Dotson vein dike. Similarly, Warner & Mardock (1987) reported general proximal HREE enrichment and distal LREE enrichment in the vein dikes. Our samples appear to fit most of the compositional trends noted previously (Warner & Mardock, 1987; Warner & Barker, 1989). A total sum of REE as oxide (without yttrium), calculated by adding measured and estimated REE abundances, is reported for each sample at the bottom of Table 1. Three of four most distal samples (21A, 23, and 6) are quartz-albite granite or aplite (Table 1). Of these, aplite samples 6 and 23 have the second and third highest REE contents (Table 1), respectively, and sample 6 also has the highest Nb concentration (2100 ppm). However, the potassium-feldspar-bearing pegmatite sample 21B has the highest REE (2.4 percent RE_2O_3) and yttrium contents (2.3 percent Y_2O_3).

PETROGRAPHY

In order to better understand the mineralogy, especially the REE-bearing minerals, the Bokan Mountain samples have been studied by light optical microscopy and by electron-microbeam instrumentation. The fine grain size precluded mineral identification by X-ray diffraction techniques. A JEOL JSM-840 SEM, equipped with a Princeton Gamma-Tech energy-dispersive X-ray analyzer, was used for detailed petrography and tentative mineral identification. Quantitative wave-length dispersive analysis was conducted with a fully-automated, five-spectrometer JEOL JXA-8900 Superprobe electron probe

microanalyzer. Microprobe operating conditions were generally 15 keV and 20 nanoamps using a focussed beam. Natural and synthetic glass, oxide, silicate, and phosphate standards were measured before each analytical session. In this report, trade names and other identifiers are given in the interest of completeness; their use does not imply endorsement by the U.S. Geological Survey. Mineral characterization of the Bokan Mountain samples, and the mineralized portions in particular, is difficult because of intergrowths, fine grain size, complex compositions, and the fact that many of the minerals appear to contain volatile constituents. Some phases were unstable under the electron beam resulting in pitting of the sample and low analytical sums; many grains were too small to permit use of a defocussed beam or raster analysis. Our study is necessarily only an overview of the mineralogy. For most minerals we have attempted to obtain some indication of an appropriate formula before assigning a name. In those cases where this has not been possible we have sometimes suggested a mineral identification with attached question mark as a designation of uncertainty. The exact nature of any of the minerals with incomplete sums should be considered tentative. Formulae for unknown minerals and for minerals with deficient sums have been calculated using a generic 24 oxygen equivalents.

Fluid inclusions are abundant in the granite and vein-dike samples, being observed as minute holes during electron-beam instrument scans of the thin sections. Primary, 2-phase (vapor + liquid) aqueous inclusions are common in quartz and less common in the feldspars and mafic phases. Healed fractures that terminate within various crystals are abundant and contain pseudosecondary 2-phase (vapor + liquid) aqueous inclusions. No daughter crystals or liquid CO_2 were observed optically. The vapor to liquid ratios in primary and pseudosecondary inclusions are qualitatively higher than those in inclusions contained in the cross-cutting healed fractures. Secondary inclusions observed as very abundant healed fractures contain 2-phase (vapor + liquid) aqueous inclusions. Some healed fractures contain coexisting liquid-rich and vapor-rich inclusions indicating vapor separation during late-stage hydrofracting.

The granite and vein-dike samples are composed primarily of quartz, potassic feldspar, albite, aegirine, amphibole, and magnetite. The modal abundances of the rock-forming minerals in the granite and vein-dike samples closely mirror the normative mineralogy reported in Table 2. The only caveat to this generalization is that in some of the samples (particularly sample 13 and, to a lesser extent, sample 15C) a substantial amount of the normative acmite is represented in the mode by amphibole. Although there is considerable variability in the modal abundance of the various rock-forming minerals, there is little variation in the composition of each mineral. We have not identified any systematic trends in the composition of the major minerals within this sample suite. The calcic pyroxenes analyzed in sample 23 (which are discussed further below) are the only noteworthy exception to the uniformity of mineral compositions. The lack of variation in the composition of the major minerals is further evidence for a close genetic link among all rocks of the suite.

Potassic feldspar in the granite and vein-dike sample suite is typically microcline with only about three mole percent albite (Table 4a). The microcline occurs in some samples as barrel-shaped grains with indistinct hourglass structure. It has been pervasively

replaced, partially along crystallographically-oriented directions, by albite (Fig. 5). The albite is quite pure (Table 4a), typically having less than one mole percent potassic feldspar. Much of the albite has grown along fractures that remain as central partings in the albite laths and may represent the fractures along which metasomatic fluids percolated. This origin may explain why many of the albites are curved and also the felty texture shown by albite in some areas. Albite may also have partly replaced potassic feldspar in the matrix of samples. To a much lesser extent albite appears to have replaced aegirine and silica along fractures. The potassic feldspar often displays incipient alteration or weathering. Alkali site occupancies are somewhat low in both feldspars (i.e. <1 cations per 8 oxygen) and this feature would be consistent with incipient alteration to clay minerals. The rocks otherwise appear to be reasonably fresh. Some of the microprobe analyses of silica phases (Table 4a) yielded somewhat deficient totals, perhaps owing to an abundance of inclusions.

Almost all of the pyroxene in the granite and vein-dike samples is aegirine (Table 4b). In some samples (e.g. 11, 13) it occurs in equant grains with grain boundaries ranging from straight to irregular. The aegirine also shows other distinct habits, occurring as needles, sheaf-like masses, and spectacular spherulitic (radiating) starbursts. We interpret these latter habits in terms of later-stage aegirine that grew rapidly, most likely due to an increase in the abundance of volatile species in the melt. Spherulites are the dominant mode of occurrence of aegirine in some of the vein dikes. However, spherulitic starbursts also occur in some of the granites and this provides a genetically significant link with the vein dikes. Aegirine also occurs (e.g. 13, 15C) as a mineral of apparent hydrothermal origin in interconnected networks of filigree that fill late-stage fractures and may replace albite. Other hydrothermal (fracture-filling) minerals include iron oxide or hydroxide, zircon, iron-aluminum-silicates, and clay minerals.

Amphibole (Table 4c), which often appears opaque in hand sample, is distinctly pleochroic (green, brown, blue, black) and has a habit similar to that of the equant aegirine grains. In sample 11, the amphibole is mostly peripheral to the aegirine and may be a later crystallization product, whereas in other rocks, such as sample 13, aegirine appears to rim amphibole. Much of the amphibole appears to be a primary igneous mineral, based on the appearance of grain boundary contacts. Aegirine and amphibole appear to have been in equilibrium as indicated by sharp grain boundaries. Both equant aegirine and amphibole are rich in oriented solid inclusions. They also both show subtle zoning of titanium contents from low levels in the interior to vanishing levels at the rim.

In terms of accessory minerals, bastnaesite, monazite, zircon, fluorite, pyrochlore, plumbopyrochlore, and betafite are ubiquitous throughout the granite and vein-dike sample suite. A major difference between the granite and the vein-dike samples is the abundance of yttrium-, REE-, and Zr-bearing silicates in the latter. Also, a stage of galena-dominated mineralization that appears to postdate much of the REE mineralization is more prominent in the vein dikes.

We turn now to a more detailed consideration of some aspects of the mineralogy, especially the REE-bearing accessory minerals. The samples are discussed in what is believed to be the approximate (parent to daughter) fractionation order, border zone granites first (samples 11, 13, 15C, and 15A) and then the (increasingly distal) vein-dike

samples (samples 17, 19-6, 19-5, 21, 6, and 23). Mineralogy provides no obvious insight into this order, which is based on ordering the groupings indicated by cluster analysis of the whole-rock chemical compositions using indicators of fractionation including the Ga/Al ratio (Table 1) and potassium abundances in the granites and lead in the vein dikes. Country rocks (samples 5 and 8) are considered at the end of the section.

Sample 11 is a granite of fine to medium grain size. In places, patches of bastnaesite several hundred micrometers across have replaced potassium feldspar and aegirine (Fig. 5). Bastnaesite also occurs as abundant inclusions in overgrowths on some aegirine grains. Other accessory minerals, typically tens of μm across, include monazite, zircon, thorite, plumbopyrochlore (in grains up to 50μm across), pyrochlore, manganiferous ilmenite, and titanium oxides. Fluorite occurs throughout the sample, mostly in the feldspar and at grain boundaries. The only minerals with significant contents of REE noted in sample 11 are monazite and bastnaesite. Electron microprobe analyses of these two minerals are given in Table 4d. The formula calculated (per 16 oxygen equivalents) for the monazite shows an excess of REE and a deficiency of phosphorous relative to the ideal composition. Microprobe analyses of accessory minerals in the present study are not expected to have the same quality as analyses of the rock-forming minerals. An additional problem is that the analytical standards differ considerably from the accessory minerals in composition. The data are presented in order to give an idea of the nature of an accessory mineral and of its absolute and relative REE abundances. The monazite and bastnaesite in sample 11 show very similar REE abundance patterns. Both minerals show examples having maxima at lanthanum and at cerium, respectively, in their REE abundance patterns (Fig. 6). About a tenth of a percent of either mineral would account for the LREE abundances in the whole rock (Fig. 4b). Although LREE enriched, the whole rock shows an inflected REE abundance pattern that represents contributions from minerals other than monazite or bastnaesite (which do not have inflected patterns), perhaps zircon.

Sample 13 is an amphibole granite of medium grain-size in which phenocrysts of microcline (up to 2 mm across), quartz, and irregularly-shaped amphibole occur in a matrix consisting largely of albite and quartz (Fig. 7a). Many of the large amphibole grains have borders of aegirine. An analysis of a representative aegirine grain (points 13.1-3) is given in Table 4b. Replicate analyses of an amphibole grain (points 13.4,5,6) are given in Table 4c. The analyses calculate well to a formula for potassic fluor-arfvedsonite using the AMPHIBOL computer program (Richard, L.R. & Clarke, D.B., Dalhousie University, 1987). Site occupancies are also given in Table 4c. It is noteworthy that A-site occupancy (Na+K) in the amphibole formulae exceeds unity and ranges from 1.011 to 1.230. An excess of alkalies in the A-site of similar arfvedsonite from Magnet Cove, Arkansas, has been explained in terms of possible lamellae of aegirine in a mixed-chain pyribole (Ross, 1984). Analyses of a very irregularly shaped finger-like matrix amphibole grain (Table 4c, points 13.13,15) yielded a composition similar to that of the large equant amphibole grains with somewhat more potassium (up to 3.65 wt.% K_2O). Arfvedsonite is again indicated but the formula calculation does not give quite as good a fit, with tetrahedral silicon assignment exceeding 8 per 23 oxygen.

Much of the quartz in this rock shows undulose extinction under crossed nicols. The

quartz-albite matrix is highly fractured. Many of the fractures appear to have opened along grain boundaries. Late-stage aegirine has crystallized as a filigree along grain boundaries and other fractures (Fig. 7b). Analysis 13.7,9 (Table 4b) is of aegirine filigree within albite adjacent to the upper right corner of the mafic grain in Fig. 7a; analysis 13.10 is of the aegirine filigree shown in Fig. 7b. The filigree has relatively high and variable aluminum contents (2 to 4.5 wt.% Al_2O_3) at about ten times the abundance in the large equant aegirine grains. It is possible that the aluminum signal for the filigree is coming from another mineral but the most straightforward interpretation is that the filigree is composed of aluminous aegirine. Analytical sums are low for the 13.7,9 analysis indicating a missing component (perhaps water or hydroxyl). Abundant zircon has similar occurrence to the aegirine filigree (Fig. 7c), forming strings of grains typically about 0.1 mm across; some zircon grains appear to be associated with brownish devitrified glass(?) or clay(?).

The large equant amphibole and pyroxene grains are full of fine inclusions, often crystallographically oriented. There are numerous round inclusions each consisting of yttrium-bearing fluorite and a small (unoriented) shrinkage bubble. The presence and size of the bubbles indicate that the fluorite crystallized from a dense fluid phase. Monazite and bastnaesite are the dominant REE bearing minerals noted in sample 13. Other accessory minerals include zircon and pyrochlore.

Sample 15C is a medium-grained granite composed of feldspar, quartz, and amphibole phenocrysts in a finer-grained matrix of microcline, albite, silica, amphibole, aegirine, and titaniferous annite. Parts of the rock have been so highly fractured as to be almost granulated. The fractures have opened along triple-junction grain boundaries in the matrix (Fig. 8a). Inasmuch as the phenocrysts of microcline and amphibole do not show this structure, we interpret the triple junctions as forming in a late volatile-rich stage of the igneous crystallization rather than in a subsequent recrystallization of the rock. Hydrothermal aegirine formed in these cracks (Fig. 8a). Zircon again shows a habit very similar to that of the filigree aegirine with perhaps somewhat more replacement of host feldspar (Fig. 8b). In more detail, zircon can be seen to have formed along triple-junction grain boundaries (Fig. 8c) in part replacing feldspar in a process yielding inclusions of hexagonal quartz crystals (Fig. 8d). There are also inclusions of bastnaesite in the zircon. Neither the aegirine nor zircon filigrees (which are both optically continuous) show triple-junction grain boundaries or cracks and presumably formed from percolating fluids subsequent to the triple-junction crystallization. Some zircon grains show deficiencies in the sum of the microprobe analyses of up to 10 percent; these zircons consistently carry yttrium and may be hydro-ribeirites (Table 4e). Hafnium was not determined but it is expected to be a component of zirconium-bearing minerals. Based on the whole-rock chemistry, hafnium is expected to be present at about two percent of the zirconium concentration. The REE abundance patterns for the zircon grains in sample 15C show considerable variety (Fig. 9) that may in part reflect competition for REE with other phases. The whole-rock REE abundance pattern (Fig. 4b) is inflected and presumably reflects both LREE-bearing minerals, like bastnaesite and monazite, and HREE-bearing minerals like zircon.

Sample 15A is a granite porphyry. Phenocrysts up to 1mm across of quartz and microcline occur in a finer grained matrix of quartz, microcline, plagioclase, and

titaniferous magnetite. The largest phenocrysts (centimeters across) appear to have been composed of a dark, pleochroic amphibole that has been largely replaced by a fine-grained mixture of crystallographically-oriented magnetite and a silica phase with lesser amounts of feldspar and a brown-colored, hydrous, iron-aluminum silicate (±K). Veins in the rock are filled with silica and the brown-colored phase. No minerals carrying significant amounts of REE, yttrium, or niobium were found in sample 15A.

Sample 17 is from the upper Dotson vein dike. The rock is a silica-rich micro-pegmatite (47% quartz in the norm). Centimeter-sized grains of microcline and fractured quartz occur in a matrix of potassic feldspar, felted albite, silica, magnetite, zircon, and a brown phase. An interesting feature of sample 17 is the absence of aegirine and amphibole and the occurrence of extensive magnetite (6% in the norm). The magnetite grains (typically 0.1 mm across) show an uneven distribution, being concentrated along phenocryst grain boundaries and in clumps in the matrix as if replacing some pre-existing mineral. The magnetite is commonly speckled with micrometer-sized inclusions of thalenite?, fergusonite?, galena, manganiferous calcite, zircon, and cassiterite that also occur as partial rims and veinlets. An occurrence of magnetite grains rimming titaniferous, magnesian fluoro-biotite in association with manganiferous ilmenite, fergusonite, and bastnaesite inclusions is shown in Fig. 10. Zircon occurs in the matrix as equant grains up to 0.1 mm across, often in linear strings as if along fractures or prior grain boundaries.

Interconnected networks of irregularly shaped open pits, up to 1 mm across, that may represent fluid inclusion or solution cavities, are common in the microcline of sample 17 (Fig. 10). Minerals present as μm-sized grains on the interior walls of the cavities include (porous) zircon, cassiterite, manganiferous ilmenite, and parisite?. Some cavities are coated with late-stage hydrothermal cerianite. Cerium oxide was not utilized in the preparation of the polished thin sections used in the present study and the habit does not resemble trapped polishing compound. The cerianite also occurs in fine (<1 μm) continuous veins that connect some of the cavities. The whole-rock REE pattern for sample 17 (Fig. 4b) shows a positive cerium anomaly relative to the pattern for other samples and this offers further support for the indigenous occurrence of a cerium mineral in this rock. Less than 0.1 weight percent of bastnaesite would account for all the LREE in the bulk chemical analysis of sample 17. The whole-rock pattern is inflected ("v"-shaped) with normalized HREE higher than LREE. The abundance of HREE presumably reflects contributions from minerals such as zircon and the tentatively identified thalenite and fergusonite.

Sample 19-6, from the middle locality along the Dotson vein dike, is a porphyry (Fig. 11a) consisting of millimeter-sized aegirine spherulites (20%) and pinkish-gray polycrystalline prismatic phenocrysts (15%) in a felsic matrix of albite and strained silica that is criss-crossed with secondary fluid inclusions along healed fractures. The silica-rich areas, which contain needles of aegirine, appear to represent crystallized melt. Aegirine also occurs as equant grains. The pinkish-gray phenocrysts are composed of a polycrystalline mixture of silica, gittinsite, zircon, and sparse aegirine similar in composition to other aegirine in the rock. Andradite occurs in the cores of the larger phenocrysts and appears to have been replaced by silica towards the rim (Figs. 11a,b). The gittinsite is full of fluid inclusions and inclusions of calcium-yttrium silicate, zircon,

cerussite, and a Pb-Th-Fe-Ca-silicate.

Sample 19-5, which was collected adjacent to sample 19-6 at the middle locality along the Dotson vein dike, appears in hand specimen to be a granite porphyry with quartz and feldspar phenocrysts set in a fine-grained speckled white and green matrix. Microscopic examination revealed slightly altered phenocrysts of microcline (mm's across) in a matrix of felted albite, aegirine, and silica, with minor zircon. The matrix is heterogeneous, consisting in part of an albite-aegirine rock and in part of a high-silica rock containing sparse aegirine needles and accessory titanite and zircon. In some parts of the rock, silica-rich areas, which macroscopically look like phenocrysts, appear, instead, to have been globules of immiscible siliceous melt set in an aegirine-albite matrix (Figs. 12a,b). The most distinctive feature of the rock are abundant globules and prismatic phenocrysts of pale pinkish hue that occur in both siliceous areas and albite-aegirine areas but are more common in the latter. They are composed of a mixture of silica, gittinsite, calcium-yttrium-silicate, andradite, zircon, (pure) calcite, and potassium feldspar in grains a fraction of a millimeter across. A (1:1) lead-chloride mineral and platy cerussite occur sparsely as inclusions, cavity fillings, and veinlets in the globules. Prismatic and rhomboid shapes may have been imposed on some globules by surrounding mineral laths and phenocrysts inasmuch as other areas containing the same mineral assemblage are distinctly rounded, having the appearance of immiscible melt globules (Fig. 12c). Alternatively, the parental phases may have both crystallized from the melt as phenocrysts and separated from it as immiscible melt globules. Perhaps a solid phase remelted owing to change in physical conditions or to a peritectic reaction with melt during crystallization. Minerals in the globules, especially the gittinsite (Fig 12d) contain numerous cavities, some of which are very elongate.

The textures in this rock appear indicative of potassium feldspar phenocrysts in association with three immiscible liquids: siliceous melt and gittinsite-globule melt in (parental?) aegirine-albite-silica melt. Perhaps when unmixing started in this sample it precipitated further unmixing. Or perhaps loss of volatiles decreased solubility of other phases in the melt, resulting in multiple immiscibility. All of the putative melts have crystallized as polymineralic solids. Compositions of minerals contained in common match closely; hence the globules appear to be in equilibrium and not accidental inclusions. Indeed grains of some minerals, such as aegirine, cross globule boundaries without apparent reaction. Analyses of aegirine in the high silica rock (lower part of Fig. 12b) and in the aegirine-albite rock (upper part of Fig. 12b) are given in Table 4b (19-5.6-8 and 19-5.12-14, respectively). Many aegirine grains in this rock contain minor patches of more calcic composition including the analyzed aegirine grain from the high-silica area (Table 4b, 19-5.9,10,11). These patches might represent residual areas of earlier calcic pyroxene that has been largely replaced by aegirine, a process common in alkaline rocks. However, calcic patches occur not only in equant aegirine but also in needles and in spherulitic aegirine showing no rim to core variation. An origin of the more calcic pyroxene in most samples by exsolution is therefore preferred. (An exception discussed below is sample 23 which contains both calcic pyroxene, seemingly in primary quench textures, in addition to grains of aegirine.)

Microprobe analyses of the gittinsite (Table 4f) yielded a formula close to

$Ca(Zr,Y,REE)Si_2O_7$. It thus appears to be a yttrium- and REE-bearing variety of this extremely rare mineral. The calcium-yttrium mineral (Fig. 12d), which showed red luminescence, was not stable under the electron beam. Microprobe analysis suggests a mineral formula approximating $CaYSi_2O_7$ (Table 4f). The analytical sum, however, is only about 80 percent. A wavelength dispersive scan did not show a carbon peak but did show fluorine. This suggests a fluor/hydroxy species, perhaps Y-tritomite. The andradite garnet (Tables 4f,4g) and zircon (Table 4f) also display low analytical sums and may be hydroxy-andradite and hydro-ribeirite, respectively. The calcium-yttrium silicate, the gittinsite, and the zircon all have chondrite-normalized REE patterns increasing towards the HREE (Fig. 13). The whole-rock REE abundance pattern (Fig. 4b) shows a maximum at ytterbium that presumably reflects the REE patterns of these minerals.

Sample 21 was collected from a lower outcrop of the Dotson vein dike, more distal from the stock than the above samples. The sample is a complex mixture of a medium-grained quartzo-feldspathic rock, finer-grained aplite, speckled with opaques, and fine-grained (<0.1mm) mineralized areas. The medium-grained rock consists of potassic feldspar phenocrysts (several millimeters across, some with patchy zoning or clouds of inclusions), albite (often with bent form and twinning), quartz with undulose extinction, magnetite, and minor biotite. In places, the aplite contains phenocryst relics composed of opaque minerals and quartz. Fluorite was observed throughout the thin section but it is particularly abundant in the fine-grained material. The mineralized patches appear to invade and, in part, replace the medium-grained rock (Fig. 14a). The mineralized areas consist of albite, rounded blebs of potassic feldspar, iron oxide, manganiferous-ilmenite, zircon, thorite, and a host of intergrown REE-, yttrium-, zirconium-, and niobium-bearing minerals.

The complexity of REE and yttrium mineral associations in sample 21 is considerable and the following is perhaps best taken only as a preliminary look. The highest REE abundances measured by microprobe were in a mineral similar in composition to synchisite, a REE-calcium fluoro-carbonate. Measured fluorine values were only at about half the expected value (Table 4h) and the mineral is perhaps hydro-synchysite. Other minerals (Figs. 14b,c) include a Y-Ca-REE fluorosilicate and a fluorine-bearing variety of yttrium (hydroxy?-)silicate (REE+Y=Si; rowlandite?, a fluorine-bearing equivalent of thalenite). The highest combined RE_2O_3 plus Y_2O_3 (62 wt%) abundances in sample 21 were found in a fluorine-free silicate (iimorite?). Another mineral (fergusonite?) has niobium in equal atomic proportions to REE plus yttrium, about 0.5 weight percent fluorine, and some silica (Table 4h). Xenotime occurs intermixed with thorite in an association with magnetite and biotite in the medium-grained rock (Fig. 14d). These minerals show a diversity of REE abundance patterns (Fig. 15) from HREE-depleted synchisite, through relatively unfractionated Y-Ca-REE-silicate, to HREE-enriched xenotime and fergusonite.

The magnetite in sample 21 is distinctive, being riddled in places with irregularly shaped inclusions of galena, and more rarely, thorite, sphalerite, and cassiterite (Fig. 14c). These minerals also occur in sparse, very fine veinlets in the magnetite and surrounding minerals, and as thin partial rims. The galena-dominated stage of mineralization appears to postdate crystallization of the major REE mineralization in this rock.

Sample 6, from the Geoduck vein system, is a medium-grained, tan-colored, felsic

aplite containing scattered black needles. Like sample 21, sample 6 appears to be a mixed-phase rock consisting about one third of disseminated, millimeter-sized patches of fine-grained (<0.1mm) multiconstituent mineralization. In contrast to the rather distinct contacts in sample 21, the mineralized patches in sample 6 tend to have more irregular and diffuse boundaries (Fig. 16a). The patches are full of irregularly shaped fluid inclusion cavities. The felsic matrix in these patches consists of silica with inclusions (mostly $\leq$0.1mm) of albite, potassium feldspar, magnetite, and rare willemite. The mineralized patches contain complex intergrowths of REE-, yttrium-, and zirconium-bearing silicates, REE-phosphate, and REE-fluorocarbonate. There is also a variety of niobium- and titanium-bearing minerals (tentatively including priorite, Y-betafite, fersmite, and pyrochlore). Many of the patches consist of intergrowths (Fig. 16b) of allanitic epidote and a yttrium-rich REE silicate (Table 4i) that may be a low-fluorine equivalent (Y-tritomite? thalenite? caysichite?) of the mineral suggested to be rowlandite in sample 21; the epidote and Y-REE silicate may represent exsolution or reaction of parental allanite. Other minerals include bastnaesite, monazite (Table 4i), apatite (Table 4i), zircon (some full of wormy cavities), and biotite. The REE abundance patterns of the analyzed minerals generally show a decrease from LREE to HREE (Fig. 17). The Y-REE silicate, however, shows a pronounced maximum near gadolinium. Although the iron content does not appear high enough, it is possible that this mineral is gadolinite, with the deficiency in the sum being due to beryllium which was relatively high (130 ppm) in the bulk analysis of sample 6. The selvage of the vein dike in contact with country rock is heavily mineralized with magnetite and fish-egg-like masses of micrometer-sized niobium oxide which fills veinlets along with biotite (Fe-rich and Mg-rich varieties), limonite, and clay? (Fig. 16c).

Sample 23, from the east Dotson vein dike, is another fine-grained brownish-colored aplite and consists of millimeter-sized rounded phenocrysts of albite in a finer-grained matrix of quartz, albite, pyroxene, and fluorite. About 15 percent of the rock consists of scattered, irregularly bounded, millimeter-sized patches that contain most of the mineralization in the sample. These patches vary in aspect from one end of the thin section to the other perhaps due to differences in cooling rate relating to distance from the contact of the vein dike with country rock. An example of a fine-grained (perhaps more rapidly cooled) type of inclusion is shown in Fig. 18a. Although mineral identifications are complicated by the feathery intergrowth texture, the inclusion appears to consist of aegirine-augite, albite, quartz, fluorite, mica, caysichite?, fersmite? (Table 4j), and plumbopyrochlore?. The aegirine-augite in the top right corner of the inclusion shown in Fig. 18a has a composition (Table 4b, points 23.10-12) mid way between aegirine and diopside (i.e. Na=Fe, Ca=Mn+Mg). Two aegirine-augite grains (Table 4b, points 23.16-20) from the essentially unmineralized matrix have a composition similar to that of the aegirine-augite in the inclusion, with somewhat higher proportions of aegirine to diopside components.

At the other end of the thin section the feathery inclusions give way to mineralized clots of coarser grain size consisting of aegirine (Table 4b, points 23.7-9), manganiferous calcite, mica, and quartz (Fig. 18b). Niobium- and REE-bearing minerals occur both distributed throughout the clot assemblage and in bifurcating veins of limited extension in both clots and matrix. At higher magnifications (Fig. 18c) some veins have the unusual

aspect of not displacing enclosing grains in the clot assemblage and thus appear to be metasomatic. The assemblages include caysichite? (REE+Ca+Y=Si; Table 4j), red betafite?, plumbopyrochlore?, monazite, and bastnaesite. Strontium-rich barite was observed in other clots, occurring as round (once-fluid?) inclusions (complete with shrinkage bubbles) in bastnaesite. The REE abundance patterns for both the caysichite? and fersmite? show some decrease towards HREE (Fig. 19). The whole-rock pattern (Fig. 4a) would be explained by the presence of about one percent caysichite?.

The mica in the clot assemblage is the low-aluminum fluoro-mica taeniolite (Tables 4j, 4k, points 23.1,3,5). Site assignments calculated using a computer program by Afifi & Essene (1988) are given in Table 4k. Lithium, an essential constituent of taeniolite, could not be determined by microprobe analysis; sample 23, however, has by far the highest lithium content (510 ppm) of any of our Bokan Mountain samples (Table 1).

Sample 5, the fine-grained, green-colored metabasalt country rock that hosts the Geoduck vein dike (sample 6), consists about 50 percent of altered feldspar, 5 percent opaque minerals, and chlorite. Sample 8, the metamorphosed granodiorite country rock, consists largely of grains of cloudy microcline (some >1mm across) and of plagioclase that has been pervasively altered to albite and epidote. Some of the quartz grains show modest fracturing. Calcic amphibole has been partially altered to chlorite, titanite, and epidote. Other accessory minerals include minor zircon, magnetite, and ilmenite.

SAMARIUM-NEODYMIUM SYSTEMATICS

The age of the Bokan Mountain stock is not as well-constrained as might be hoped. Lanphere and others (1964) reported potassium-argon ages on two riebeckite samples (weathered out of Bokan Mountain peralkaline granites) of 181±8 and 186±8 Ma; hornblende samples from granitic country rocks from the West Arm of Kendrick Bay and the South Arm, located 3 km and 6 km southeast of Bokan Mountain, respectively, yielded ages of 431±21 Ma and 446±22 Ma. De Saint-Andre and others (1983) studied the uranium-lead geochronology of zircons from two Bokan Mountain granitic rock types, the fine-grained aegirine (±arfvedsonite) granite occurring south of Ross-Adams, and the Ross Adams (80% albite) syenite that they suggested is closely associated, both spatially and genetically, with the uranium-thorium mineralization. They obtained a concordia intercept age of 171±5 Ma, which they considered approximately equal to the potassium-argon ages of Lanphere and others (1964). Armstrong (1985) studied rubidium-strontium isotopic systematics of the Bokan Mountain granite and country rocks. Four quartz-monzonite country rocks and a gabbro yielded an isochron age of 432±19 Ma. The initial ratio of 0.7039±0.0004 was considered reasonable for Phanerozoic volcanic arc rocks. The age obtained for the country rocks was considered a good fit with the prior potassium-argon dates. The data for the Bokan Mountain stock granites showed some scatter which Armstrong (1985) thought might be due to a 101±3 Ma uranium-thorium mineralization event proposed by De Saint-Andre and others (1983) to explain scatter in uranium-lead dates. Seven selected samples yielded a Rb-Sr isochron indicating an age of 151±5 Ma and an initial ratio of 0.711±0.001. Five other granites gave model ages ranging from 122 to 139 Ma. All of these Rb-Sr ages are younger than the prior K-Ar determinations, which Armstrong (1985) interpreted in terms of excess radiogenic argon, and the zircon concordia

intercept age, which Armstrong interpreted in terms of putative analytical and geologic difficulties of the lead isotope data.

Armstrong's (1985) interpretations may be correct but the discrepancies and lack of agreement are unsettling. In hopes of improving this situation we have studied the samarium-neodymium systematics of our suite of samples from Bokan Mountain. This isotopic system is known to be relatively robust in the face of some of the challenges that can degrade results from other dating techniques because of the general immobility of the REE. In addition, the high levels of REE in the Bokan Mountain granitic samples might obviate concerns about variation in initial ratios owing to contamination of melt by country rock during emplacement.

All of the present isotopic measurements were performed at USGS/Denver. Fresh rock chips were washed with 2N HCl and distilled water in an ultrasonic bath in order to eliminate surface contamination. After drying, the samples were pulverized using a hardened alloy tool-steel mortar and pestle. Approximately 70 mg sized samples were spiked with ^{149}Sm and ^{150}Nd, then dissolved in concentrated ultraclean HF + HNO_3 in PFA Teflon vials with screw-top caps on a hot plate at 80°C for about a week. REE were separated through a cation-exchange resin using 6N HCl. Sm and Nd were separated by continuous elution through a high pressure cation-exchange resin column with 0.2M α-hydroxyisobutyric acid. Nd was measured as an element on an Isomass 54R mass spectrometer, using a triple filament mode with Ta side filaments and Re center filaments. Sm was measured on an NBS 12" radius 60 degree mass spectrometer using triple filaments as for Nd. The $^{143}Nd/^{144}Nd$ ratios are normalized to a $^{146}Nd/^{144}Nd$ value of 0.7219; the mean for 30 analyses of the La Jolla Nd standard (Lugmair and others, 1976) was 0.511862 ± 10. In light of these results, no instrumental bias correction was applied to the Nd data reported here. Concentration uncertainties of Sm and Nd are less than 0.1 percent and 0.05 percent, respectively. Blank determinations for Sm and Nd were made at the time the analyses were performed and yielded whole-procedure blank values of 3 x 10^{-11}g and 5 x 10^{-11}g, respectively. No blank corrections were needed, therefore, for any of the measured data.

$^{143}Nd/^{144}Nd$ isotopic analyses and associated $^{147}Sm/^{144}Nd$ ratios for Bokan Mountain granites, vein dikes, and country rocks are given in Table 5. The results for the granite and vein-dike samples do not yield an isochron within acceptable error. The scatter is illustrated in Fig. 20 which displays evolution of $^{143}Nd/^{144}Nd$ through time for these samples. A useful isochronous relationship (as indicated by intersection of the isotopic evolution lines within an acceptable spread in age) is clearly lacking. All of the prior age estimates for the Bokan Mountain stock fall within the scatter of the present samarium-neodymium data. The cause for the scatter is not known. It may be due to alteration of the feldspar. A factor that might exacerbate alteration and weathering effects is the abundance in these samples of cracks and microscopic cavities that would give ready access to percolating fluids. The trapped fluids may also have corrosive compositions. Furthermore, the vein-dike samples contain an unusually diverse group of REE-bearing minerals (carbonates, phosphates, oxides, silicates) and it is entirely possible that some of these may be more readily soluble than typical rock-forming silicates on which Sm-Nd ages are usually determined. For these reasons we suspect that lack of a closed system may be

the underlying basis for the failure of our samples to define an isochron.

Any reasonable age (i.e. younger than their host rocks) for the Bokan Mountain stock granite and vein-dike samples indicates that they were derived from depleted source material. That is to say the lines in Fig. 20 showing evolution of their $^{143}Nd/^{144}Nd$ fall above (on the MORB side of) the chondritic evolution line. The data are consistent with derivation of Bokan Mountain granite and vein-dike samples from moderately depleted (i.e. Sm/Nd higher than chondritic) source material. If the Bokan Mountain samples were not contaminated during emplacement then the degree of depletion is most consistent with arc or ocean island basalt source material. Country rock samples (5, 7, and 8) were also derived from depleted source material as shown in Fig. 21. The isotopic data preclude the Bokan Mountain stock granites being derived by melting of country rock such as the sample 8 granodiorite. If this granodiorite were generated in the Ordovician or Silurian, the general age given for Wales Group rocks, then it might have formed from material similar to the source from which the Bokan Mountain granites and vein dikes were subsequently derived, at least in terms of neodymium isotopic composition. Such source material would presumably be moderately depleted basalt. If there was a common parent, however, the genetic process must have been quite different for country rock sample 8 and the Bokan Mountain stock granites judging from the quite different REE abundance patterns among other effects. The lack of an appreciable europium anomaly in country rock sample 8 (Fig. 4c), which might favor an origin via bimodal (Daly Gap) magmatism, is in contrast to the extensive feldspar fractionation manifested by the depletion of europium in the Bokan Mountain stock granites (Figs. 4a,b,c). The neodymium isotopic data for the basaltic dike (sample 7) indicate that the basalt was from a highly depleted source and that it is either a MORB or possibly an arc basalt, both of which would be consistent with the REE abundance pattern. The metabasalt country rock (sample 5) has Sm/Nd lower than chondritic and has also evolved from depleted source material. The present results are all consistent with the depleted nature of the Prince of Wales samples reported on by Samson and others (1989). In contrast to many Phanerozoic orogenic belts, which samarium-neodymium and rubidium-strontium isotopic studies show to be composed largely of reworked pre-existing continental crust, this part of southeastern Alaska does not appear to have been proximal to old continental crust for any extended period of time. The Alexander terrane appears to have formed as mantle-derived crust in a volcanic arc, probably in an intra-oceanic setting (Samson and others, 1989).

DISCUSSION

Our petrographic results are in accord with prior studies of Bokan Mountain rocks with a few exceptions. The amphiboles we have analyzed in the granites are arfvedsonite and this is in agreement with the findings of Collot (in De Saint-Andre and others, 1983; cf. Thompson and others, 1982). This has petrogenetic significance in that arfvedsonite is stable to higher temperatures than riebeckite (Wones & Gilbert, 1982) and its occurrence hence places less constraint on the igneous conditions that seem indicated for many of our samples. The conclusion of Staatz (1978) that bastnaesite is the only REE mineral in the central and southeastern part of the I and L system (which would include our samples 17, 19-5, 19-6, 21, and 23, by his usage) is clearly not correct. He also found monazite to be

rare, whereas it is a common mineral in our samples. Furthermore, the microprobe analyses of REE-bearing phases offer little support for the suggestion by Staatz (1978) that REE abundance patterns with maxima at neodymium are due to negative cerium anomalies.

A number of minerals have been reported for the first time in this paper as occurring at Bokan Mountain. These include taeniolite and gittinsite. Taeniolite, the low-aluminum lithium fluoro-mica found in sample 23, is an exceedingly rare mineral. We are aware of only two other occurrences in the United States, one in contact metasomatic rocks bordering syenite at the Magnet Cove Complex, Arkansas (Miser & Stevens, 1938) and the other in a alkalic mafic diatreme at Coyote Peak, California (Erd and others, 1983). Gittinsite was found in the recrystallized phenocrysts and putative immiscible melt globules in samples 19-5 and 19-6. Gittinsite was first identified in samples from an agpaitic syenite complex at Kipawa, Quebec (Ansell and others, 1980) and has subsequently been found at the Strange Lake alkalic complex on the Quebec-Labrador border (Roelofsen-Ahl & Peterson, 1989) and in the Khaldzan-Buregtey peralkaline granitoids of western Mongolia (Kovalenko and others, 1995). These occurrences bear striking resemblance to Bokan Mountain in terms of their peralkaline igneous rocks, sodic pyroxenes and amphiboles, and enrichments of zirconium, REE, and niobium.

The REE-bearing minerals we have analyzed show a wide diversity of chondrite-normalized REE abundance patterns. This diversity extends to the same mineral type in different samples (e.g. monazite in samples 11 and 6) and even to the same mineral type within a sample (e.g. zircon in sample 15C). We generally discount contamination as a cause for these differences. The observed REE patterns are presumed to reflect both REE partition coefficients and REE abundances in the immediate crystallization environment. We note that the minerals show a much greater diversity of REE patterns than shown by the whole rocks and suggest that this may be due to closed system competition for REE during crystallization of the minerals. The rough parallelism of parts of the whole-rock REE patterns for most of the stock and vein-dike samples suggests that these samples have a close genetic link to each other. Differences in the absolute abundances of REE in these samples may be due in part to the dilution effect of phases with low REE concentrations, such as quartz, feldspar, and aegirine. The similarity in the REE patterns suggests that the REE in these samples are likely dominated by the same few (perhaps two or three) major REE-bearing components. These phases may have very similar REE patterns regardless of the rock in which they occur. The slopes of the LREE in all the stock and vein-dike patterns, and especially the pattern for aplite sample 23 (Fig. 4c), indicate that one or more of the phases contributing REE is LREE-enriched with increasing depletion toward heavier REE. The petrographic studies suggest monazite, bastnaesite, and other REE-bearing carbonate minerals as possible candidates. However, the pattern may have been imposed on the rock not by any given mineral but by a magmatic fluid, possibly carbonatite. East Dotson sample 23, with the greatest decrease in abundances from LREE to HREE (Fig. 4c), has the highest carbonate content of any of the stock or vein-dike samples (Tables 1, 2). Carbonatites, such as those at Mountain Pass, are typically rich in LREE (Olson and others, 1954). The patterns in Figs. 4a and 4b further suggest a component phase with enriched but relatively unfractionated HREE and another REE-bearing phase with HREE showing increasing enrichment up to ytterbium or lutetium.

Minerals such as zircon, Ca-Y-silicate, or the phase parental to the gittinsite-bearing assemblage are among candidates for petrogenetically significant HREE-bearing minerals.

The europium anomalies give an even better indication of the close genetic bond between the stock and vein-dike samples. Clearly, the stock and vein-dike samples displayed in Figs. 4a, b, and c have pronounced negative europium anomalies. This is in distinct contrast to the patterns of the country rock samples (Fig. 4c), which lack europium anomalies. The europium anomalies in the stock and vein-dike samples are unusual in that they all show very similar depletions in the range 0.25 to 0.30 (Table 1). Considering the observed ± 15 percent range of Eu/Eu^* in terms of likely sampling-errors, analytical-errors, and curve-fitting errors, it is concluded that the europium anomalies might be identical in all of our stock and vein-dike samples. The magnitude and invariance of the europium anomalies provide several petrogenetic insights. The similarity of the europium anomalies of the Bokan Mountain granites and vein dikes indicates that the REE in each of these samples are very closely linked genetically. All of the rock samples, whether granite, pegmatite, or aplite, albite-rich or potassic, give no indication of any intervening fractionation of europium relative to other REE. The neodymium isotopic results on the Bokan Mountain stock granites and vein dikes indicate that the granite was most likely derived from the mantle or possibly from primitive mantle-derived material such as MORB or island-arc basalt. It is very unlikely that any sizable volume of such source materials would have large negative europium anomalies. Therefore, the anomalies presumably developed during the fractionation event that produced the Bokan Mountain granites by crystallization and separation of feldspar. The size of the europium anomaly indicates extensive fractionation. Further, the invariance of the stock and vein-dike europium anomalies can be interpreted several ways. The most likely explanation is that all of our stock and vein-dike samples (or more precisely the phases dominating their REE abundances) were generated at exactly the same paragenetic stage. MacKevett (1963) concluded that the thorium-uranium mineralization, the pegmatites, and the aplites were all coeval. Thompson (1988) concluded that the mineralization event was rapid and essentially contemporaneous with the hydrothermal alteration. This conclusion must be tempered by the caveat that it is not impossible that europium anomalies had stopped evolving in these rocks either because conditions became sufficiently oxidizing for the europium to be effectively all in the trivalent state or because fractionation of REE-rich minerals lacking europium anomalies effectively swamped any feldspar fractionation effect. However, studies of redox effects on europium partitioning (Philpotts, 1970) and the generally non-anomalous (i.e. trivalent not tetravalent) behavior of cerium in these rocks provide no evidence to support the former possibility and the second possibility might not be consistent with continued enrichment of REE in the system.

Although a greater number of accessory minerals were found in sample 15C than in sample 15A, the whole rock analyses indicate that both border-zone granites are low in trace elements, including REE. Both rocks have about an order of magnitude less REE than the presumed parental granites 11 and 13. Because the amount of fractionation required to build up trace element contents from those in samples 15C and 15A appears prohibitive if they were earlier in the differentiation sequence than granites 11 or 13, and because some evidence of such extensive fractionation such as a change in europium anomaly might

be expected, the preferred explanation is that samples 15C and 15A crystallized later than samples 11 and 13 and that fluid carrying most of the components of the accessory minerals was lost from samples 15C and 15A to the vein-dike system in the interim. This is consistent with the low accessory mineral content of sample 15C and the virtual absence of accessory minerals other than zircon and fluorite in the thin section of sample 15A. The relatively large size of the relict amphibole phenocrysts in sample 15A might indicate the presence of a second fluid phase or vapor at this stage. It is also consistent with Thompson's (1988) identification of post-devolatilization granites. However, the europium anomaly data suggest that the entire process may have taken place at the same stage of feldspar fractionation and presumably with a single depressurization event. Inasmuch as both the aegirine-granite sample 11 and the amphibole-rich granite sample 13 appear to have formed prior to volatile loss based on their trace element abundances, the devolatilization may not have taken place exactly at a change-over from aegirine to amphibole crystallization as suggested by Thompson (1988).

The unusual abundance and mobility of zirconium and other elements in the Bokan Mountain stock granites and vein dikes is an extreme example of phenomena that are common in alkalic systems. Excess sodium in melts is known to suppress crystallization of zirconium-bearing minerals and hence to lead to zirconium enrichment in melts (Dietrich, 1968). Similarly the presence of fluorine is known to dramatically increase the solubility of zirconium and niobium in experimental granite melts (Keppler, 1991). Rubin and others (1993) claim that zirconium in alkalic rocks occurs mostly in aegirine and amphibole where it is more readily extracted by hydrothermal fluids. Alkaline magma similar to that at Bokan Mountain is frequently saturated with a diversity of fluid phases that are known to transport typically immobile elements such as zirconium and the REE (e.g. Belkin and others, 1996).

One of the more interesting petrogenetic questions at Bokan Mountain is whether the vein dikes are of igneous or hydrothermal origin. Only the Geoduck vein-dike sample 6 appears to have a distinctly non-igneous composition with 84.5 percent silica (Table 1) and 72 percent normative quartz (Table 2). All of the other Bokan Mountain stock granite and vein-dike samples range in composition from 75.3 to 65.6 percent silica. Of these, however, upper Dotson vein-dike sample 17 with 47 percent normative quartz also appears to be outside the range for normal siliceous granites, and sample 15A with 41 percent normative quartz is perhaps borderline. As mentioned above, some vein dikes were noted in the field to have silica cores. This is one of the reasons for using the term "vein" in their appellation. Such high-silica material might normally be considered to be of hydrothermal origin. The occurrence of this material in the vein dikes opens the possibility that the samples with high silica values or excessive normative quartz might be hydrothermal, at least in part, and possibly the other samples as well. The almost pure compositions of the potassium feldspar and albite revealed by the microprobe analyses indicate low-temperature crystallization whether from a volatile-rich melt or an aqueous fluid.

It is noted that the high silica Geoduck vein-dike sample 6 is a fine-grained aplite. Aplites are not uncommon in general association with pegmatite. They are often interpreted as igneous rocks formed, perhaps, by depressurization quenching of a previously volatile-rich melt. Pegmatite may form from volatile-rich melt, hydrothermal fluid, or

vapor. Upper Dotson vein-dike sample 17, with 47 percent quartz in the norm and modal potassium feldspar phenocrysts up to several millimeters across, might constitute (micro-) pegmatite. Mechanisms can be visualized for producing high silica rocks via igneous processes. Accumulation of quartz phenocrysts is one possibility. Assimilation of siliceous material by magma might also result in excess silica. Of particular relevance for the present suite of samples is the process of liquid immiscibility. Immiscibility is a well-known process in igneous differentiation and is particularly common in alkaline rocks (Philpotts, 1990). Several of the vein-dike samples, as discussed above, have textures that are indicative of liquid immiscibility. It was suggested that middle Dotson vein-dike sample 19-5 might have consisted at one time of three immiscible liquids in association with crystalline phases. One of these was a high-silica liquid and this might argue for reconsideration of the origin of high silica cores in vein dikes. The high volatile contents that may be indicated by some microprobe analyses of silica phases would tend to keep siliceous melts fluid at lower temperatures. In addition, the occurrence of round inclusions of barite and of fluorite, both with small shrinkage bubbles, indicates the presence of other fluid phases in the system. The high volatile content of the magma that is indicated by the abundance of fluid inclusions and by the occurrence of carbonates, hydroxides, and fluorite, perhaps offers other means of enriching silica by magmatic processes. Streaming of fluorine in particular might be expected to provide a strong solvent and possible enricher of silica (and zirconium) in late stage melts. Given the igneous aspect of the samples, including the typical occurrence of mineralization as scattered pockets rather than veins, mechanisms other than hydrothermal activity may have been responsible for enriching silica in these rocks. At the same time there is ample evidence for hydrothermal processes. We interpret the monomineralic filigrees of aegirine, zircon, iron oxide, and other phases observed at grain boundaries in the samples and the volume for volume replacements by albite, bastnaesite, and other minerals as being of hydrothermal origin. The extensive enrichment of trace elements, such as the more than twenty-five-fold enrichment of zirconium in going from the granites to vein-dike sample 19-5 (Fig. 3), would seem improbable in bulk crystallizing magma and appears to imply enrichment by partitioning into a solid, fluid, or vapor phase. It may be highly significant that the largest general compositional differences between the vein dikes and the border granites appears to be the increased abundances of calcium, zirconium, yttrium, and carbonate, and these also appear to be the major components determined by the petrography of the minerals in the prismatic phenocrysts and putative immiscible globules in samples such as 19-5 and 19-6 from the middle Dotson vein dike. Given the occurrence of this mineralization in both phenocryst and globule forms, an origin via crystal accumulation and subsequent remelting cannot be ruled out.

It is interesting to speculate whether the sodic metasomatism at Bokan Mountain (and other alkalic complexes) might be related to a release of sodium associated with the change in the nature of the iron-bearing minerals noted above from sodium-iron silicates to oxides. One of the characteristic features of the Bokan Mountain uranium mineralization is its association with abundant iron oxide and hydroxide. This abundance of late-stage iron minerals might be a complement to the widespread albitic metasomatism, with both perhaps relating ultimately to destabilization and breakdown of sodium-iron

silicates. This process would also appear to offer a mechanism for generating iron-rich skarns which are common on Prince of Wales Island.

We have evaluated the chemical data for Bokan Mountain rocks in terms of a wide variety of petrogenetic and tectonic discriminants. These all give essentially the same results. The Bokan Mountain granites (e.g. 11, 13, 15C), as pointed out by many previous workers, fall into the peralkaline field (molar $Na_2O+K_2O>Al_2O_3$) of the Shand index. According to the discriminant criteria offered recently by Maniar & Piccoli (1989), Bokan Mountain stock granites 11, 13, and 15C are anorogenic, with the relatively low titanium somewhat favoring a central epeirogenic uplift granitoid (like the Nigerian granitoids) over a rift-related granitoid (like the Oslo granitoids). By their criteria, Bokan Mountain country rock sample 8 appears to represent a metaluminous island arc or continental arc granitoid. Sample 8 is close in composition to the "I-type" (igneous protolith) granitoids of Whalen and others (1987), with some of the trace elements (Zr, Nb, Y, Ce) tending towards "M-type" (melting of subducted oceanic crust or overlying mantle). Granites 11, 13, and 15C fit well into their "A-type" (anorogenic or alkaline) granites. Specific characteristics include gallium/aluminum of 7 - 8 x 10^{-4} and sum of alkalies of about nine. Gallium/aluminum ratios are given in Table 1; they reach quite extraordinary levels in these rocks (almost $15x10^{-4}$ in Geoduck vein-dike sample 6). A-type granites, in general, are characterized by relatively high abundances of silica, iron, alkalies, gallium, niobium, yttrium, zirconium, zinc, and REE; relatively low abundances of aluminum, magnesium, calcium, and vanadium; and sizable negative europium anomalies. Clearly the Bokan Mountain stock granites fit all of these criteria very well (Table 1). However, it is worth noting that Whalen and others (1987) conclude that this designation may not be highly significant in terms of tectonic classification inasmuch as A-type granites can occur "in a variety of tectonic settings and do not necessarily indicate an anorogenic or rifting environment."

CONCLUSIONS AND PETROGENETIC MODEL

The neodymium isotope data indicate depleted sources (i.e. Sm/Nd > chondritic) for the Bokan Mountain stock granites and vein dikes. The magma may therefore have arisen in the mantle as a plume or subduction zone melt or by melting of the depleted (mantle derived) crust that characterizes the Alexander terrane. There is some support for the idea that A-type granites form from residues remaining in the lower crust after extraction of orogenic granites (Whalen and others, 1987) which might favor a subduction zone setting. The timing of the fusion event that produced the Bokan Mountain stock might be related to initial juxtaposition of the Alexander terrane with North America.

The magma, once formed, underwent extensive crustal fractional crystallization involving feldspar as manifested by the sizable negative europium anomaly in the REE abundance patterns of the granites and vein dikes. This differentiation would have modified the chemistry of the magma and possibly, via contamination, the isotopic ratios. The appropriate source and the extensive fractionation led to enrichment of yttrium, zirconium, hafnium, REE, niobium, uranium, thorium, and other elements, to anomalously high but subeconomic levels. The step that concentrated these elements to ore levels was the formation of the vein dikes. Thompson (1988) has made a persuasive case that emplacement of the vein dikes was associated with caldera collapse.

It is unlikely that the vein dikes simply represent further fractional crystallization of granitic magma. There is no evidence of the extensive suite of intermediate rocks that would have had to crystallize in order to effect the substantial enrichment of many elements observed in the vein dikes. Further, the very similar size of the europium anomalies in the Bokan Mountain granites and in the vein dikes argues that these rocks are essentially at the same stage in terms of feldspar crystallization. It appears likely that the enrichments were effected by favorable partitioning of these elements into separating solid, fluid, or vapor phases that were concentrated in the formation of the vein dikes.

If Thompson (1988) is correct that the vein dikes are associated with venting of the magma chamber, they could have formed from fluids or vapor released from the magma by depressurization of the system. There is evidence of hydrothermal activity in the vein dikes. The quartz cores occurring in some of them might be hydrothermal. The low temperatures that Thompson (1988) reports for some of the mineralization are certainly more akin to hydrothermal temperatures than typical magmatic temperatures. Similarly the grain-boundary filigrees of aegirine, zircon, bastnaesite, and other phases appear to be hydrothermal, as well as the replacement of potassium feldspar phenocrysts by albite, bastnaesite, and other minerals. This system was rich in volatiles and there appears to be ample evidence of late-stage deuteric and hydrothermal processes.

Standing in opposition to the interpretation that the vein dikes are hydrothermal, or at least totally hydrothermal, is the petrography of the samples which shows polymineralic assemblages and textures that appear to be igneous. The apparent occurrence of up to three immiscible melts further supports an igneous origin. One model that might reconcile the attractive concept of depressurization hydrothermal mineralization with seemingly igneous features of the rocks, would involve depressurization immiscibility. Loss of volatile fluxes from the magma during venting may have resulted in liquid immiscibility with the more mobile (and trace element-rich) melt(s) finding readier egress from the system via the vein dikes. This material may have quenched in the vein dikes which show evidence of continued immiscibility in terms of globules and distributed areas of mineralization. The vein dikes appear to be products of both magmatic processes and subsequent hydrothermal activity.

The wide diversity and complex mineralogy of the yttrium-, REE-, and zirconium-bearing phases in these rocks is of scientific interest. It might also be of interest in considerations of possible beneficiation. However, it appears unlikely that many of the analyzed yttrium-, REE-, and zirconium-bearing minerals had much effect on the course of the enrichment inasmuch as they generally occur as fine-grained quench products or as late stage replacements. This conclusion is consistent with the rather restricted range in relative REE abundance patterns of the whole-rocks compared to the wide range of patterns manifested by the minerals themselves. While this study shows that enrichment of yttrium, REE, zirconium, and niobium can occur in samples of relatively low radioactivity, the generally radioactive nature of the vein dikes coupled with their quenched nature provide little evidence favoring larger bodies of non-radioactive material in the vicinity of Bokan Mountain. The small widths of the vein dikes lessens their likely value as potential resources unless peculiarly attractive beneficiation properties could be identified.

Acknowledgments.-We thank Jim Barker of Interior Development, Fairbanks, Alaska, and R."Red" Dotson, resident on the claim at the time of our visit. Their local knowledge and assistance with the logistics were of inestimable help in the collection of samples and in the appreciation of the geological context. We also thank Gary McWilliams, Captain of the research vessel HYAK, for providing efficient, cost-effective transportation and for mineralogic insights; and Holly Hughes for board. Finally we thank our former colleagues Marta Flohr, Carter Hearn, and Mac Ross for useful in-house reviews of the manuscript.

REFERENCES CITED

Afifi, A.M., and Essene, E.J., 1988, MINFILE: a computer program for storage and manipulation of chemical data on minerals: American Mineralogist, v. 73, p. 446-448.

Ansell, H.G., Roberts, A.C., Plant, A.G., and Sturman, B.D., 1980, Gittinsite, a new calcium zirconium silicate from the Kipawa agpaitic syenite complex, Quebec: Canadian Mineralogist, v. 18, p. 201-203.

Armstrong, R.L., 1985, Rb-Sr dating of the Bokan Mountain granite complex and its country rocks: Canadian Journal of Earth Sciences, v. 22, p. 1233-1236.

Baedecker, P.A., ed., 1987, Methods for geochemical analysis: U.S. Geological Survey Bulletin 1770, 151 p.

Barker, J.C., and Mardock, C.L., 1988, Lithophile metal, REE-Y-Nb deposits on southern Prince of Wales Island, Alaska, in Carson, D.J.T., and Vassiliou, A.H., eds., Process mineralogy VIII: The Minerals, Metals, and Materials Society, p. 139-157.

Bazard, D.R., Butler, R., Gehrels, G.E., and Soja, C.M., 1994 New constraints for Late Silurian-Devonian paleogeography of the Alexander terrane, southeastern Alaska: Geological Society of America Abstracts with Programs, v. 26, no. 7, p. A-384.

Belkin, H.E., De Vivo, B., Lima, A., and Torok, K.,1996, Magmatic (silicates/saline/sulfur-rich/CO_2) immiscibility and zirconium and rare-earth element enrichment from alkaline magma chamber margins: evidence from Ponza Island, Pontine Archipelago, Italy: European Journal of Mineralogy, v. 8, p.1401-1420.

Berg, H.C., Jones, D.L., and Richter, D.H., 1972, Gravina-Nutzotin belt: Tectonic significance of an Upper Mesozoic sedimentary and volcanic sequence in southern and southeastern Alaska: U.S. Geological Survey Professional Paper 800-D, p. D1-D24.

Berg, H.C., Jones, D.L., and Coney, P.J., 1978 Map showing pre-Cenozoic tectono-stratigraphic terranes of southeastern Alaska and adjacent areas: U.S. Geological Survey Open-File Report 78-1085, 2 sheets, scale 1:1,000,000.

Churkin, Michael, Jr., and Eberlein, D.G., 1977 Ancient borderland terranes of the North American Cordillera: correlation and microplate tectonics: Geological Society of America Bulletin, v. 88, p. 769-786.

De Saint-Andre, B., Lancelot, J.R., and Collot, B., 1983, U-Pb geochronology of the Bokan Mountain peralkaline granite, southeastern Alaska: Canadian Journal of Earth Sciences, v. 20, p. 236-245.

Dietrich, R.V., 1968, Behavior of zirconium in certain artificial magmas under diverse P-

T conditions: Lithos v. 1, p. 20-29.
Erd, R.C., Csamanske, G.K., and Meyer, C.E., 1983, Taeniolite, an uncommon lithium-mica from Coyote Peak, Humbolt County, California: The Mineralogical Record, Jan-Feb, p. 39-40.
Gehrels, G.E., 1992, Geologic map of the southern Prince of Wales Island, southeastern Alaska: U.S. Geological Survey Miscellaneous Investigations Map I-2169, scale 1:63,360.
Gehrels, G.E., and Berg, H.C., 1994, Geology of southeastern Alaska, in Plafker, G., and Berg, H.C., eds., The Geology of Alaska: Boulder, Colorado, Geological Society of America, The Geology of North America, v. G-1, p. 451-467.
Gehrels, G.E., Dickinson, W.R., Ross, G.M., Stewart, J.H., and Howell, D.G., 1994, Provenance of detrital zircons in strata of the Cordilleran miogeocline and selected outboard terranes: Geological Society of America Abstracts with Programs, v. 26., no. 7, p. A-384.
Gehrels, G.E., and Saleeby, J.B., 1987, Geologic framework, tectonic evolution and displacement history of the Alexander terrane: Tectonics, v. 6, p.151-173.
Haeussler, P.P., Coe, R.S., and Onstott, T.C., 1992, Paleomagnetism of the Late Triassic Hound Island volcanics: revisited: Journal of Geophysical Research, v. 97, p. 19,617-19,639.
Hillhouse, J.W., 1977, Paleomagnetism of the Triassic Nikolai Greenstone, McCarthy quadrangle, Alaska: Canadian Journal of Earth Sciences, v. 14, p. 2,578-2,592.
Hillhouse, J.W., and Gromme, C.S., 1984, Paleomagnetism of the Triassic Hound Island volcanics, Alexander terrane, southeastern Alaska: Journal of Geophysical Research, v. 85, p. 2,591-2,602.
Keppler, H., 1991, Influence of fluorine on the solubility of high field strength trace elements in granite melts: EOS, Transactions of the American Geophysical Union, Fall Meeting Program with Abstracts, v. 72, p. 532-533.
Kovalenko, V.I., Tsaryeva, G.M., Goreglyad, A.V., Yarmolyuk, V.V., Troitsky, V.A., Hervig, R.L., and Farmer, G.L., 1995, The peralkaline granite-related Khaldzan-Buregtey rare metal (Zr, Nb, REE) deposit, western Mongolia: Economic Geology, v. 90, p. 530-547.
Lanphere, M.A., McKevett, E.M., Jr., and Stern, T.W., 1964, Potassium-argon and lead-alpha ages of plutonic rocks, Bokan Mountain area, Alaska: Science, v. 145, p. 705-707.
Lugmair, G.W., Marti, K., Kurtz, J.P., and Scheinin, N.B., 1976, History and genesis of lunar troctolite 76535 or: How old is old?: p.2009-2033 in Proc.Lunar.Sci.Conf.7th, Pergamon Press, New York.
MacKevett, E.M., Jr., 1963, Geology and ore deposits of the Bokan Mountain uranium-thorium area, southeastern Alaska: U.S. Geological Survey Bulletin 1154, 125 p.
Maniar, P.D., and Piccoli, P.M., 1989, Tectonic discrimination of granitoids, Geological Society of America Bulletin, v. 101, p. 635-643.
McClelland, W.C., and Gehrels, G.E., 1990, Geology of the Duncan Canal shear zone: Evidence for Early to Middle Jurassic deformation of the Alexander terrane, southeastern Alaska: Geological Society of America Bulletin, v. 102, p. 1378-1392.

Miser, H.D., and Stevens, R.E., 1938, Taeniolite from Magnet Cove, Arkansas: American Mineralogist, v. 23, p. 104-110.
Olson, J.C., Shawe, D.R., Pray, L.C., and Sharp, W.N., 1954, Rare-earth mineral deposits of the Mountain Pass District, San Bernardino County, California: U.S. Geological Survey Professional Paper 261, 75 p.
Philpotts, A.R., 1990, Principles of Igneous and Metamorphic Petrology, Prentice Hall, New Jersey, 498 p.
Philpotts, J.A., 1970, Redox estimation from a calculation of Eu^{2+} and Eu^{3+} concentrations in natural phases: Earth and Planetary Science Letters, v. 9, no. 3, p. 257-268.
Philpotts, J.A., and Schnetzler C. C., 1968, Genesis of continental diabases and oceanic tholeiites considered in light of rare-earth and barium abundances and partition coefficients, in Ahrens, L. H., ed., Origin and distribution of the elements: Oxford, England, Pergamon Press, p. 939-947.
Philpotts, J.A., Schnetzler, C. C., and Hart, S. R., 1969, Submarine basalts: Some K, Rb, Sr, Ba, and rare-earth data bearing on their alteration, modification by plagioclase and possible source materials: Earth and Planetary Science Letters, v. 7, p. 293-296.
Philpotts, J.A., Tatsumoto, M., Li, X., and Wang, K., 1991, Some Nd and Sr isotopic systematics for the rare earth deposit at Bayan Obo, China: Chemical Geology, v. 90, p. 177-188.
Roelofsen-Ahl, J.N., and Peterson, R.C., 1989, Gittinsite: A modification of the thortveitite structure: Canadian Mineralogist, v. 27, p. 703-708.
Ross, Malcom, 1984, Ultra-alkalic arfvedsonite and associated richterite, acmite, and aegirine-augite in quartz syenite, Magnet Cove igneous Complex, Arkansas: (abs) EOS, Transactions, American Geophysical Union, v. 65, p. 293.
Rubin, J.N., Henry, C.D., and Price, J.G., 1993, The mobility of zirconium and other "immobile" elements during hydrothermal alteration: Chemical Geology v. 110, p. 29-47.
Saleeby, J.B., 1994, Tectonic history of the Insular Suture Zone of southeastern Alaska: Geological Society of America Abstracts with Programs, v. 26, n. 7, p. A-384.
Samson, S.D., McClelland, W.C., Patchett, P.J., Gehrels, G.E., and Anderson, R.G., 1989, Evidence from neodymium isotopes for mantle contributions to Phanerozoic crustal genesis in the Canadian Cordillera: Nature, v. 337, p. 705-709.
Savage, N.M., 1994, Terrane affinities of the Middle and Late Devonian conodonts from the Wadleigh limestone, southeastern Alaska: Geological Society of America Abstracts with Programs, v. 26, no. 7, p. A-384.
Staatz, M.H., 1978, I and L uranium and thorium vein system, Bokan Mountain, southeastern Alaska: Economic Geology, v. 73, p. 512-523.
Thompson, T.B., 1988, Geology and uranium-thorium mineral deposits of the Bokan Mountain Granite Complex, southeastern Alaska: Ore Geology Reviews, v. 3, p. 193-210.
Thompson, T.B., Pierson, J.R., and Lyttle, T., 1982, Petrology and petrogenesis of the Bokan Granite Complex, southeastern Alaska: Geological Society of America

Bulletin, v. 93, p. 898-908.
Warner, J.D., and Barker, J.C., 1989, Columbium- and rare earth element-bearing deposits at Bokan Mountain, southeast Alaska: U.S. Bureau of Mines Open File Report 33-89, 196 p.
Warner, J.D., and Mardock, C.L., 1987, Rare earth element-, niobium-, thorium-, and uranium-bearing dikes at Bokan Mountain, southeast Alaska [abs]: Geological Society of America Abstracts with Programs, v. 19, no. 6, p. 461.
Whalen, J.B., Currie, K.L., and Chappell, B.W., 1987, A-type granites: geochemical characteristics, discrimination and petrogenesis: Contrib.Mineral.Petrol., v. 95, p. 407-419.
Wones , D.R., and Gilbert, M.C., 1982, Amphiboles in the igneous environment: Chap 3 in Amphiboles, Veblen, D.R., and Ribbe, P.H., eds., Reviews in Mineralogy, v. 9B, Mineralogical Society of America, Washington, D.C., 390 pp.

Table 1: Chemical composition of rock samples (major/minor elements in wt.%, trace elements in ppm by wt.).

location:	Country rock	Geoduck	Country rock	Country rock	S.E. Stock	S.E. Stock	Border zone
rock type:	meta-basalt	Q Ab aplite	meta-bslt dike	granodiorite	aeg. granite	amph. granite	flt.gran.porph
sample #:	APP-91-5	APP-91-6	APP-91-7	APP-91-8	APP-91-11	APP-91-13	APP-91-15A
SiO2	52.4	84.5	43.8	67.7	74.0	74.2	71.8
TiO2	0.85	0.32	1.38	0.35	0.18	0.19	0.27
Al2O3	16.1	4.44	16.4	15.9	10.9	10.6	9.02
Fe2O3	3.3	2.69	2.4	1.4	3.62	2.9	8.5
FeO	5.8	0.64	8.4	1.2	0.44	1.3	2.8
MgO	6.38	0.15	8.98	1.25	0.02	0.02	0.01
CaO	7.97	0.36	10.3	3.63	0.02	0.04	0.03
Na2O	4.13	2.28	1.59	4.78	4.64	4.95	4.02
K2O	0.71	0.15	0.35	1.93	4.77	4.12	1.95
P2O5	0.14	0.02	0.11	0.11			
MnO	0.22	0.18	0.18	0.07	0.06	0.10	0.02
H2O+	1.9	0.3	4.4	1.3	0.2	0.13	0.39
H2O-	0.05	0.20	0.12	0.04	0.07	0.04	0.17
CO2	0.04	0.02	2.10	0.14			0.01
F	0.07	0.05	0.08	0.07	0.06	0.11	0.03
Cl	0.019		0.009	0.030	0.005		
O (F, Cl, S)	0.03	0.02	0.06	0.04	0.03	0.05	0.07
sum	100.1	96.3	100.5	99.8	99.0	98.6	99.1
As				1.2		2	1.2
Ba	200	35	240	1100	24	34	19
Be		130			6	8	5
Co	29.0	1.6	59	6.9	0.11	0.12	0.16
Cr	170	12	150	19		3	3
Cs	0.4	0.3	0.2	0.12	0.97	0.77	0.60
Cu	6	16	87	23		2	1
Ga	18	35	19	18	40	40	42
Hf	1.9	105	2.4	2.5	32	11.5	43.7
Li	5	2	13		88	120	2
Mo		6.4			1.5	2.2	1.2
Nb	1.9	2100	1.9	1.8	51	130	32
Ni	48	3	140	10			
Pb		130		6	25	23	16
Rb	27.5	16	13	37	250	230	82
Sb	0.35	8.3	0.13	0.15	0.10	0.24	0.15
Sc	36.0	0.75	33.6	5.2	0.35	0.33	0.18
Sn		82			10	11	
Sr	380	76	300	840	2	6	3
Ta	0.16	112	0.16	0.17	4.2	9.9	2.7
Th	1.71	217	0.21	3.86	19.5	137	12.3
U	0.63	141		1.26	7.2	11.6	8.04
V	270	11	220	52			4
Y	23	2100	23	5	19	70	40
Zn	108	220	107	28	235	320	140
Zr		5600	110	90	1100	390	1600
La	9.0	1200	2.9	17.4	200	290	20
Ce	19.6	2420	9.1	31	390	620	44
Nd	11	780	9.8	12	170	240	22
Sm	3.1	237	3.4	2.3	21	48	6.5
Eu	1.04	22.6	1.2	0.63	1.1	3.2	0.66
Tb	0.63	51.3	0.72	0.21	0.89	3.6	1.62
Ho	0.75	140	1.4				4
Yb	2.5	190	2.6	0.65	17.3	16.6	16
Lu	0.36	22.2	0.37	0.085	2.8	2.3	2.67
Eu/Eu*	0.95	0.26	0.97	1.01	0.25	0.26	0.27
RE2O3 %	0.007	0.70	0.005	0.008	0.10	0.16	0.018
10000Ga/Al	2.1	15	2.2	2.1	6.9	7.1	8.8

Table 1 (continued)

location:	Border zone	U. Dotson	M. Dotson	M. Dotson	L. Dotson	L. Dotson	E. Dotson
rock type:	float granite	QF pegmatite	QF pegmatite	QF pegmatite	Ab granite	QF pegmatite	Q Ab aplite
sample #:	APP-91-15C	APP-91-17	APP-91-19-5	APP-91-19-6	APP-91-21A	APP-91-21B	APP-91-23
SiO2	75.2	74.1	69.0	69.5	75.3	65.0	65.6
TiO2	0.19	0.27	0.52	0.40	0.20	0.14	0.36
Al2O3	10.5	8.15	5.50	7.72	12.3	11.1	13.0
Fe2O3	2.3	3.8	8.02	5.11	0.62	0.87	2.51
FeO	1.9	1.9	0.56	0.56	0.68	0.28	0.12
MgO	0.03	0.15	0.11	0.10	0.45	0.13	1.22
CaO	0.04	0.01	2.78	2.83	0.87	0.47	2.60
Na2O	5.07	2.64	4.57	4.54	7.01	1.28	8.48
K2O	3.37	3.18	2.19	2.33	0.36	7.94	0.71
P2O5					0.01	0.07	0.09
MnO	0.10	0.06	0.18	0.23	0.08	0.08	0.49
H2O+	0.24	0.29	0.18	0.18	0.17	0.13	0.06
H2O-	0.04	0.02	0.04	0.06		0.04	0.02
CO2		0.02	0.18	0.16	0.41	0.53	1.10
F	0.15	0.04	0.06	0.08	0.38	0.34	0.28
Cl		0.004	0.011	0.013	0.005	0.005	
O (F, Cl, S)	0.06	0.02	0.03	0.04	0.16	0.14	0.12
sum	99.1	94.6	93.9	93.8	98.7	88.3	96.5
As	2						
Ba	34	79	53	57	90	150	96
Be	7	30	25	24	7	49	120
Co	0.14	0.56	0.4	0.3	1.4		4.9
Cr	1.7	7		19	5		3
Cs	1.0	0.65	0.55	0.60	0.56	2.0	0.55
Cu	1	1	2	10	3	19	19
Ga	41	44	28	42	19	45	31
Hf	25	430	537	420	11.2	290	9.8
Li	160	9	11	10	60	4	510
Mo	2.5	1.7		1.8		1.8	4.7
Nb	60	77	69	600	100	630	1700
Ni			2		4	3	5
Pb	18	44	400	1000	130	200	2300
Rb	180	290	260	310	41	740	150
Sb	0.22	2.4	1.9	2.0	0.18	1.3	0.9
Sc	0.34	1.9	1.67	1.16	3.3	1.8	3.5
Sn			120	110			24
Sr	5	5	15	50	58	40	200
Ta	4.4	10.4	7.2	57.3	14.5	48	113
Th	28.4	86	30	116	48	490	41
U	6.1	64	95	98	19.4	148	95
V		8	3		4		44
Y	28	140	1800	2200	530	18000	380
Zn	280	170	620	610	310	220	1600
Zr	920	19000	24000	19000	450	15000	330
La	26	102	41	540	230	3200	1140
Ce	56	270	78	1130	390	5900	1950
Nd	20	110	60	530	150	2450	710
Sm	4.5	33	28	186	47	770	198
Eu	0.40	4.3	4.9	18.7	4.85	79	16.4
Tb	0.94	18	24.6	49.6	13.8	295	19.6
Ho	2.6	60	90	110	20	500	
Yb	14	335	490	390	52	1360	12.2
Lu	2.28	46	67	52.6	5.6	153	0.99
Eu/Eu*	0.25	0.26	0.30	0.26	0.26	0.23	0.30
RE2O3 %	0.018	0.17	0.19	0.49	0.14	2.4	0.53
10000Ga/Al	7.4	10	9.6	10	2.9	7.7	4.5

(footnote Table 1)

Additional determinations: total S, #7, 0.05%, #15A, 0.11%; Au, #15A, 0.019 ppm; Cd, #23, 9 ppm; Se, #7, 1.84 ppm; W, #21B, 3.8 ppm. Analysts: Phil Baedecker, Paul Briggs, Mike Doughten, David Fey, Judy Gillison, Mal Kavulak, John Marinenko, Jim Mee, Dave Siems, and Carol Skeen. Meta-bslt = meta-basalt; aeg.= aegirine; amph.= amphibole; flt.gran.porph.= float granite porphyry; F = feldspar. Blank values in the tables indicate that a component was not detected or was determined with insufficient precision. A dash ("-") indicates that no determination was attempted.

Table 2: Normative Mineralogy

sample:	APP-91-5	APP-91-6	APP-91-7	APP-91-8	APP-91-11	APP-91-13	APP-91-15A
cb	0.09	0.05	4.81	0.31			0.02
ap	0.33	0.06	0.28	0.28			
cm	0.04	0.00	0.03	0.00		0.00	0.00
il	1.65	0.63	2.72	0.67	0.35	0.37	0.52
fr	0.12	0.10	0.15	0.12	0.12	0.23	0.06
Z		1.16	0.02	0.02	0.23	0.08	0.33
or	4.27	0.92	2.15	11.58	28.51	24.70	11.67
ab	35.60	19.98	14.00	41.07	29.85	32.04	34.45
ac					8.69	8.50	
ns						0.19	
an	23.76	1.27	38.06	16.40			
C		0.08			0.13	0.23	0.34
mt	4.85	1.76	3.56	2.01	0.95		8.40
hm		1.57					2.66
di	12.14	-0.00	5.50	0.19		0.00	
wo			0.00				
hy	16.60	0.37	25.14	3.53	0.13	2.33	0.02
Q		72.04		23.79	31.36	31.91	41.40
ol	0.53		3.43				
py			0.10				0.21
normative feldspar mole fractions:							
X_an	0.36	0.05	0.69	0.23	0.00	0.00	0.00
X_ab	0.57	0.91	0.27	0.61	0.52	0.58	0.76
X_or	0.06	0.04	0.04	0.16	0.48	0.43	0.24

Table 2 (continued)

APP-91-15C	APP-91-17	APP-91-19-5	APP-91-19-6	APP-91-21A	APP-91-21B	APP-91-23	sample
	0.05	0.41	0.37	0.91	1.29	2.51	carbonate
				0.03	0.18	0.22	apatite
0.00	0.00		0.00	0.00		0.00	chromite
0.36	0.53	1.02	0.79	0.38	0.29	0.71	ilmenite
0.31	0.08	0.13	0.17	0.79	0.76	0.58	fluorite
0.19	3.89	5.06	4.05	0.09	3.29	0.07	zircon
20.11	19.40	13.35	14.32	2.15	52.01	4.34	orthoclase
35.59	23.06	16.60	27.80	60.07	12.00	65.13	albite
6.81		20.51	10.70			7.51	acmite
						0.15	sodium silicate
			0.00	0.16		0.00	anorthite
0.33	0.49			0.32	1.35		corundum
0.03	5.70	0.77	1.32	0.92	0.38		magnetite
	0.01	0.65	0.71		0.70		hematite
	0.00	0.29	0.27			4.91	diopside
		5.35	5.48		0.13	0.33	wollastonite
3.46	0.37			1.17			hypersthene
33.65	46.71	35.85	34.01	32.82	30.17	13.44	quartz
							olivine
							pyrite
	mole fractions:						
0.00	0.00	0.00	0.00	0.00	0.00	0.00	X_anorthite
0.66	0.55	0.57	0.67	0.96	0.19	0.94	X_albite
0.35	0.45	0.43	0.33	0.03	0.81	0.06	X_orthoclase

Table 3: Inter-element correlation coefficients (negative above diagonal) for granite and vein dike samples.

	Ti	Al	Fe +2	Mg	Ca	Na	K	P	Mn	LOI	CO2	F	Cl	As	Ba	Be	Co	Cr	Cs	Cu
Al																				
Fe +2								(4).999												
Ca	0.812																			
Mn				0.832	0.741															
LOI				0.740										(3)1.00						
H2O+			0.764																	
CO2				0.911					0.755	0.910										
Cl					(6).967				(6).993											
As		(3).999																		
Ba										0.741		0.798								
Co				0.970					0.863		0.843					0.758				
Cs							0.917													
Cu										0.842						0.822				
Ga																				
Hf																				
Li				0.846		0.753			0.781								0.823			
Mo																(9).913				
Nb																0.972				0.841
Pb				0.862	0.748				0.956		0.826						0.843			
Rb							0.884												0.875	
Sc				0.812							0.816									
Sr				0.936					0.903	0.800	0.872					0.784	0.968			0.751
Ta									0.759							0.946	0.749			0.893
Th															0.748					
U																				0.825
V				(6).922					(6).928								(6).963			
Y															0.818			(8).915	0.845	
Zn				0.872	0.752				0.958		0.815		(6).971				0.846			
Zr																				
La										0.741					0.853					0.837
Ce															0.833					0.837
Nd															0.844					0.799
Sm															0.836					0.792
Eu															0.833				0.745	0.761
Tb															0.828			(8).901	0.817	
Ho										(8).850										(8).838
Yb																		(8).847	0.739	
Lu																				

Numbers of samples for correlations involving less than all eleven samples are given in parentheses. Diagonal is marked by black cells. LOI is "loss on ignition".

Table 3 (continued)

	Hf	Li	Mo	Nb	Pb	Rb	Sb	Sn	Sr	Th	U	Y	La	Ce	Nd	Sm	Eu	Tb	Ho	Yb
Al							0.743													
Fe +2																				
Ca																				
Mn																				
LOI																				
H2O+																				
CO2																				
Cl																				
As																				
Ba																				
Co																				
Cs																				
Cu																				
Ga			(9).813																	
Hf																				
Li																				
Mo																				
Nb			0.929																	
Pb		0.788																		
Rb																				
Sc																				
Sr		0.767		0.776	0.888															
Ta		0.852	(9).852	0.980					0.841											
Th																				
U																				
V		(6).968			(6).959				(6).938											
Y						0.848		(6).945		0.923										
Zn		0.847			0.969				0.856											
Zr	0.998							(6).927												
La										0.920		0.916								
Ce										0.934	0.745	0.914	0.999							
Nd						0.746				0.938		0.944	0.995	0.994						
Sm						0.754				0.941		0.954	0.988	0.989	0.997					
Eu						0.774				0.945	0.738	0.969	0.978	0.979	0.992	0.998				
Tb						0.836				0.940		0.996	0.936	0.936	0.961	0.971	0.983			
Ho						(8).850				(8).973		(8).981	(8).975	(8).971	(8).984	(8).986	(8).990	(8).990		
Yb						0.884		(6).968		0.848		0.939	0.793	0.795	0.837	0.861	0.890	0.938	(8).953	
Lu						0.876		(6).955		0.809		0.904	0.744	0.747	0.792	0.819	0.852	0.903	(8).926	0.996

Table 4a: Mineral compositions (determined by electron microprobe analysis).

mineral:	Potassium feldspar	Albite	Silica
sample:	11,15C,15A	11,13,15C,15A	11,15A,19-5
run #:	a	a	a,l
n:	18	9	8
wt %			
SiO2	64.97 ± 1.26	69.97 ± 2.64	96.22 ± 2.43
Al2O3	18.43 ± 0.35	19.42 ± 0.34	0.14 ± 0.13
Fe2O3 t	0.42 ± 0.38	0.91 ± 0.89	0.05 ± 0.03
Na2O	0.30 ± 0.05	10.36 ± 0.98	0.02 ± 0.02
K2O	15.45 ± 0.17	0.05 ± 0.04	0.09 ± 0.08
BaO	0.02 ± 0.02	0.03 ± 0.03	0.04 ± 0.04
total	99.66 ± 1.30	100.40 ± 1.60	96.54 ± 2.24
cations per	8 oxygen equivalents	8 oxygen equivalents	16 oxygen equivalents
Si	3.007 ± 0.016	3.028 ± 0.041	7.985 ± 0.012
Al	0.996 ± 0.018	0.985 ± 0.020	0.013 ± 0.013
Fe 3+	0.015 ± 0.013	0.029 ± 0.029	0.003 ± 0.002
Na	0.027 ± 0.005	0.872 ± 0.104	0.003 ± 0.003
K	0.916 ± 0.020	0.002 ± 0.002	0.009 ± 0.009
Ba	0.000 ± 0.000	0.001 ± 0.001	0.001 ± 0.001
total	4.964 ± 0.017	4.912 ± 0.089	8.013 ± 0.010
X Ab	0.03 ± 0.00	1.00 ± 0.00	
X Or	0.97 ± 0.00	0.00 ± 0.00	

"n" is the number of points analyzed. "Fe2O3 t" is total iron as Fe2O3.
MgO, CaO, MnO, and SrO were below detection limits.

Table 4b

mineral:	Aegirine			Aegirine-augite							
sample:	13.1-3	13.7,9	13.10	19-5.6-8	19-5.12-14	23.7-9	19-5.9	19-5.10	19-5.11	23.10-12	23.16-20
run #:	m	m	m	m	m	m	m	m	m	m	m
n:	3	2	1	3	3	3	1	1	1	3	5
wt %											
SiO2	51.32	51.04	52.66	51.61	51.79	51.72	53.80	52.43	52.16	52.68	53.56
TiO2	1.22	0.22	0.09	0.61	0.85	0.97	1.58	1.12	0.28	0.33	0.33
ZrO2	0.22	0.01	0.03	0.04	0.09	0.03	0.12	0.07	0.02	0.02	0.03
Al2O3	0.30	3.59	2.00	0.35	0.33	0.37	0.34	0.32	0.32	0.34	0.34
Fe2O3 t	32.64	29.11	32.15	32.84	32.36	30.53	31.95	31.58	30.67	17.58	20.94
MgO	0.01		0.01	0.15	0.20	0.44	0.23	0.27	0.36	5.76	4.43
CaO	0.27	0.06	0.08	0.28	0.43	0.67	2.06	4.14	6.94	11.80	9.28
MnO	0.10	0.03	0.09	0.18	0.23	0.53	0.48	0.71	1.00	3.67	2.88
Na2O	14.03	13.63	12.08	12.20	12.32	13.94	13.06	11.71	9.96	7.38	8.96
K2O		0.01	0.02			0.02					0.02
total	100.09	97.68	99.19	98.26	98.60	99.23	103.50	102.28	101.69	99.53	100.76
cations per 6 oxygen equivalents											
Si	1.971	1.975	2.008	2.004	2.003	1.995	1.986	1.969	1.973	2.001	2.012
Ti	0.035	0.006	0.002	0.018	0.025	0.028	0.044	0.032	0.008	0.009	0.010
Zr	0.008	0.001	0.001	0.002	0.003	0.001	0.004	0.002	0.001	0.001	0.001
Al	0.013	0.164	0.090	0.016	0.015	0.017	0.015	0.014	0.014	0.015	0.015
Fe 3+	0.947	0.851	0.926	0.963	0.945	0.889	0.891	0.895	0.876	0.504	0.594
Mg	0.001		0.001	0.009	0.012	0.026	0.013	0.015	0.020	0.327	0.249
Ca	0.011	0.003	0.003	0.012	0.018	0.028	0.082	0.167	0.282	0.482	0.375
Mn	0.003	0.001	0.003	0.006	0.008	0.018	0.015	0.023	0.032	0.118	0.092
Na	1.049	1.026	0.896	0.921	0.927	1.046	0.938	0.855	0.733	0.545	0.654
K		0.001	0.001			0.001					0.001
total	4.038	4.025	3.930	3.950	3.956	4.047	3.987	3.973	3.940	4.003	4.002

Table 4c

mineral:	Arfvedsonite				
sample:	13.4	13.5	13.6	13.13	13.15
run #:	k	k	k	k	k
n:	1	1	1	1	1
wt %					
SiO2	51.80	52.27	51.37	51.67	51.39
TiO2	0.99	0.93	0.93	0.00	0.05
Al2O3	0.58	0.62	0.00	0.93	0.08
FeO t	32.47	31.56	31.48	31.84	32.15
MgO	0.15	0.19	0.14	0.01	
CaO	0.02	0.09	0.95		
MnO	1.06	1.23	1.17	1.14	1.38
Na2O	9.49	9.54	9.54	7.66	8.20
K2O	1.90	1.73	1.73	3.34	3.65
F	2.13	2.89	2.89	1.56	2.10
Cl				0.01	
O (F,Cl)	0.90	1.22	1.22	0.66	0.88
total	99.69	99.83	98.98	97.50	98.12
cations per 23 oxygen equivalents					
#T Si	7.776	7.839	7.774	8.139	8.074
#T Al	0.103	0.110			
#T Fe3+	0.122	0.051	0.226		
#T Ti					
T site	8.000	8.000	8.000	8.139	8.074
#C Al				0.173	0.015
#C Fe3+	2.399	2.394	2.479	1.218	1.593
#C Ti	0.112	0.105	0.106		0.006
#C Mg	0.034	0.042	0.032	0.002	
#C Fe2+	1.555	1.513	1.280	2.976	2.632
#C Mn	0.135	0.156	0.150	0.152	0.184
#C Ca	0.003	0.014	0.154		
C site	4.238	4.226	4.200	4.522	4.429
#B Mg					
#B Fe2+					
#B Mn					
#B Ca					
#B Na	2.000	2.000	2.000	2.000	2.000
B site	2.000	2.000	2.000	2.000	2.000
#A Ca					
#A Na	0.762	0.774	0.800	0.340	0.498
#A K	0.364	0.331	0.334	0.671	0.732
A site	1.126	1.105	1.134	1.011	1.230
sum	15.364	15.331	15.334	15.671	15.732
anions					
#C Cl				0.003	
#C F	1.011	1.371	1.383	0.777	1.043

Table 4d

mineral:	Monazite		Bastnaesite	
sample:	11	11	11	11
run#:	g	g	g	g
grain #:	7	14	23	24
wt %				
SiO2	0.72	0.25	0.23	0.46
TiO2		0.07	0.05	
Al2O3	0.01			
FeO t	0.56			
MgO	0.02			
CaO	0.04	0.07	0.08	0.08
K2O	0.01	0.04	0.03	0.00
P2O5	24.14	23.36	0.01	0.01
Nb2O5			0.65	0.65
Y2O3	0.28		0.07	
ZrO2	2.52	2.62		
La2O3	21.49	9.56	17.88	10.64
Ce2O3	35.94	34.56	35.75	36.54
Pr2O3	2.38	5.09	4.06	5.12
Nd2O3	7.70	17.89	18.71	22.56
Sm2O3	0.27	1.32	1.59	2.06
Gd2O3		0.75	0.68	0.65
Dy2O3		0.09		0.29
F	0.87	0.84	7.59	7.26
Cl	0.02	0.07	0.06	0.12
O(F,Cl)	0.37	0.37	3.21	3.08
total	96.61	96.19	84.22	83.35
cations	per 16 oxygen eq.		per 24 oxygen eq.	
Si	0.124	0.045	0.122	0.251
Ti		0.009	0.019	
Al	0.003			
Fe	0.080			
Mg	0.004			
Ca	0.008	0.013	0.046	0.049
K	0.003	0.009	0.019	0.003
P	3.514	3.499	0.002	0.005
Nb			0.159	0.159
Y	0.026		0.020	
Zr	0.211	0.226		
La	1.363	0.624	3.568	2.134
Ce	2.263	2.239	7.084	7.276
Pr	0.149	0.328	0.801	1.014
Nd	0.473	1.131	3.616	4.382
Sm	0.016	0.080	0.296	0.387
Gd		0.044	0.122	0.117
Dy		0.005		0.050
total	8.238	8.251	15.874	15.826
anions				
F	0.474	0.468	12.994	12.490
Cl	0.006	0.021	0.059	0.108

MnO and Na2O were not detected.

Table 4e

mineral:	Zircon			
sample:	15C	15C	15C	15C
run#:	g	g	g	g
grain #:	1	6	10	11
wt %				
SiO2	33.93	33.93	30.25	30.50
TiO2	0.07	0.04		
Al2O3		0.02		
FeO	0.04	0.00	0.06	0.06
MgO		0.01	0.00	
CaO	0.05	0.07	0.01	0.04
MnO	0.13	0.08		
K2O	0.01	0.01	0.01	0.01
P2O5	0.06	0.06	1.47	1.50
Nb2O5	0.73			
Y2O3	0.34	0.17	4.34	3.97
ZrO2	64.72	63.98	54.05	55.11
La2O3	0.05	0.06		0.02
Ce2O3	0.25	0.26	0.04	
Nd2O3		0.47		
Sm2O3		0.33	0.01	0.09
Gd2O3	0.28	0.48	0.05	0.25
Dy2O3	0.29			
Er2O3	0.16	0.03	0.57	0.69
Yb2O3	0.08	0.01	1.12	0.97
F	0.10	0.07	0.23	0.09
Cl	0.01			0.01
O (F,Cl)	0.04	0.03	0.10	0.04
total	101.26	100.06	92.10	93.26
cations per 16 oxygen equivalents				
Si	4.076	4.122	4.010	3.992
Ti	0.006	0.004		
Al		0.003		
Fe	0.004	0.000	0.007	0.007
Mg		0.003	0.001	
Ca	0.007	0.009	0.001	0.006
Mn	0.014	0.009		
K	0.002	0.002	0.001	0.002
P	0.006	0.006	0.165	0.166
Nb	0.040			
Y	0.022	0.011	0.306	0.277
Zr	3.792	3.791	3.494	3.518
La	0.002	0.003		0.001
Ce	0.011	0.012	0.002	
Nd		0.020		
Sm		0.014	0.001	0.004
Gd	0.011	0.019	0.002	0.011
Dy	0.011			
Er	0.006	0.001	0.024	0.028
Yb	0.003	0.000	0.045	0.039
total	8.012	8.029	8.059	8.050
anions				
F	0.039	0.026	0.096	0.038
Cl	0.001			0.002

Na2O and Pr2O3 were not detected.

Table 4f

mineral:	Zircon		Gittinsite		CaYSilicate		Andradite
sample:	19-5	19-5	19-5	19-5	19-5	19-5	19-5
run #:	b	c	b	c	b	c	c
n:	2	4	2	15	2	3	5
wt %							
SiO2	33.64	32.12	41.27	40.26	32.46	33.48	33.34
Fe2O3 t	0.05	0.74	0.03	0.17	0.04	0.02	22.69
CaO	0.33	1.50	18.40	18.30	14.10	15.88	32.34
Y2O3	4.19	3.95	1.51	1.85	24.42	26.01	1.33
ZrO2	58.60	54.35	38.28	37.73	0.00	0.00	4.26
La2O3	0.01			0.05	0.06	0.03	0.05
Ce2O3	0.10	0.04	0.03	0.04	0.51	0.31	0.03
Pr2O3					0.14		0.18
Nd2O3	0.15		0.02				
Dy2O3	0.46						0.02
Er2O3	0.50	0.50	0.25	0.33	1.63	2.29	0.26
Yb2O3	0.75	0.74	0.38	0.38	1.93	2.13	0.26
total	98.78	93.93	100.16	99.12	75.29	80.14	94.76
cations	per 16 ox. equiv.		per 14 ox. equiv.		per 24 ox. equiv.		
Si	4.167	4.158	4.095	4.055	7.657	7.478	6.166
Fe+3	0.005	0.070	0.002	0.013	0.006	0.002	3.126
Ca	0.044	0.208	1.957	1.975	3.545	3.800	6.411
Y	0.277	0.273	0.080	0.099	3.064	3.091	0.130
Zr	3.540	3.434	1.852	1.853			0.152
La	0.000			0.000	0.005	0.002	0.001
Ce	0.004	0.002	0.001	0.001	0.044	0.025	0.001
Pr					0.012		0.005
Nd	0.006		0.000				
Dy	0.019						0.000
Er	0.020	0.021	0.008	0.009	0.120	0.161	0.012
Yb	0.028	0.029	0.012	0.012	0.140	0.145	0.003
total	8.112	8.204	8.003	8.022	14.629	14.774	15.893

Table 4g		
mineral:	Andradite	
sample:	19-5.3	19-5.5
run #:	m	m
n:	1	1
wt %		
SiO2	33.50	33.53
TiO2	0.54	0.46
Al2O3	4.87	5.05
Fe2O3 t	25.70	23.24
CaO	33.60	32.66
MnO	0.29	0.18
total	98.50	95.12
#Si IV	5.68	5.80
#Al IV	0.32	0.20
T site	6.00	6.00
#Al VI	0.65	0.83
#Ti VI	0.07	0.06
#Fe +3	3.28	3.11
O site	4.00	4.00
#Ca	6.10	6.06
#Mn +2	0.04	0.03
A site	6.00	6.00
#O	23.87	23.93

Table 4h						
mineral:	Synchisite	Rowlandite?	Ilmorite?	YCaREESi	Fergusonite?	Xenotime
sample:	21	21	21	21	21	21
run #:	e	e	e	e	e	e
n:	4	4	2	4	3	1
wt %						
SiO2	0.07	28.37	16.32	17.36	6.81	1.96
TiO2		0.06	0.01		1.61	
Al2O3	0.02					
FeO t	0.00	2.25	0.01	1.30	4.14	0.03
CaO	17.57	0.35	0.06	7.31	1.08	0.03
MnO		0.27			0.37	
P2O5	0.02	0.01	0.02		0.07	31.74
Nb2O5	0.44	0.04		0.07	34.74	
PbO		0.22	0.25	0.24	0.55	0.26
Y2O3	9.28	37.94	50.46	32.65	22.15	45.42
La2O3	5.23	0.26	0.01	1.31	0.08	
Ce2O3	14.04	1.89	0.05	3.71	0.18	
Pr2O3	1.89	0.34	0.01		0.04	
Nd2O3	10.65	3.02	0.65	3.45	0.30	0.37
Sm2O3	4.27	2.11	0.65	1.35	0.35	0.27
GdO3	7.95		4.52			
Dy2O3		1.37		2.79		
Er2O3		2.18	2.77	0.97	2.96	2.87
Yb2O3		2.10	2.19	1.01	3.87	1.49
F	3.12	4.34		4.32	0.45	0.04
O (F)	1.31	1.83		1.82	0.19	0.02
total	73.23	85.28	77.98	76.02	79.56	84.47
cations per 24 oxygen equivalents						
Si	0.030	6.913	4.987	5.210	1.937	0.419
Ti		0.011	0.001		0.347	
Al	0.012					
Fe	0.001	0.453	0.002	0.205	0.987	0.006
Ca	8.810	0.088	0.021	2.424	0.332	0.008
Mn		0.055			0.090	
P	0.007	0.002	0.006		0.016	5.758
Nb	0.090	0.004		0.009	4.512	
Pb		0.014	0.020	0.019	0.043	0.015
Y	2.286	4.670	8.205	5.709	3.380	5.180
La	0.906	0.023	0.001	0.150	0.008	
Ce	2.417	0.169	0.006	0.423	0.019	
Pr	0.322	0.031	0.002		0.005	
Nd	1.785	0.264	0.071	0.382	0.030	0.028
Sm	0.689	0.179	0.068	0.146	0.035	0.020
Gd	1.235		0.458			
Dy		0.107		0.278		
Er		0.167	0.266	0.095	0.267	0.193
Yb		0.155	0.204	0.097	0.340	0.097
total	18.589	13.306	14.319	15.149	12.346	11.725
anions						
F	4.547	3.357		4.698	0.408	0.026

Table 4i					
mineral:	YREESilicate	Silica	Epidote	Apatite	Monazite
sample:	6	6	6	6	6
run #:	e	e	e	e	e
n:	3	6	10	1	2
wt %					
SiO2	25.34	91.70	33.64	0.58	0.11
TiO2	0.13	0.18	0.01		
Al2O3		0.17	17.16	0.68	0.01
FeO t	5.87	0.49	13.95	0.05	
CaO	2.78	0.23	11.00	20.20	0.01
MnO		0.03	2.35		
P2O5	0.03	0.03	0.03	29.96	30.20
Nb2O5	0.01	0.10	0.18		
PbO	0.12	0.13	0.13		
Y2O3	26.97		2.10	0.06	
La2O3	0.06	0.08	4.28	14.97	41.94
Ce2O3	0.54	0.07	6.41	19.17	26.08
Pr2O3	0.14	0.03	0.75	1.43	0.67
Nd2O3	2.47	0.04	4.07	3.03	2.39
Sm2O3	2.73	0.11	0.73	0.29	0.58
GdO3	6.95	0.05	0.93		0.64
Dy2O3		0.03			0.64
Er2O3	0.46	0.05	0.14		0.09
Yb2O3	0.12				
F	0.07	0.02	0.04	1.48	0.35
O (F)	0.03	0.01	0.02	0.62	0.15
total	74.75	93.53	97.89	91.27	103.55
cations per 24 oxygen equivalents					
Si	6.903	11.725	6.015	0.128	0.025
Ti	0.026	0.020	0.001		
Al		0.029	3.605	0.176	0.002
Fe	1.338	0.098	2.085	0.009	
Ca	0.811	0.042	2.093	4.772	0.003
Mn		0.012	0.358		
P	0.007	0.046	0.004	5.593	5.910
Nb	0.001	0.006	0.014		
Pb	0.011	0.006	0.006		
Y	3.879		0.207	0.007	
La	0.006	0.005	0.286	1.217	3.576
Ce	0.054	0.003	0.425	1.547	2.207
Pr	0.013	0.002	0.049	0.115	0.057
Nd	0.238	0.002	0.262	0.238	0.196
Sm	0.254	0.005	0.046	0.022	0.046
Gd	0.624	0.002	0.056		0.048
Dy		0.002			0.048
Er	0.039	0.004	0.008		0.006
Yb	0.010				
total	14.214	12.008	15.519	13.823	12.124
anions					
F	0.059	0.010	0.025	1.030	0.252

Table 4j

mineral:	Fersmite?	Caysichite?	Taeniolite
sample:	23	23	23
run #:	f	f	f
n:	1	2	6
wt %			
SiO2	0.58	23.46	53.71
TiO2	7.80	0.04	0.21
Al2O3			4.35
FeO t	1.09	0.61	0.26
MgO		0.02	20.71
CaO	9.95	8.69	0.05
MnO	1.14	1.12	0.11
Na2O	2.23	0.01	0.09
K2O	0.02	0.07	9.59
P2O5	0.04	0.02	0.00
Nb2O5	41.77	0.21	0.14
PbO			0.07
Y2O3		5.55	0.01
La2O3	0.32	6.36	0.01
Ce2O3	1.75	13.53	0.01
Pr2O3	0.23	1.21	
Nd2O3		6.68	
Sm2O3		2.07	0.01
Gd2O3		1.43	0.02
Dy2O3	0.39	0.57	
Er2O3		0.03	0.02
Yb2O3			0.01
F	2.27	0.96	11.97
Cl	0.02	0.04	0.00
O (F,Cl)	0.96	0.41	5.04
total	68.63	72.26	96.32
cations per 24 oxygen equivalents			
Si	0.182	7.051	8.423
Ti	1.842	0.010	0.024
Al			0.801
Fe +2	0.286	0.152	0.034
Mg		0.009	4.838
Ca	3.348	2.810	0.008
Mn	0.303	0.286	0.014
Na	1.359	0.008	0.027
K	0.006	0.028	1.919
P	0.009	0.005	0.001
Nb	5.931	0.029	0.010
Pb			0.003
Y		0.887	0.001
La	0.037	0.706	
Ce	0.202	1.490	
Pr	0.027	0.132	
Nd		0.716	
Sm		0.214	
Gd		0.142	
Dy	0.040	0.055	
Er		0.003	0.001
Yb			
total	13.571	14.733	16.105
anions			
F	2.251	0.910	5.922
Cl	0.012	0.018	0.000

ZrO2 was not detected.

Table 4k

mineral:	Taeniolite			
sample:	23.1	23.3	23.5	23.1,3,5
run #:	j	j	j	j
n:	1	1	1	3
wt %				
SiO2	52.54	55.42	55.39	54.45
TiO2	0.19	0.21	0.21	0.20
Al2O3	4.04	3.07	2.49	3.20
FeO t	1.44	0.70	0.97	1.04
MgO	20.74	21.43	20.78	20.98
MnO	0.38	0.22	0.22	0.27
BaO	0.07	0.05		0.04
Na2O	0.13	0.04	0.07	0.08
K2O	9.61	9.86	9.91	9.79
F	10.69	11.13	10.84	10.89
Cl		0.01		
O (F,Cl)	4.50	4.69	4.56	4.58
total	95.33	97.45	96.32	96.37
#Si IV	7.643	7.833	7.920	7.800
#Al IV	0.357	0.167	0.080	0.200
#Fe IV				
#Ti IV				
T site	8.000	8.000	8.000	8.000
#Al VI	0.336	0.345	0.340	0.340
#Ti VI	0.021	0.022	0.023	0.022
# Fe 3+				
#Fe 2+	0.175	0.083	0.116	0.124
#Mn 2+	0.047	0.026	0.027	0.033
#Mg	4.498	4.515	4.429	4.481
O site	5.076	4.992	4.934	5.000
#Ba	0.004	0.003		0.002
#Na	0.037	0.011	0.019	0.022
#K	1.783	1.778	1.808	1.790
A site	1.824	1.792	1.827	1.814
#O	19.082	19.022	19.098	19.067
#F	4.918	4.975	4.902	4.932
#Cl		0.002		0.001
Charge	0.920	0.980	0.900	0.930

Table 5: Sm-Nd Isotopic Systematics

sample	147Sm/144Nd	error	143Nd/144Nd	error	wt. in g
APP-91-5	0.16038	0.000222	0.512733	0.000018	0.06392
APP-91-7	0.204743	0.000133	0.513004	0.000025	0.07290
APP-91-8	0.099014	0.000078	0.512562	0.000026	0.07326
APP-91-11	0.06517	0.000287	0.512781	0.000025	0.06090
APP-91-13	0.111374	0.000248	0.512817	0.000034	0.07421
APP-91-15A	0.162792	0.000256	0.512869	0.000025	0.07280
APP-91-15C	0.22081	0.000291	0.512925	0.000021	0.07354
APP-91-17	0.213365	0.000491	0.512899	0.000019	0.06936
APP-91-19-5	0.440181	0.00373	0.513198	0.000017	0.08477
APP-91-19-6	0.162794	0.000662	0.51287	0.000019	0.07457
APP-91-21A	0.209398	0.00165	0.512973	0.000025	0.07114
APP-91-21B	0.359252	0.0472	0.513266	0.00003	0.07778
APP-91-6	0.216306	0.0133	0.512885	0.000044	0.07409
APP-91-23	0.142137	0.00501	0.512891	0.000032	0.07740

Errors are 2-sigma, absolute.

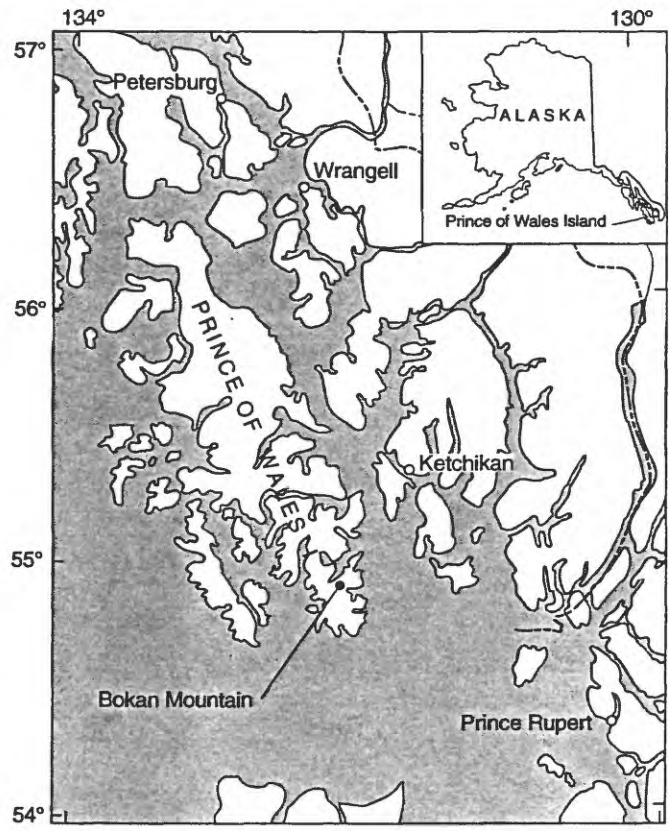

Fig. 1. Location of Bokan Mountain on Prince of Wales Island, southeastern Alaska.

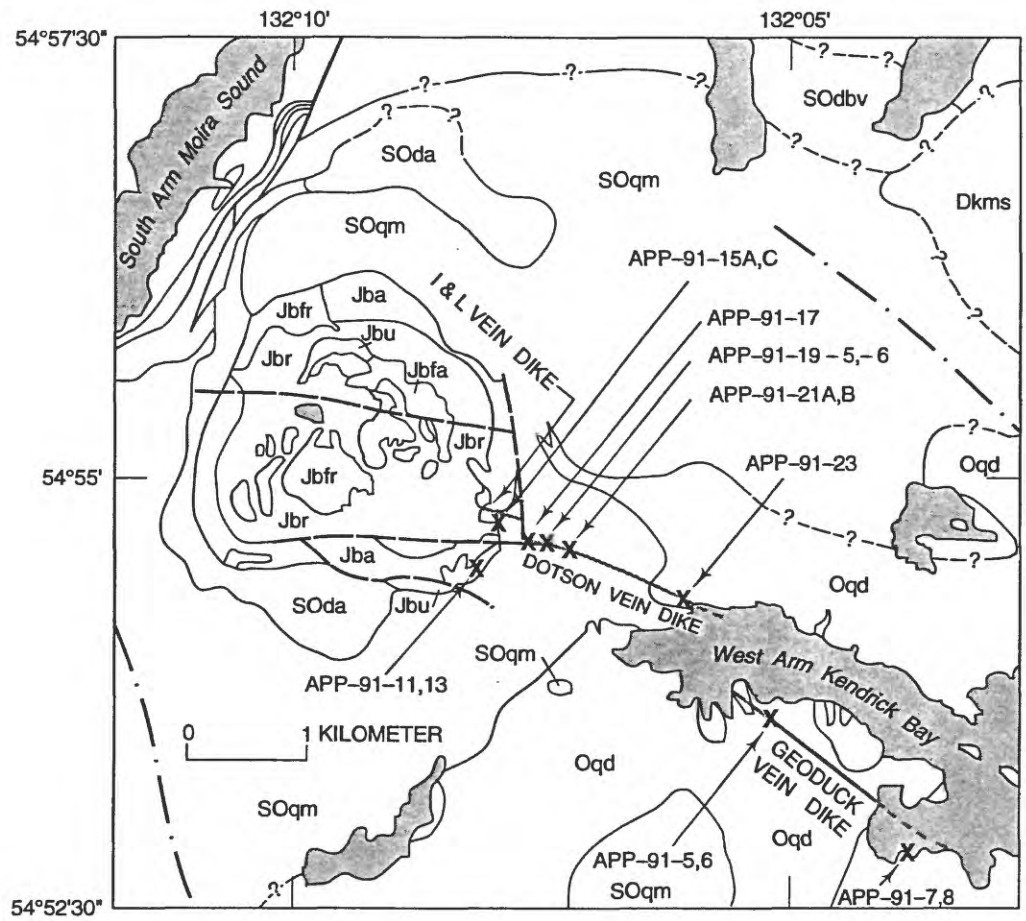

Fig. 2. Sample sites (X) and the location (after Warner and Barker, 1989) of the Dotson, Geoduck, and I & L vein dikes on the southeast flank of Bokan Mountain. Geologic map modified from Gehrels (1992); all map units from Gehrels (1992). Bokan Mountain Granite map units (all Jurassic): Jbr, riebeckite granite porphyry; Jba, aegirine granite porphyry; Jbfr, fine-grained riebeckite granite porphyry; Jbfa, felty-aegirine granite; Jbu, granite, undivided. Country rock map units: Dkms, mudstone and siltstone unit of Early Devonian Karheen Formation; SOda and SOdbv, argillite and shale unit and basaltic to andesitic volcanic rock unit, respectively, of Ordovician and Early Silurian(?) Descon Formation; SOqm, Late Ordovician and (or) Early Silurian quartz monzonite and granite; Oqd, Late Ordovician quartz diorite and diorite. Faults are shown by long-dash lines where approximately located and by dash-dot lines where inferred from aerial photographs.

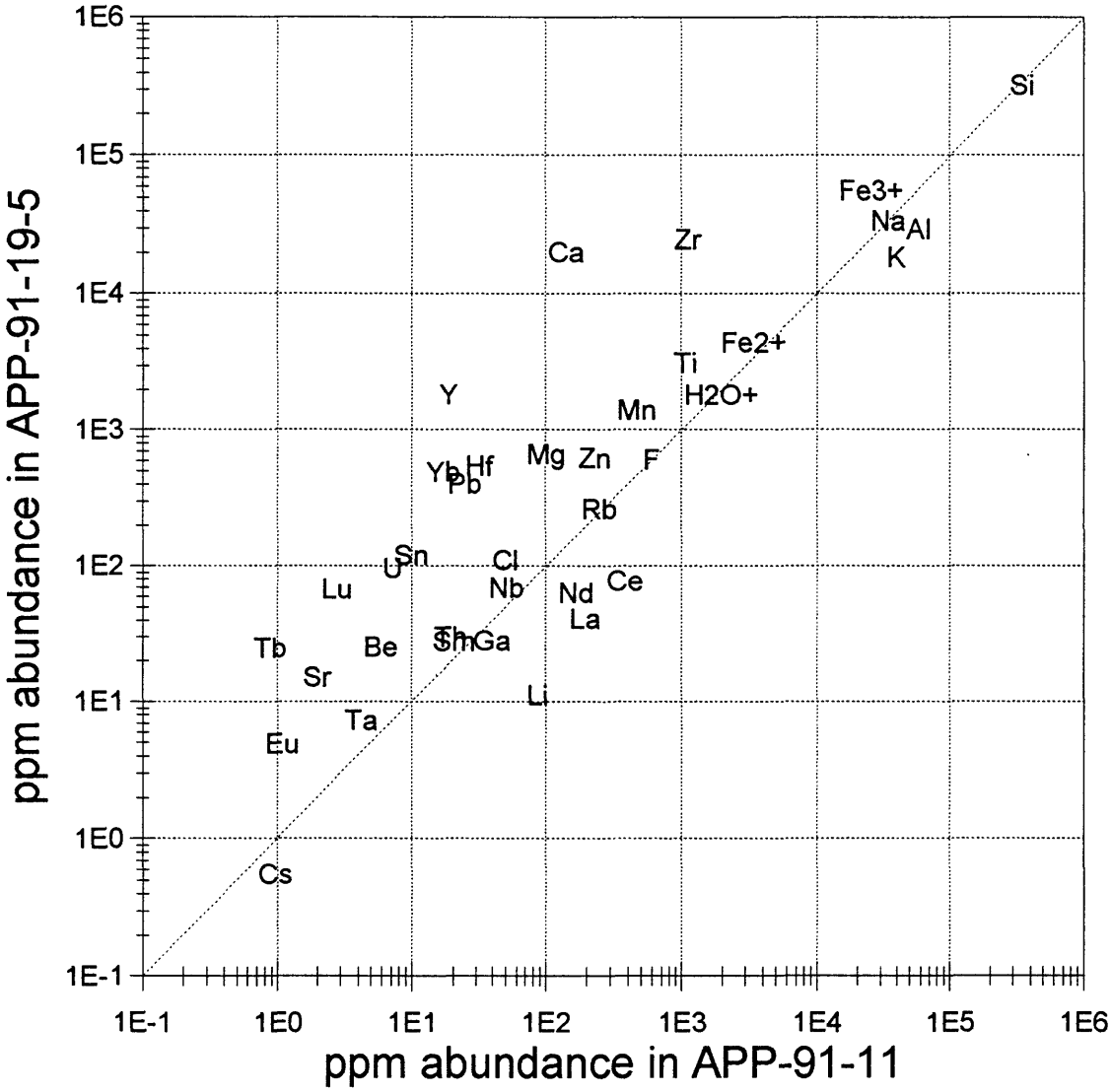

Fig. 3. Element-by-element abundance comparison of middle Dotson vein-dike sample 19-5 and Bokan Mountain stock granite sample 11 showing enrichment of Ca, Zr, Hf, Y HREE, Pb, U, and Sn, and depletion of Li, in the vein dike. Abundances are in parts per million (ppm).

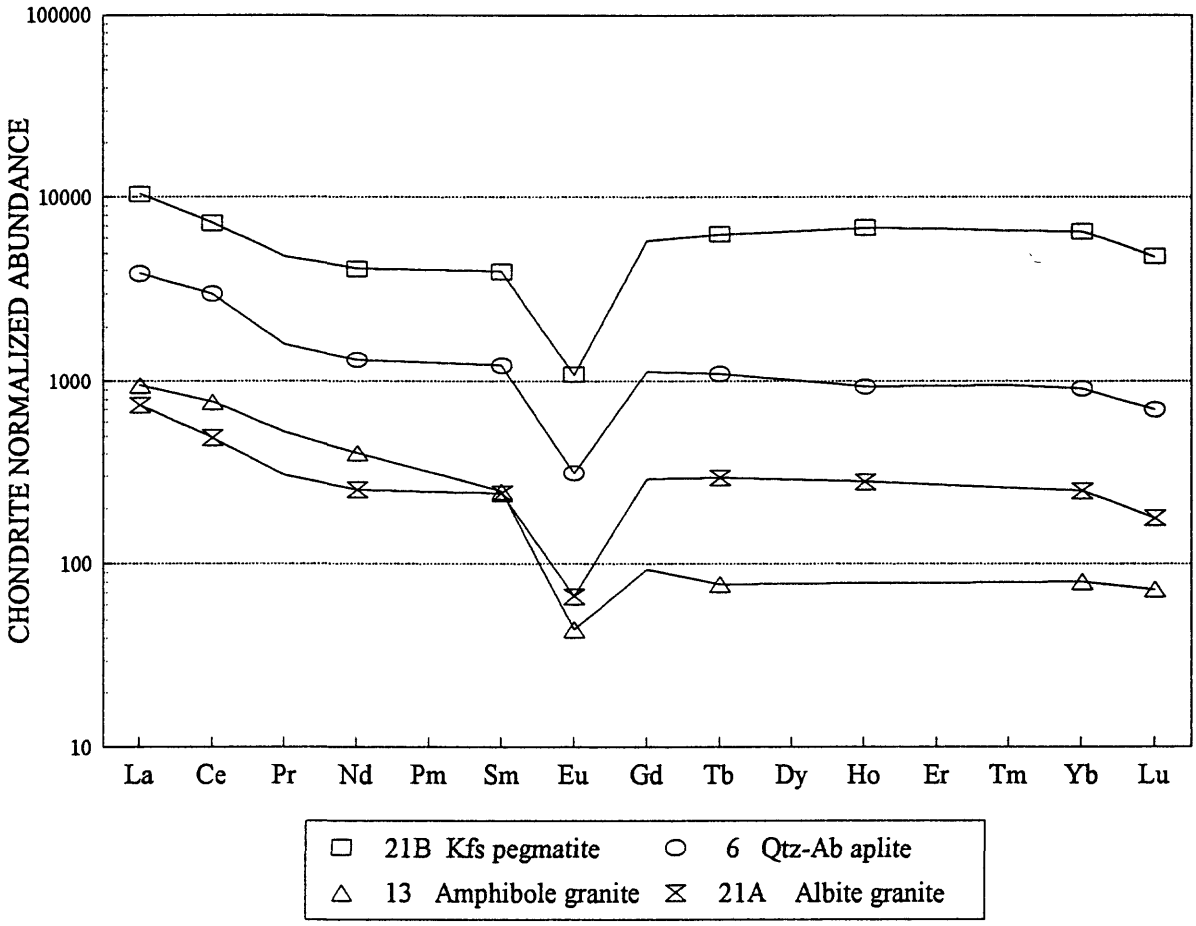

Fig. 4a. Chondrite-normalized REE abundance patterns for samples from Bokan Mountain stock granite (sample 13), the Dotson vein dike (samples 21A and 21B), and the Geoduck vein dike (sample 6) (The patterns are interpolated from measured values represented by the symbols).

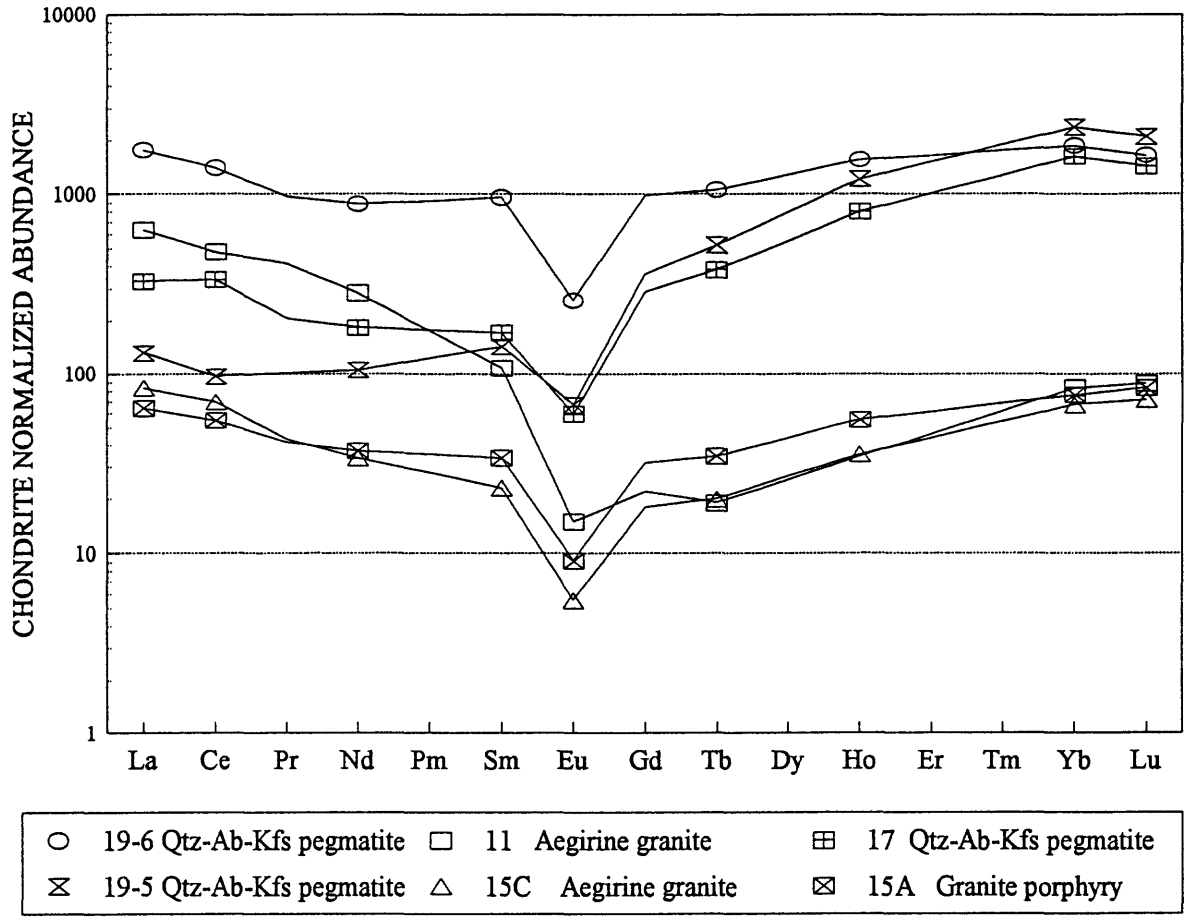

Fig. 4b. Chondrite-normalized REE abundance patterns for samples from Bokan Mountain stock granite (sample 11, 15A, and 15C) and the Dotson vein dike (samples 17, 19-5, and 19-6).

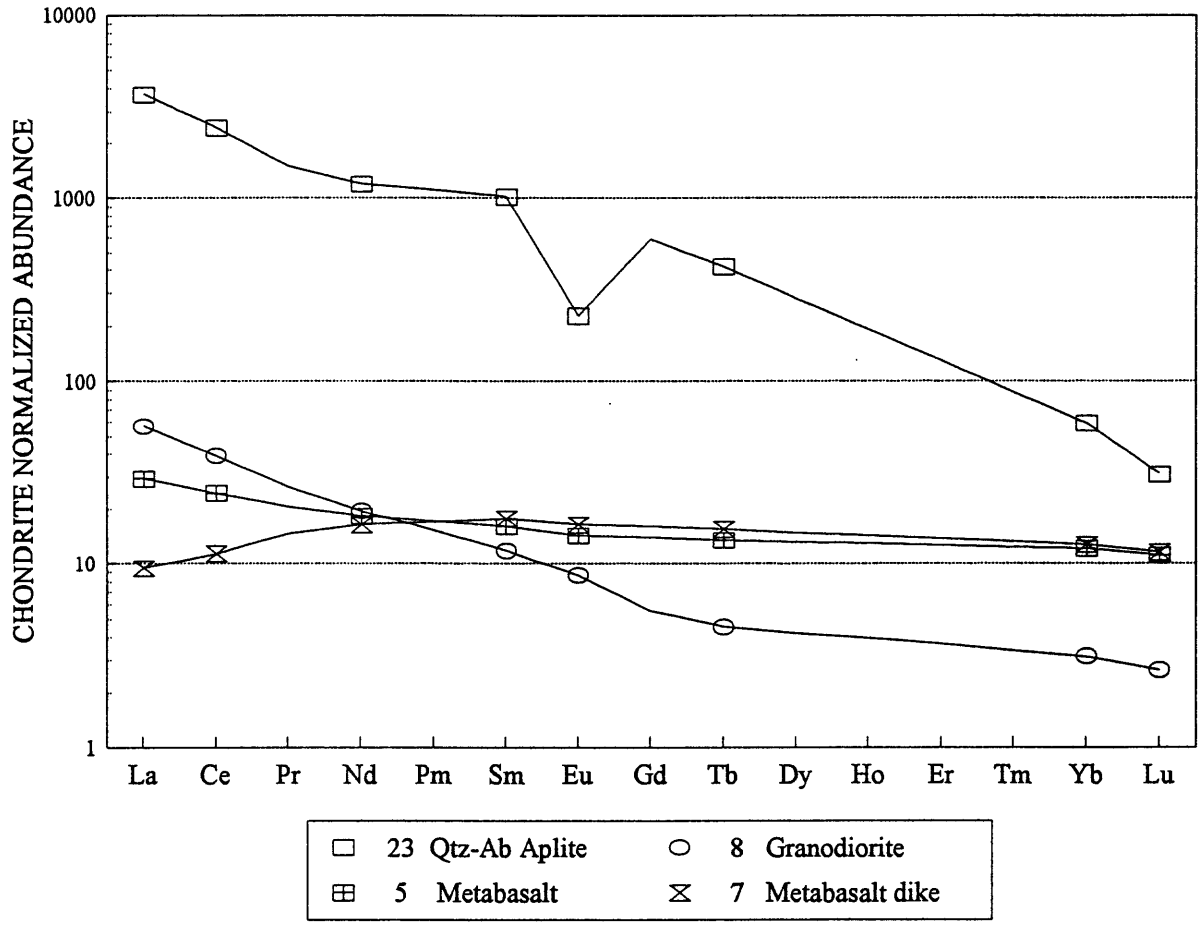

Fig. 4c. Chondrite-normalized REE abundance patterns for samples from Bokan Mountain area country rocks (samples 5, 7, 8) and east Dotson vein dike (sample 23).

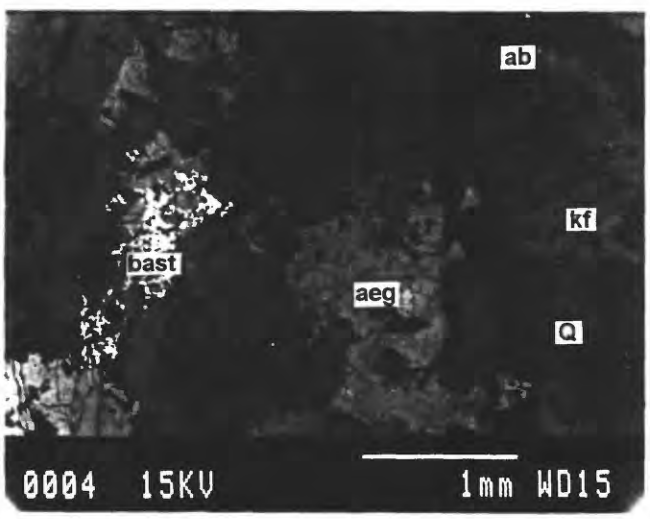

Fig. 5. Scanning electron microscope (SEM) backscattered electron (BSE) image of Bokan Mountain stock granite sample 11 showing equant grains of potassium feldspar (kf) that have been partly replaced by albite (ab). The lower right quadrant of the photograph is occupied largely by quartz (Q) and aegirine (aeg). Some aegirine grains have overgrowths that are flecked with inclusions of bastnaesite. Late hydrothermal bastnaesite (bast) replaces a variety of minerals on the left side of the image. The lower bar indicates photograph sequence number 4, taken at a working distance of 15 mm, with an electron beam accelerating voltage of 15 kV; a 1 mm scale bar is also shown.

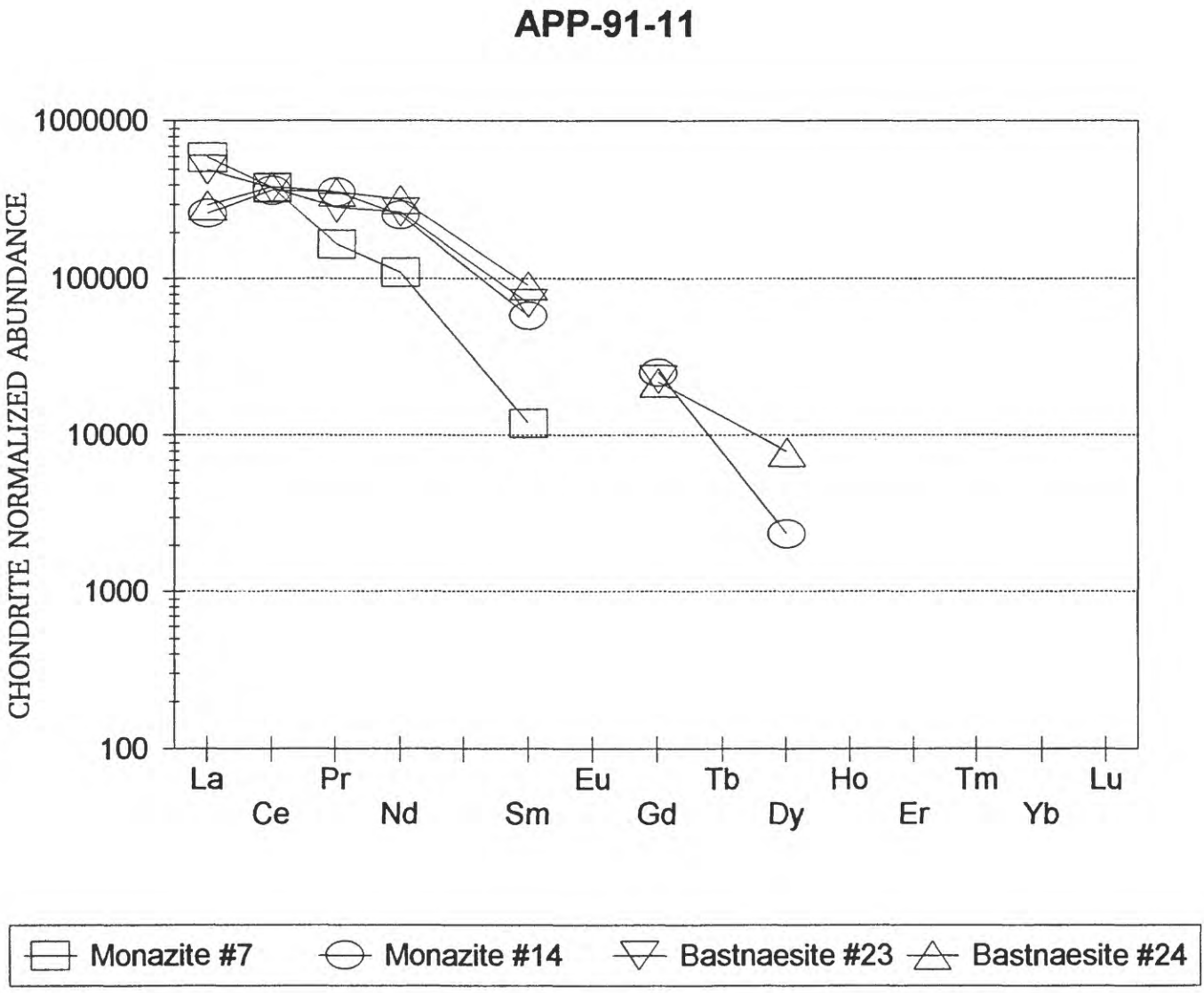

Fig. 6. REE abundance patterns for two monazite grains and two areas of bastnaesite in Bokan Mountain stock granite sample 11, determined by electron probe microanalysis. Grain #'s refer to data in Table 4d.

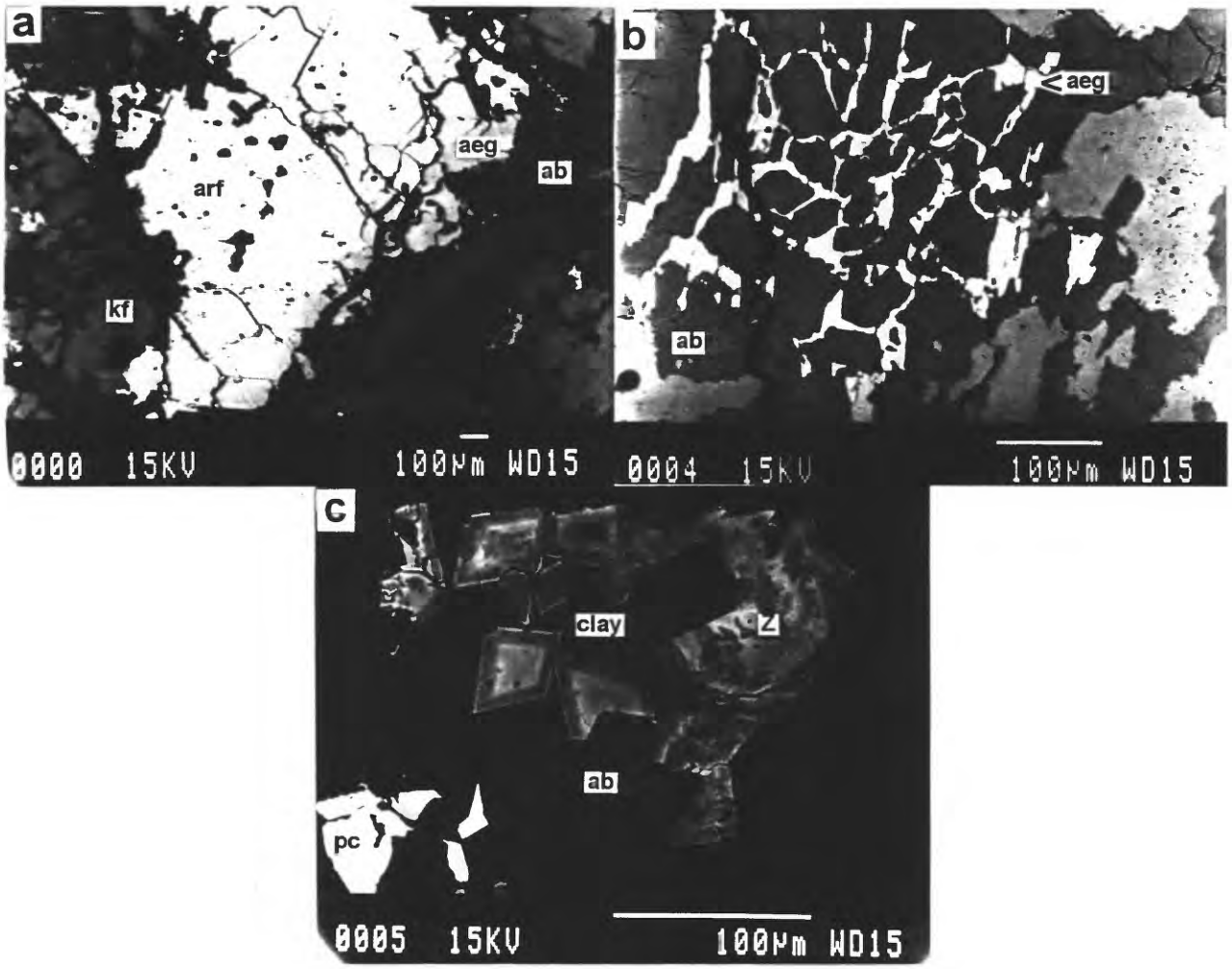

Fig. 7. SEM-BSE images of Bokan Mountain stock granite sample 13 showing (a) a composite phenocryst composed of arfvedsonite (arf), with good cleavage, and aegirine (aeg) surrounded by potassium feldspar (kf) that has been partly replaced by albite (ab); a few laths of albite have replaced arfvedsonite and aegirine along cracks; the mafic minerals have solid inclusions of pyrochlore, bastnaesite, and monazite, and round (once-fluid?) inclusions of fluorite with yttrium-enriched rims; ghost-like filigrees of hydrothermal aegirine occur in albite on the right side of the phenocryst; (b) a filigree of hydrothermal aegirine (aeg) has replaced albite (ab) along a fracture system or grain boundaries; (c) zoned crystals of zircon (Z) occur with a brown Al-Fe silicate (clay?) and pyrochlore with tantalum enriched cores (pc), all within albite (ab); inasmuch as no compositional differences were noted within the zircons, the zoning may be due to water or hydroxyl ions; the zircon, clay?, and pyrochlore are believed to be of hydrothermal origin.

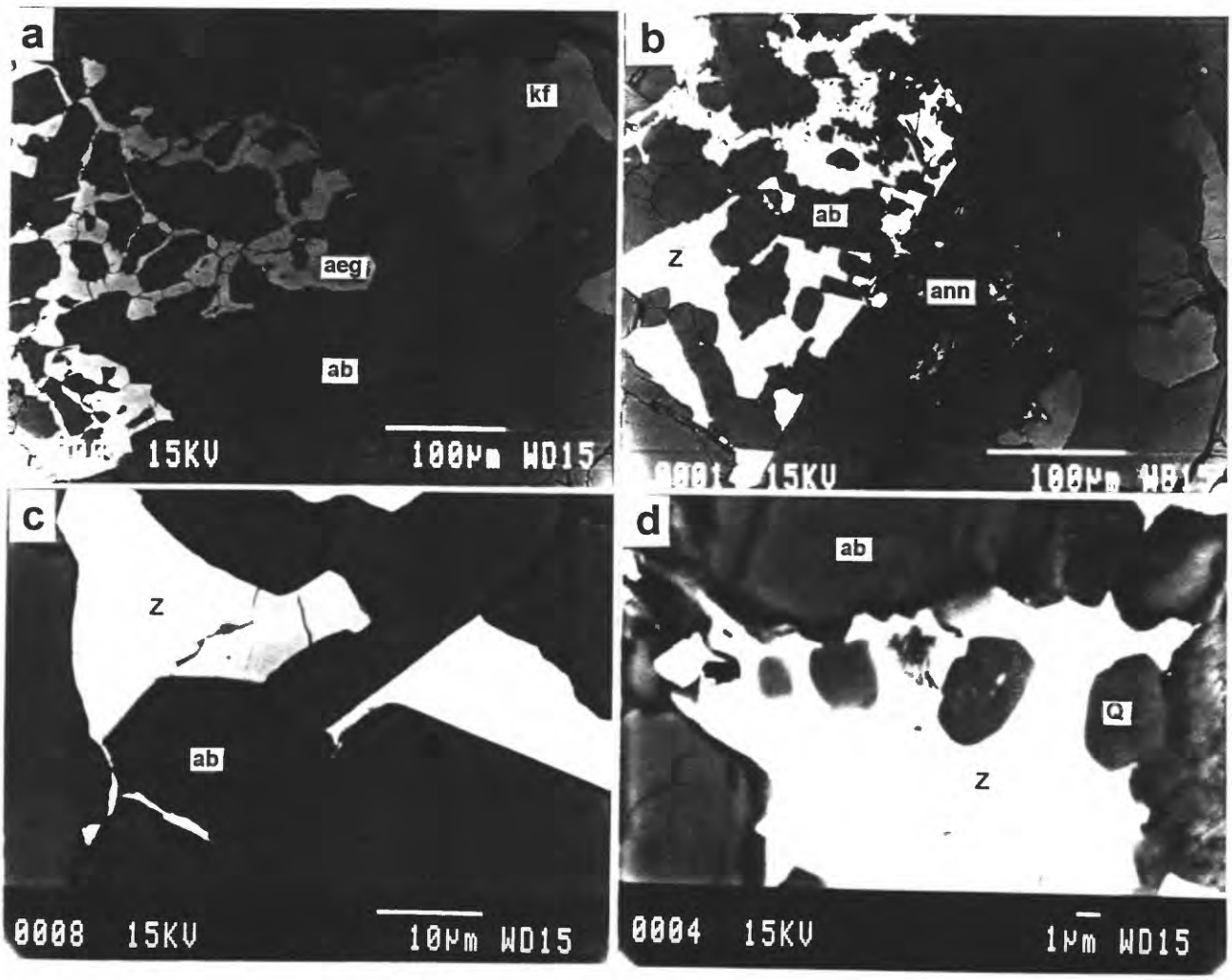

Fig. 8. SEM-BSE images of Bokan Mountain stock granite sample 15C showing (a) triple-junction grain boundaries for potassium feldspar (kf) and albite (ab) along which a filigree of hydrothermal aegirine (aeg) has subsequently formed, (b) optically continuous grain-boundary metasomatic zircon filigree (Z) replacing albite (ab) containing titaniferous annite (ann), (c) crystallization of zircon (Z), some thorium-bearing, along triple junction grain boundaries in albite (ab), and (d) hexagonal quartz crystals (Q) in zircon (Z) replacing albite (ab); bastnaesite can occur in both albite and zircon.

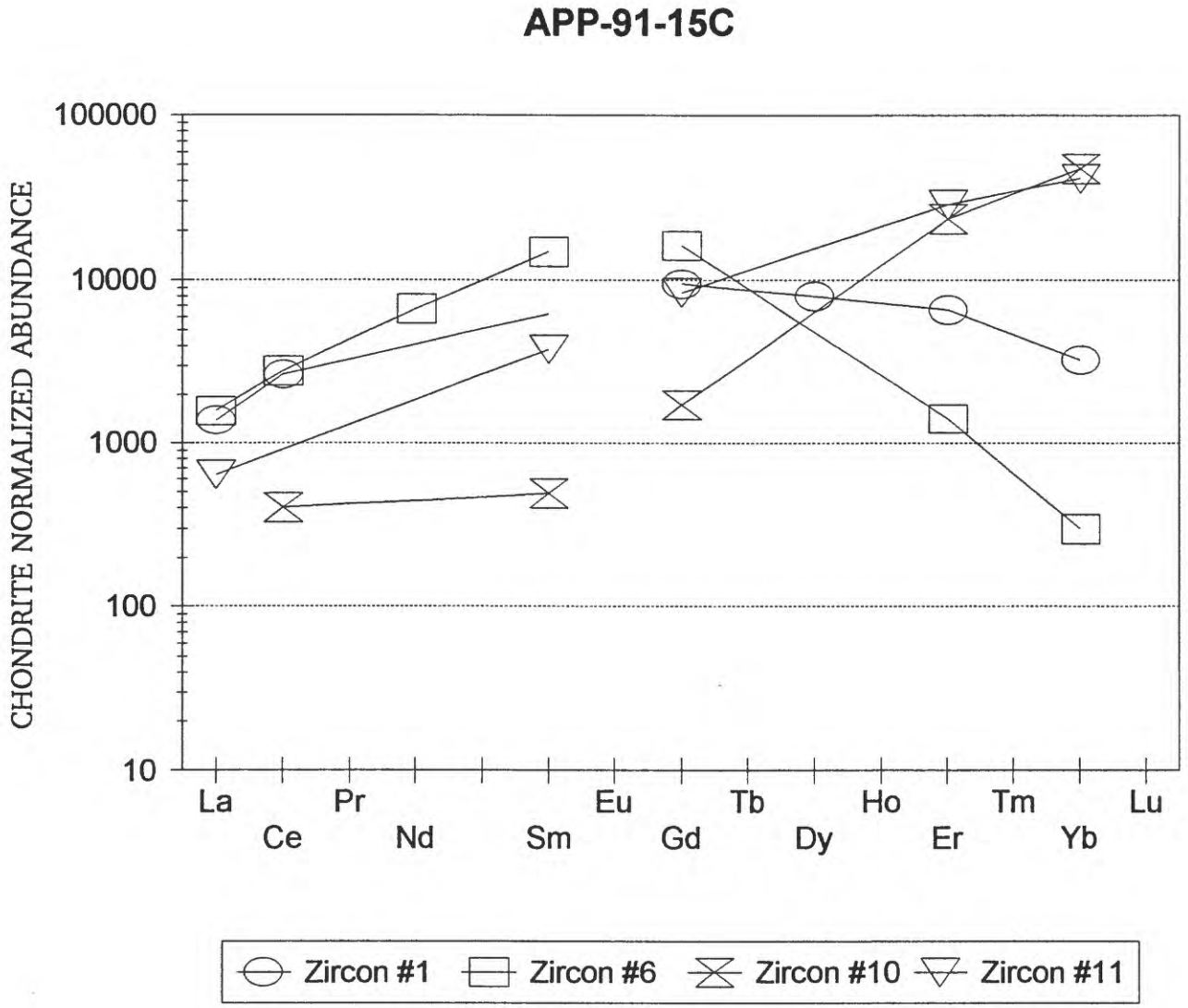

Fig. 9. REE patterns for four individual zircon grains from Bokan Mountain stock granite sample 15C. Grain #'s refer to data in Table 4e.

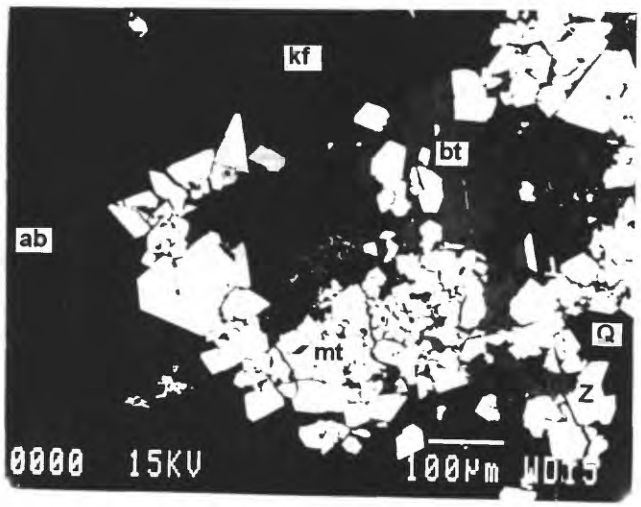

Fig. 10. SEM-BSE image of upper Dotson vein-dike sample 17 showing a cluster of magnetite grains (mt) between potassium feldspar (kf) and quartz (Q) grains. The potassium feldspar is partly replaced by albite (ab) along cracks and in places (upper left) is honeycombed with irregular solution cavities. Many of the grains on the quartz side of the magnetite cluster are zircons (Z). The magnetite surrounds an area of magnesian fluoro-biotite (bt) with inclusions of manganiferous ilmenite, fergusonite, and bastnaesite. The cavities to the lower left of the magnetite cluster appear to be coated with cerianite.

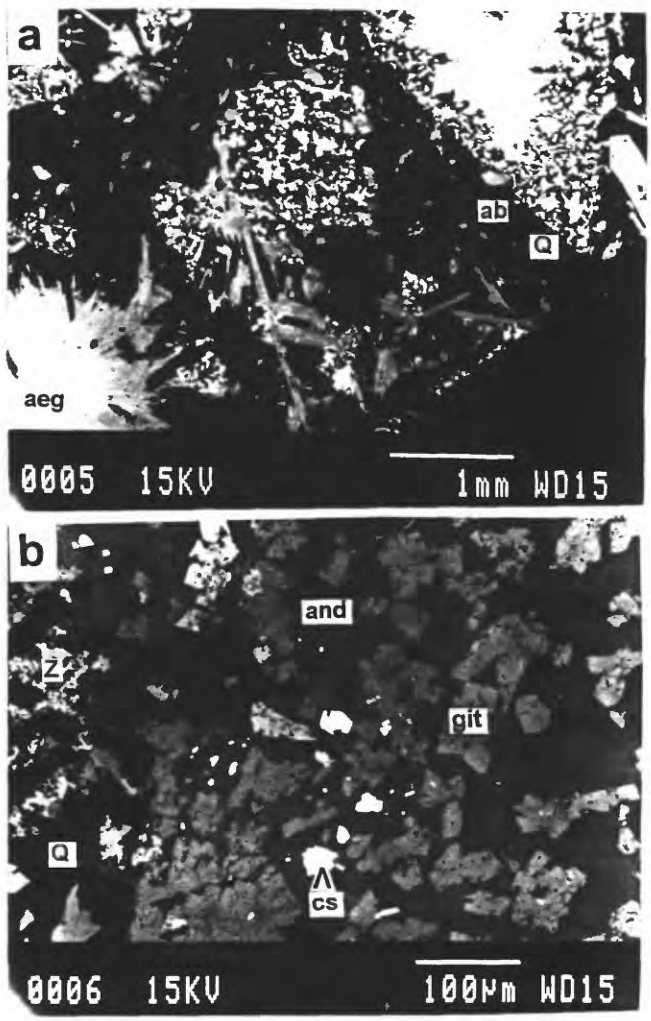

Fig. 11. SEM-BSE image of middle Dotson vein-dike sample 19-6 showing (a) spherulites, needles, and laths of aegirine (aeg), and polymineralic phenocrysts in a matrix of silica (Q) and albite (ab), and (b) at greater magnification, within the largest phenocryst, porous gittinsite clusters (git), some with inclusions of a Ca-Y silicate, occur in a matrix of silica (Q) and of andradite (and); the lighter gray grains in the upper left are zircon (Z); the central white patches are cerussite (cs); the white lath at the bottom of the image is an unidentified lead silicate.

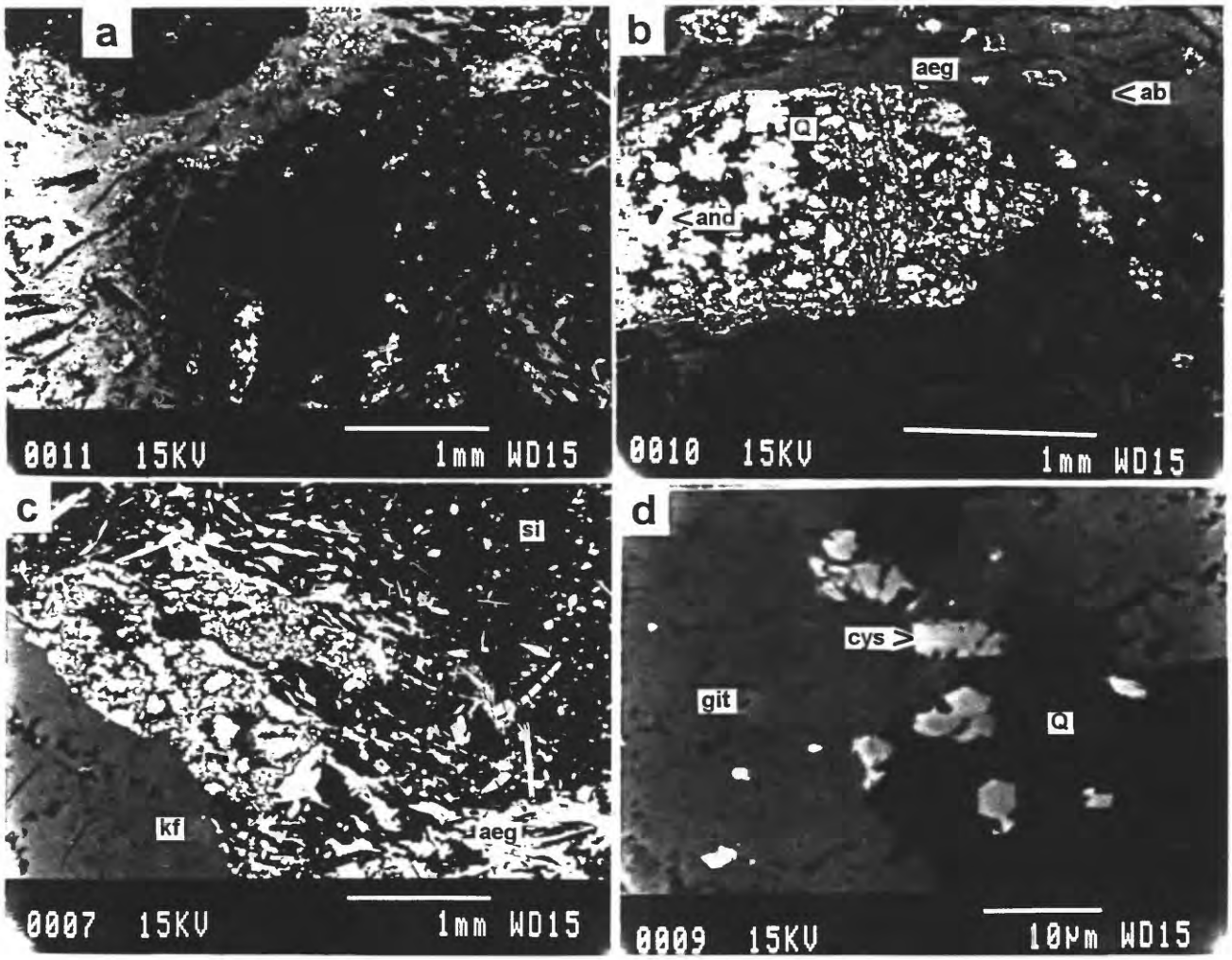

Fig. 12. SEM-BSE image of middle Dotson vein-dike sample 19-5 showing (a) polymineralic globules occurring in both siliceous melt and in an aegirine-albite meniscus; (b) a prismatic globule consisting largely of gittinsite and Ca-Y silicate set in a matrix of andradite (and) and of silica (Q), occurring at the contact between an aegirine (aeg) and albite (ab) rock (melt), in the upper part of the image, and an immiscible siliceous melt containing aegirine needles in the lower part of the image; (c) a crystal of potassium feldspar (kf) that occurs in a matrix of silica (si) flecked with aegirine needles (aeg); a globule of immiscible melt appears to be wetting the feldspar; (d) at higher magnification the globule is seen to be composed of porous gittinsite (git) and crystals of Ca-Y silicate (cys) in a matrix of silica (Q); the bright inclusions in gittinsite in the lower left of the image are a Pb-Cl mineral and cerussite; Ca-Y-Pb-silicate, aegirine, aegirine-augite, calcite, and porous zircon also occur in the assemblage.

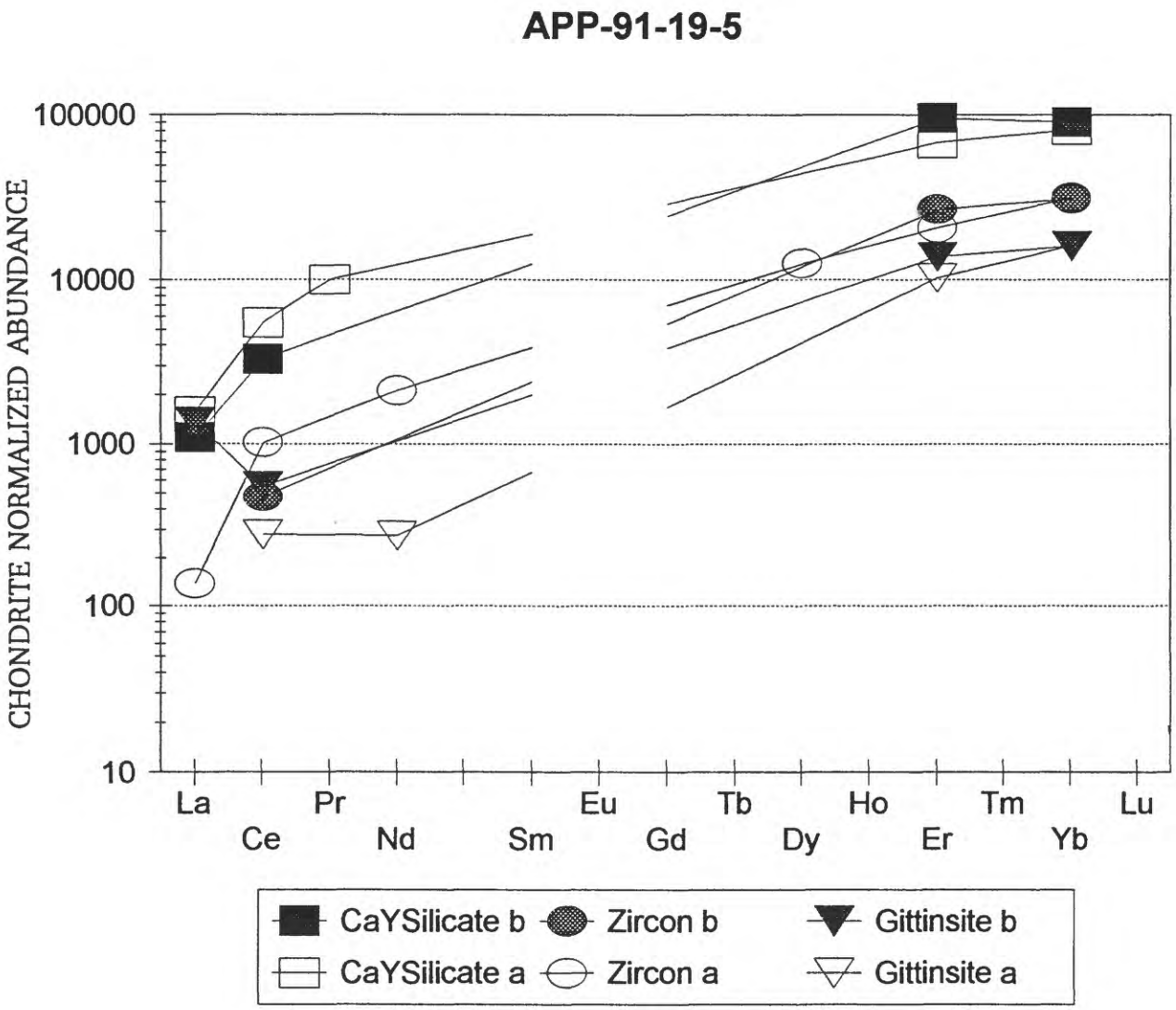

Fig. 13. REE patterns for average compositions of calcium-yttrium silicate, zircon, and gittinsite from two separate microprobe analytical runs on middle Dotson vein-dike sample 19-5.

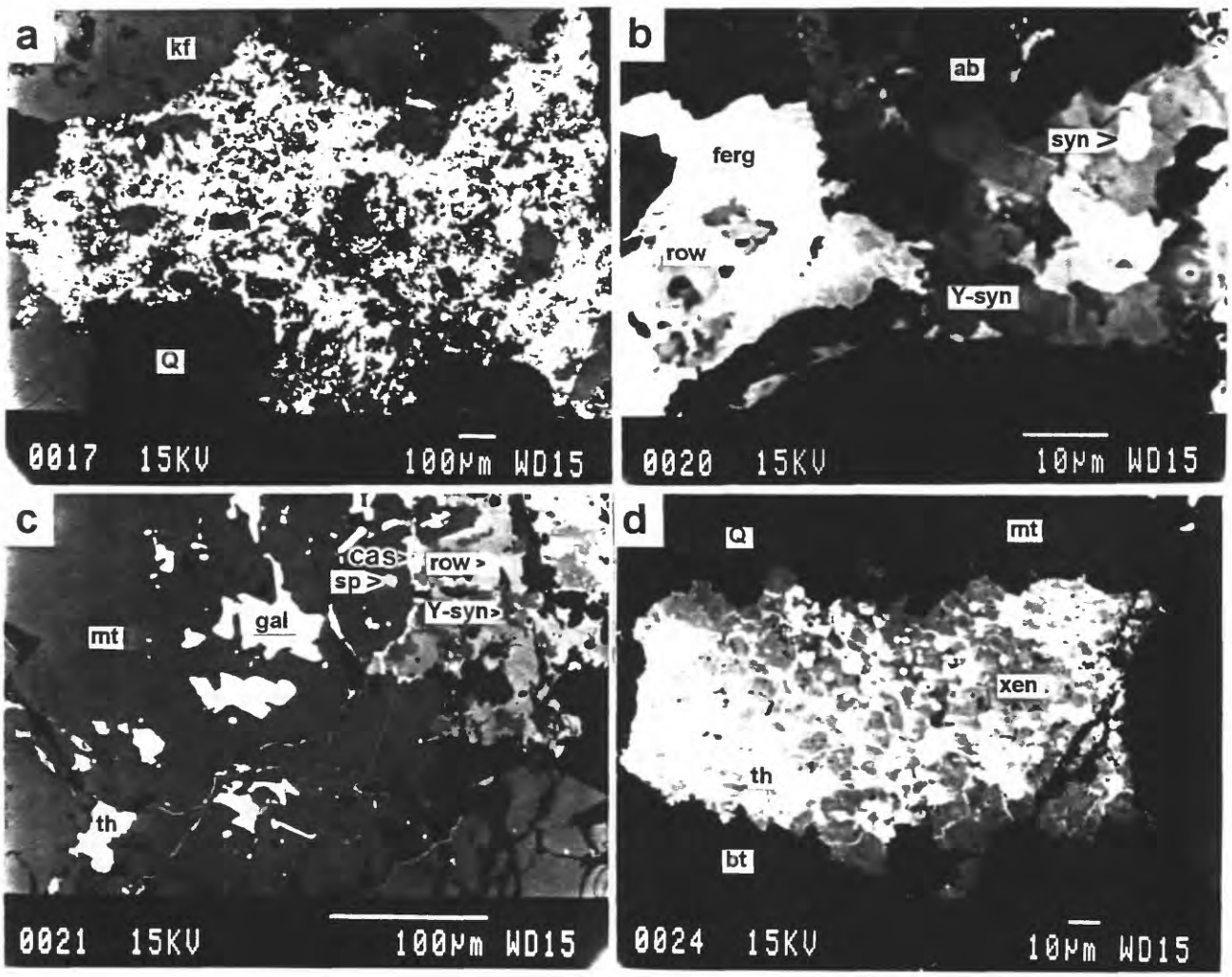

Fig. 14. SEM-BSE image of lower Dotson vein-dike sample 21 showing (a) rounded grains of potassium feldspar (kf) with silica (Q) that appears to have been replaced by a phase now consisting of fine-grained yttrium-, REE-, and niobium-bearing carbonates, silicates, and oxides which in more detail (b) consists largely of intergrown synchisite (syn), Y-synchisite (Y-syn; grain on right shows damage from electron beam), rowlandite? (row), and fergusonite? (ferg) in albite (ab). (c) Elsewhere in the section a magnetite grain (mt) contains patches of inclusions of irregularly-shaped galena (gal), thorite (th), sphalerite (sp), and cassiterite (cas). Cassiterite also occurs on the eastern margin of the magnetite where it abuts REE mineralization composed of rowlandite? (row) and Y-synchisite (Y-syn). Fine veins of galena cut both the magnetite and the REE-bearing minerals. (d) A fractured grain of xenotime (xen) with inclusions of thorite (th) occurs within silica (Q), biotite (bt), and magnetite (mt).

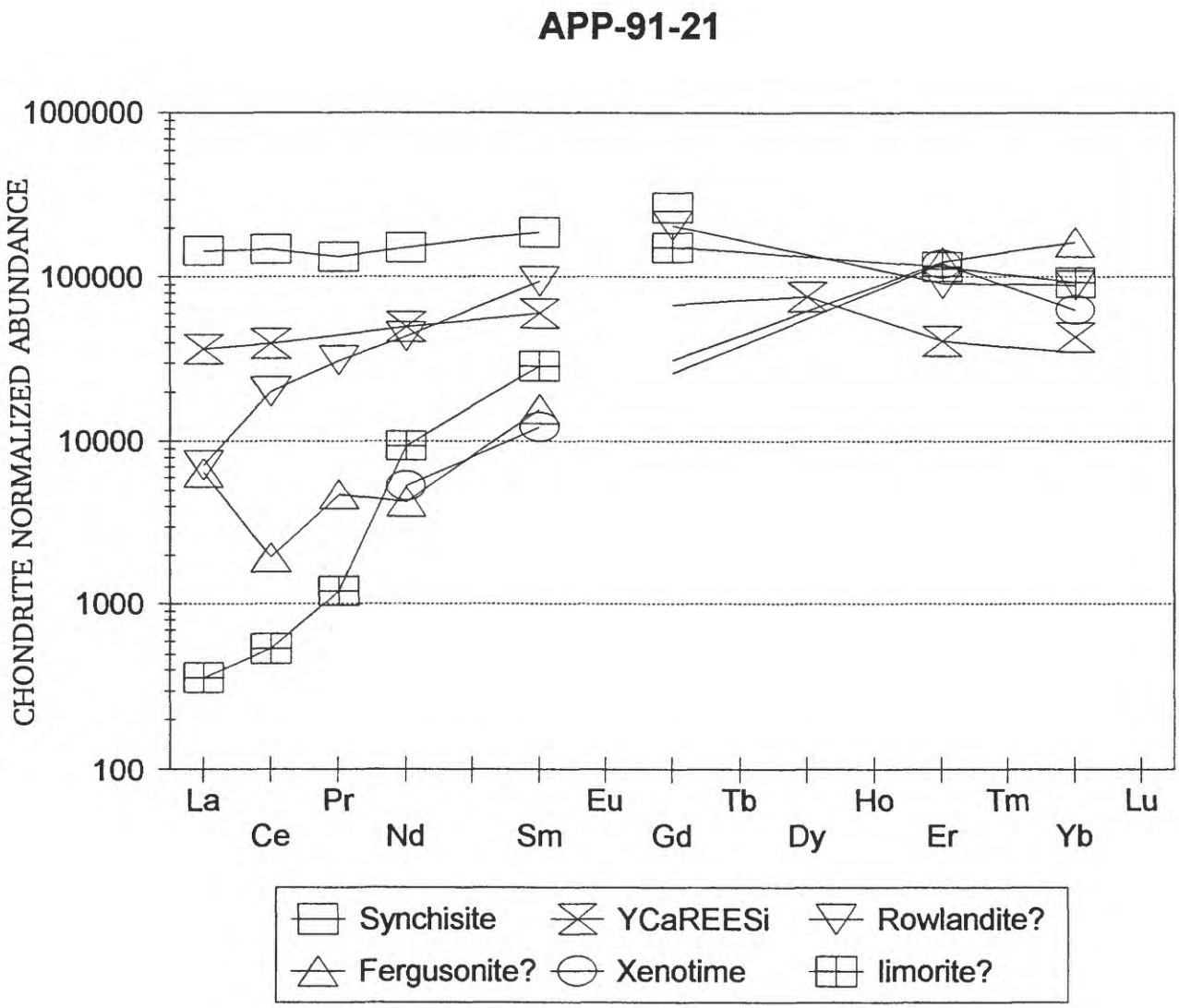

Fig. 15. REE patterns for minerals from lower Dotson vein-dike sample 21.

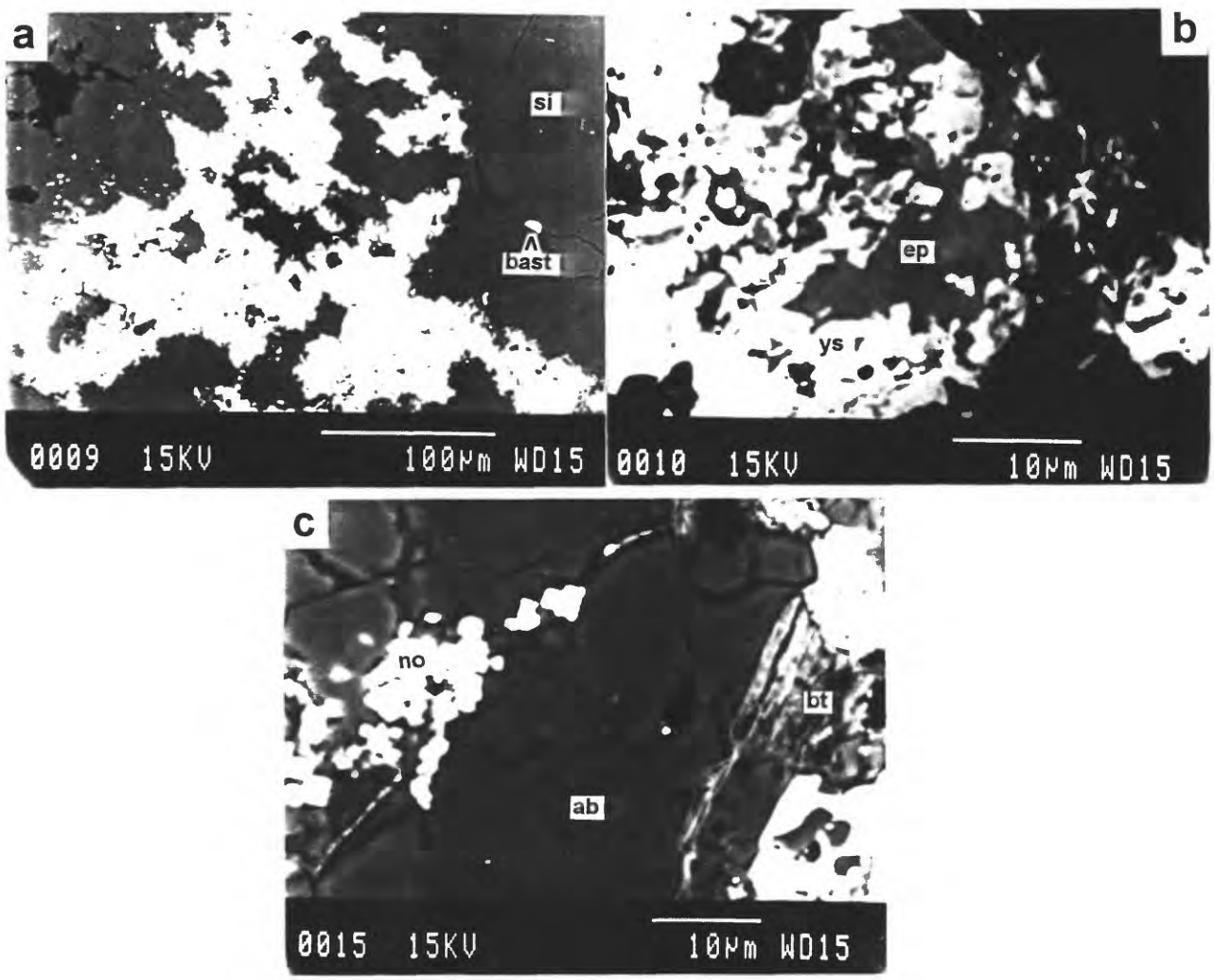

Fig. 16. SEM-BSE image of Geoduck vein-dike sample 6 showing (a) irregular patches of yttrium- and REE-bearing mineralization in a matrix of silica (si). A 10 μm grain of bastnaesite (bast) occurs in a crack in the silica on the right side of the photograph. Cavities of highly irregular shape are abundant in both mineralized and siliceous areas. Some cavities are open, some have coatings of a tetravalent cerium mineral (crandallite?), and others are filled with aluminum-iron silicate (clay?). The mineralization may have been deposited in miarolitic cavities. (b) At higher magnification, much of the mineralization is seen to consist of an Y-REE silicate (ys) and allanitic epidote (ep). (c) Close to the selvage of the vein dike, cracks in albite (ab) are filled with μm-sized grains of a niobium oxide phase (no), biotite (bt), iron oxide or hydroxide, and clay?.

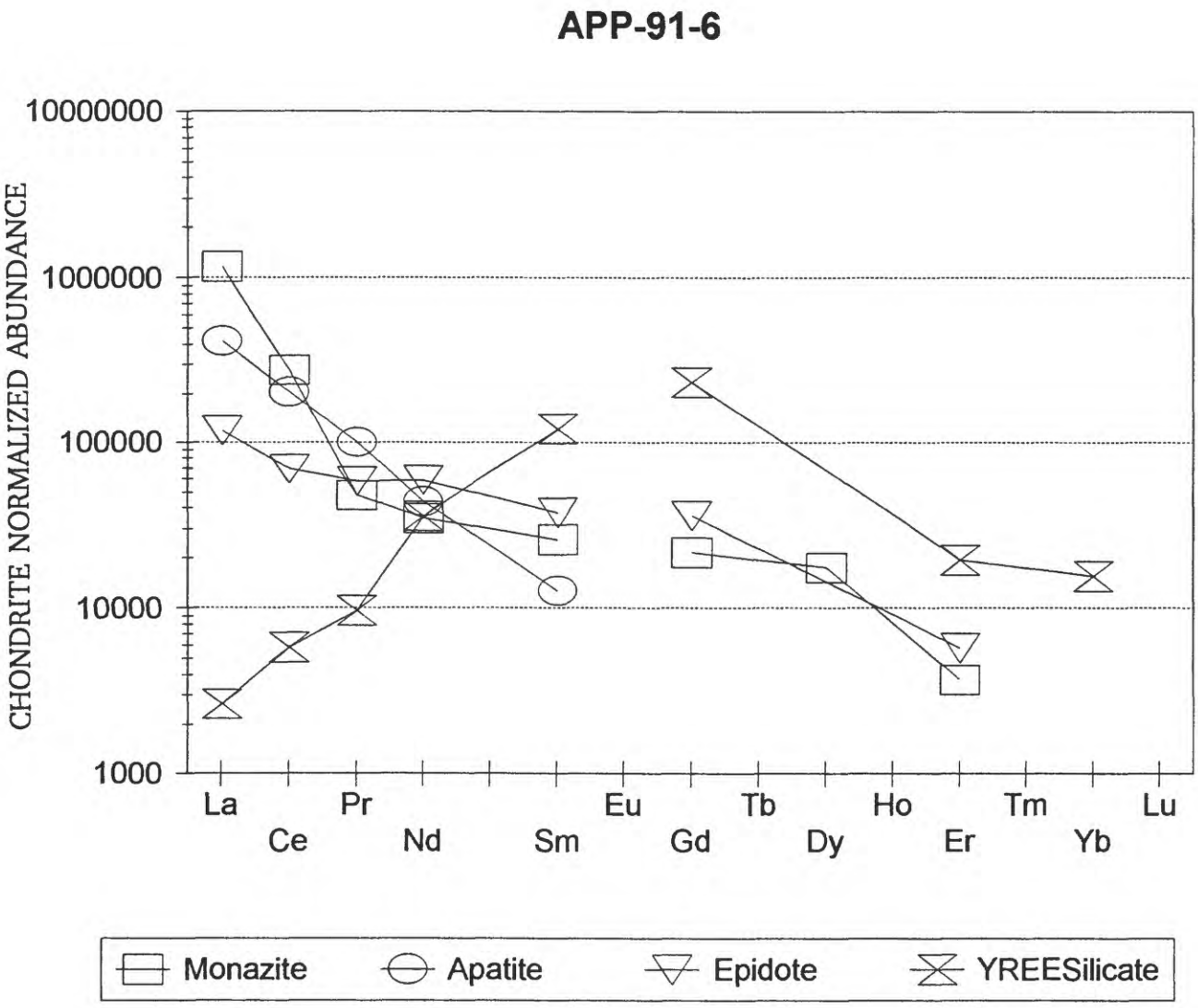

Fig. 17. REE patterns for monazite, apatite, allanitic epidote, and an yttrium-REE silicate in the Geoduck vein-dike sample 6.

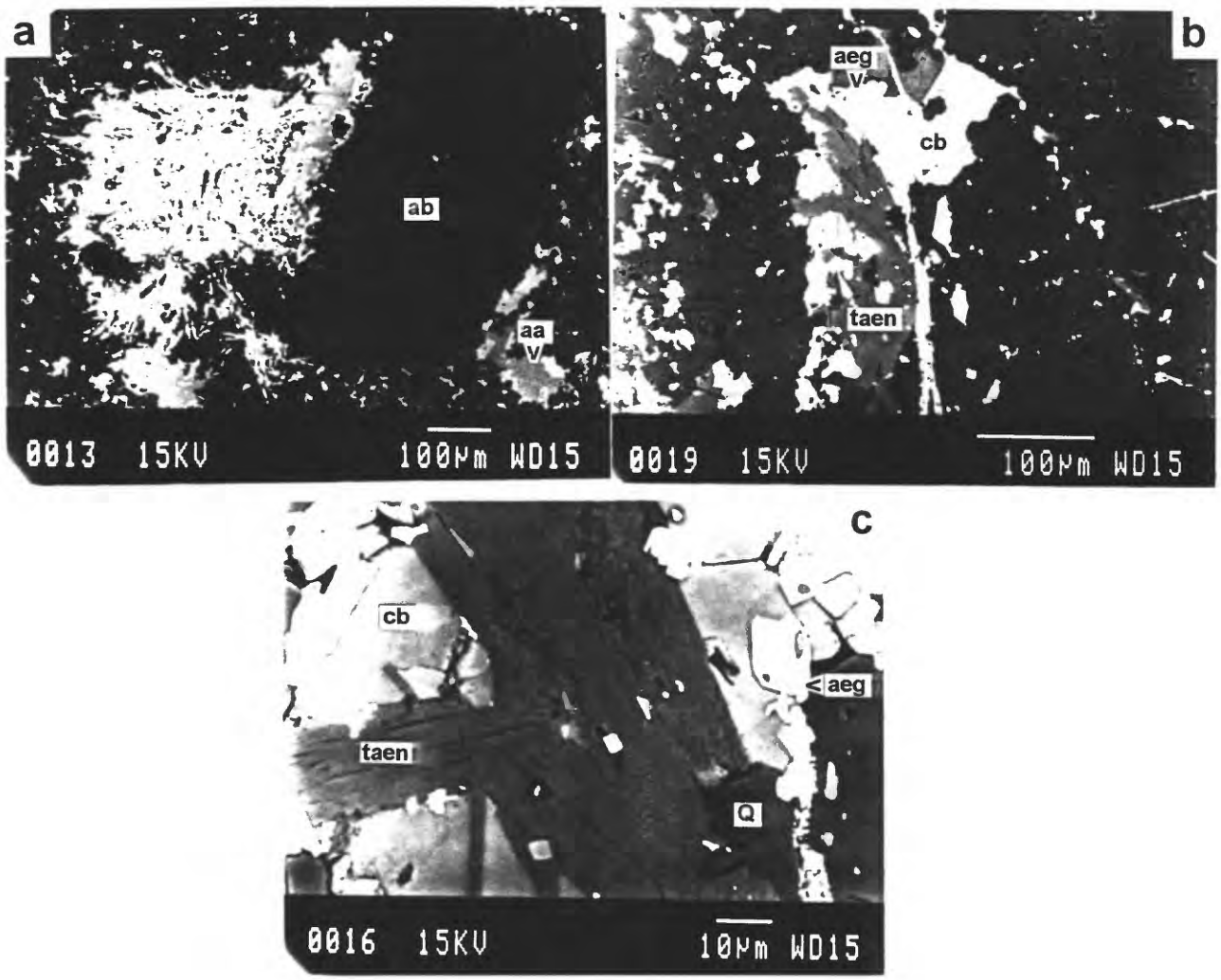

Fig. 18. SEM-BSE images of east Dotson vein-dike sample 23 showing (a) a distinct patch of feathery mineralization in a matrix of albite (ab) and aegirine-augite (aa). The mineralized area contains aegirine-augite, albite, silica, fluorite, and fine intergrowths of fersmite?, caysichite?, bastnaesite, and plumbopyrochlore. (b) A clot composed of aegirine (aeg), manganiferous calcite (cb), and taeniolite (taen) occurs in a matrix of silica and albite; mineralization occurs both disseminated in the clot and in short bifurcating veins. (c) At higher magnification within the clot, taeniolite (taen), with basal cleavage, occurs with carbonate (cb), aegirine (aeg), and silica (Q). Grains of caysichite? occur disseminated in the clot and in the vein where they are accompanied by fersmite?, plumbopyrochlore, bastnaesite, monazite, and strontium-bearing barite. The veins do not appear to displace enclosing minerals and may be metasomatic replacements.

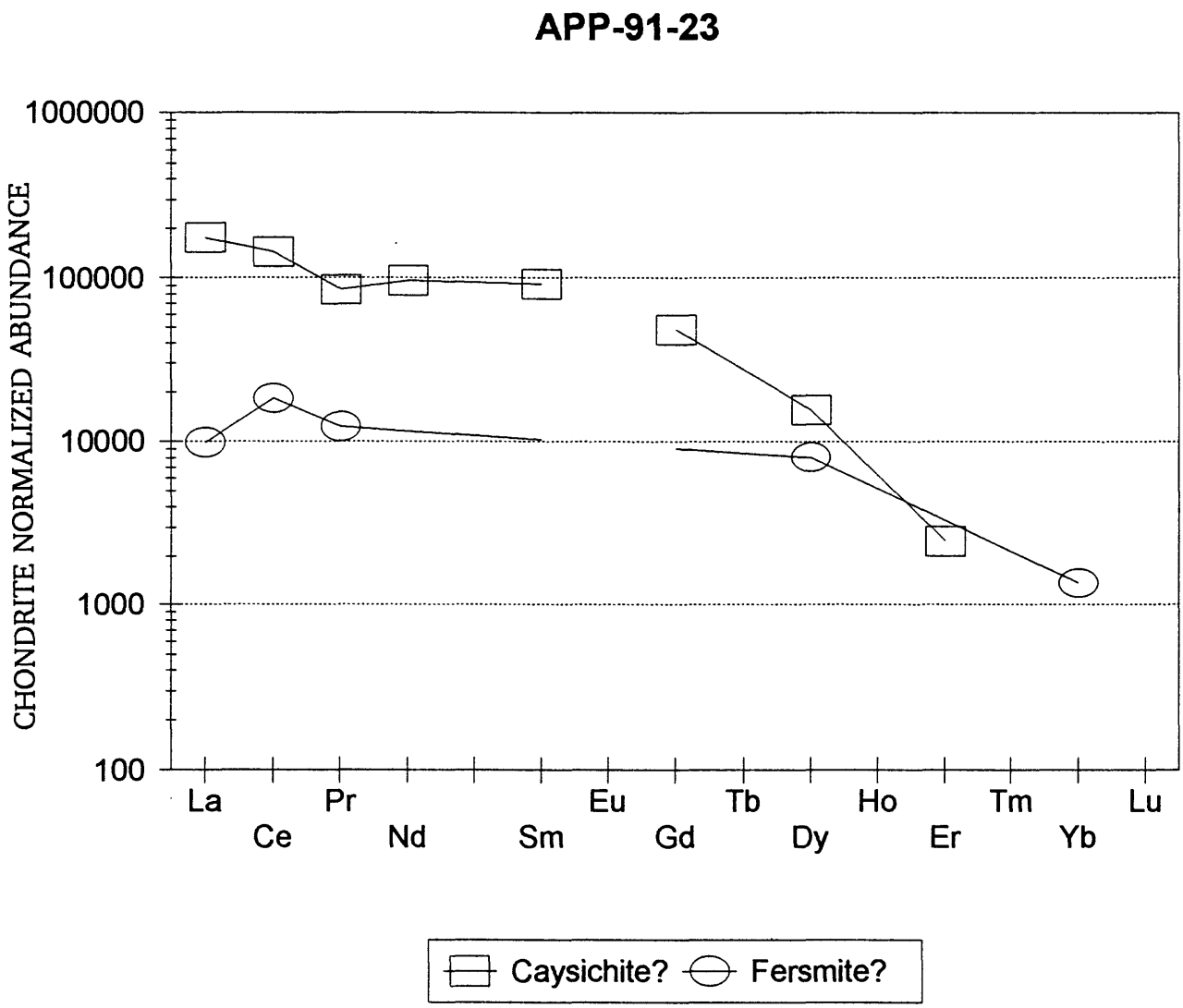

Fig. 19. REE patterns for caysichite? and fersmite? in east Dotson vein-dike sample 23.

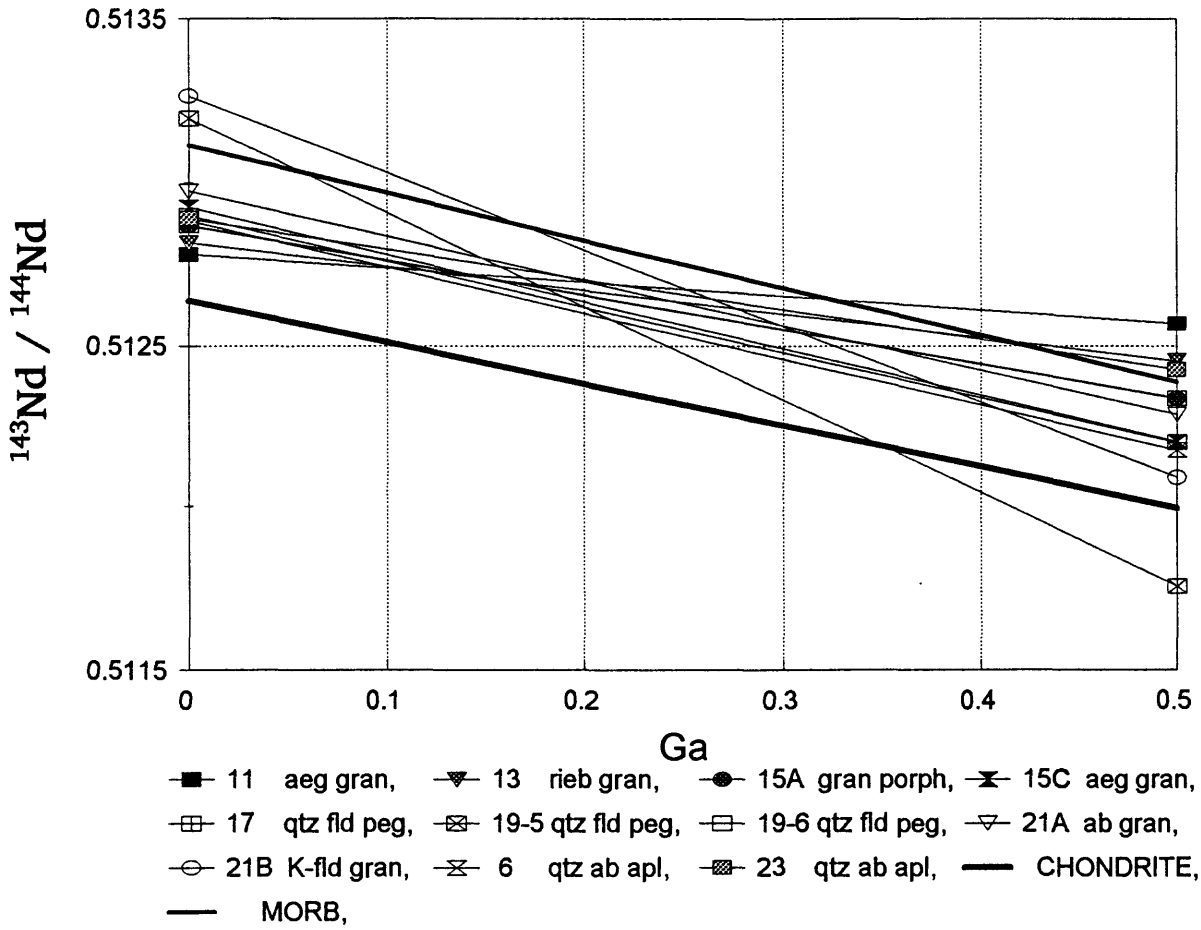

Fig. 20. Diagram showing evolution of $^{143}Nd/^{144}Nd$ as a function of time, based upon measured $^{147}Sm/^{144}Nd$ ratios in Bokan Mountain stock granites and vein dikes. Evolution lines for chondrites (CHOND) and for mid-ocean-ridge basalt (MORB) are shown for reference. Undisturbed isotopic systems with unique initial ratios would yield intersection of evolution lines at the age when the system became closed.

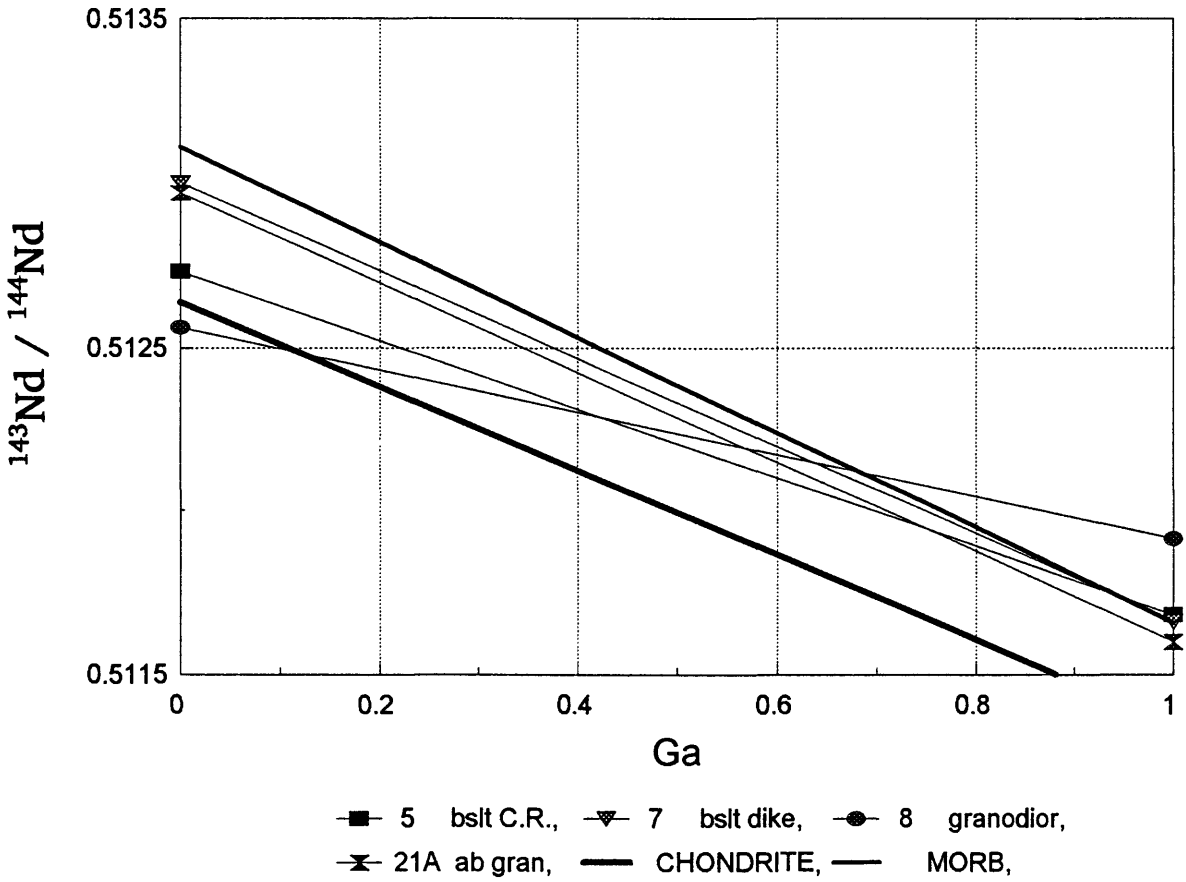

Fig. 21. Diagram showing evolution of $^{143}Nd/^{144}Nd$ as a function of time, based upon measured $^{147}Sm/^{144}Nd$ ratios in country rocks from the vicinity of Bokan Mountain.